Technische Universität München

Physik-Department

Lehrstuhl für Biophysik E22

Forces, Thermodynamics and Structure of Artificial Glycocalyx Models in Two and Three Dimensions

Matthias F. Schneider

Vollständiger Abdruck der von der Fakultät für Physik der Technischen Universität München zur Erlangung des akademischen Grades eines

Doktors der Naturwissenschaften (Dr. rer. Nat.)

genehmigten Dissertation.

Vorsitzender: Univ.-Prof. Dr. M. Kleber

Gutachter: 1. Univ.-Prof. Dr. E. Sackmann

2. Univ.-Prof. Dr. J. Friedrich

Diese Dissertation wurde am 22.04.2003 bei der Technischen Universität München eingereicht und durch die Fakultät für Physik am 06.06.2003 angenommen.

Danke an …

… Prof. E. Sackmann für die exzellenten Vorraussetzung in seinem Labor

… Dr. M. Tanaka, der mir die Freiheit ließ, eigene Ideen zu verwirklichen ohne sein Begeisterung an meiner Arbeit zu verlieren

… Prof. R. R. Schmidt und Christian Gege für ihre ausgezeichneten Synthesen

… Prof. G.G. Fuller und seiner Arbeitsgruppe in Stanford für ihr wissenschaftliches "know how" und die Gastfreundschaft

… PD Dr. A. Boublicht und Prof. D. Andelman deren theoretische Überlegungen zu meinen experimentellen Resultaten zu einem tiefergehenden Verständnis beitrugen

… Dr. Michael Rappolt für die Kooperationsbereitschaft und die Berechnung von Elektronendichteprofilen

… PD. U. Rothe und Dr. G. Bendas für ihre Flusskammerexperimente

… Gerald Mathe und Florian Rehfeld für die Einführung und Unterstützung bei der Ellipsometrie

… den ehemaligen Ulf Rädler, Julia Nissen und Heiko Hillebrandt für die vielen kleinen Tips und Tricks beim Präperieren und Umgang mit Chemikalien, sowie Roman Zantl und Frank Artzner für ihre theoretische wie praktische Hilfe bei der Röntgenstreuung

… Zeno Gutenberg der stets seine gesammelte Erfahrung zur Verfügung stellte und immer Zeit fand über grundsätzliche biophysikalischen Fragenstellungen zu diskutieren

… Laurent Limozine der mir die Präparation von riesen Vesikeln beibrachte und mir mit seiner Erfahrung am Mikroskop bis in den späten Abend zur Verfügung stand

… Oli Purucker und Klaus Adelkofer für ihre Organisation und Hilfsbereitschaft

sowie den Rest der Tanaka Gruppe Stefan, Uwe (alias Murrat) und Jockey (alias Joachim) für die gute Atmosphäre und ausserlaborlichen Aktivitäten

… unseren Werkstattleitern Erwin und Rudi die durch ihre Ideen und Kompetenz erst zum gelingen vieler Experimente beidrugen

… alle übrigen Mitglieder des Lehrstuhls E22, die für das ausgezeichnete Arbeitsklima im Institut maßgeblich waren

… meinen Bruder Stefan für seine Unterstützung nicht nur bei medizinisch relevanten Fragen sowie seiner Gattin Birgit in deren „Tegernseeer Häusle“ ein Großteil dieser Arbeit verfasst wurde

… meiner Freundin Vanessa für ihre vielen sprachlichen Korrekturen und Tips, aber v.a. für die nötige moralische Unterstützung

… meinen Eltern ohne deren Unterstützung und Vertrauen es nie zu dieser Arbeit gekommen wäre

Meinen Eltern Afra und Theo

1 SUMMARY 1

2 INTRODUCTION 5

3 MATERIAL AND METHODS 11

3.1 Film balance and Langmuir-Blodgett-Technique 11
3.1.1 Physical principles of the film balance technique 12
3.1.2 The design of the trough with Wilhelmy plate 13
3.1.3 Fluorescence Film balance 14
3.1.4 Film Preparation and Langmuir-Blodgett transfer 15

3.2 Ellipsometry 16

3.3 Interfacial Rheology 21
3.3.1 Theory of Surface Rheology and measuring principle 21
3.3.2 Experimental Setup 22

3.4 Differential Scanning Calorimetry (DSC) 24
3.4.1 Theory of Calorimetry 24
3.4.2 Experimental Setup 25

3.5 X-Ray Scattering 26
3.5.1 Physical Principles of X-Ray Scattering 27
3.5.2 Experimental Setup 29

3.6 Chemicals and Chemical Structures 30

4 RESULTS AND DISCUSSION 33

4.1 Glycolipids with Linear Head group Conformation (Lac1-3) 34
4.1.1 Pressure Area Isotherms 34

4.1.2 Swelling Behaviour of glycolipid monolayer 38
4.1.3 Rheology at the Air/Water Interface (Schneider, Lim et al. 2002) 43
4.1.4 Calorimetry and X-Ray Scattering on Glycolipid Dispersions 49
4.1.5 Summary 60

4.2 Glycolipids with Branched or Bent Head Group Conformation (Lewis X, Gentiobiose) 61
4.2.1 Monomolecular Films of Gentiobiose Lipids. 62
4.2.2 Monomolecular Films of Lewis X Lipids. 66
4.2.3 Summary 70

4.3 Phase Behaviour of Fluorinated Lipids and Artificial Microdomains 71
4.3.1 Stripe-like Phase Formation in Fluorinated Lipid Monolayer (Schneider, Andelman et al. 2003) 72
4.3.2 Design of Artificial Glycolipid Microdomains by Fluorinated Lipids (Gege, Schneider, et al 2003) 81
4.3.3 Summary 89

5 CONCLUSIONS AND OUTLOOK 90

A. Viscoelasticity of PEG-lipids 93

B. Preparation of Giant Unilamellar Vesicles (GUVs) 95

1 Summary

The glycocalyx, a network of oligo- and polysaccharide chains with glycolipids, glycoproteins, and proteoglycans on the extracellular membrane surface serves as a hydrophilic “cushion” between cells in addition to stabilizing the structure of animal cell membranes by a combination of various physical forces (generic interactions). Furthermore, it contains specific recognition sites for counterpart lectins and cell adhesion receptors (specific interaction). The interplay of these generic and specific interactions often mediates adhesion and recognition between

cells, in which the condensation of cell surface receptors builds functional microdomains, which can serve as a prerequisite for cell contact formation. Although such phenomena have been widely studied, the physical basis of glycocalyx function has not yet been experimentally understood and still little is known regarding the interaction mechanisms on a molecular level. Despite a number of reports on the effects of ethylene glycol chains (as a glycocalyx model system) on the morphology and interfacial properties of membranes, studies of the thermodynamic and elastic properties of glycolipids themselves in a well-defined artificial model system are still missing. Consequently, a set of synthetic glycolipids with various carbohydrate head groups and lipid anchors (synthesized by Dr. C. Gege and Prof. R.R. Schmidt, Universität Konstanz) was used to study the mechanical, morphological and thermodynamic properties of glycocalyx model systems and the relationship to the molecular structure of these glycolipids. Furthermore, the formation of functional microdomains, important for specific interactions between membranes was studied using synthetic glycolipids with biofunctional relevant head groups.

In Chapter 4.1.1 and 4.1.2 thermodynamic phase behaviour and hydration forces in synthetic glycolipid monolayers were measured by a combination of Langmuir film balance experiments and ellipsometry under controlled humidity conditions. As model systems for the study of the impact of saccharide chain length, synthetic lipids with linear oligolactose head groups were used. Thermodynamic parameters such as phase transition entropy and latent heat could be quantitatively estimated by the application of the Clausius-Clapeyron equation and were found to be comparable to those of phospholipids. Under controlled humidity conditions the strength of hydration (disjoining pressure) could be precisely set, yielding to quantitative force-distance relationships perpendicular to the membrane surface. The hydration of the oligolactose chains could be treated within the theoretical framework of polymer “brushes”. Analysis within this framework, as well as examination of the film balance experiments, indicates increasing entropic contributions from the head group as a result of the elongation of the saccharide chain. The monomolecular film of elongated sugar chains can therefore be viewed as a “soft cushion”.

To get deeper insight into the relationship between molecular structure and macroscopic physical properties (i.e. chain melting, lamellar spacing, lateral packing and degree of hydration) the thermotropic phase behaviour of oligolactose lipids were studied by a combination of differential scanning calorimetry (DSC) and small and wide angle x-ray scattering and are presented in Chapter 4.1.4. The hydrophobic/hydrophilic balance (competition between enthalpic contribution from chain-chain interaction and entropic contribution from carbohydrate-carbohydrate interaction) was found to be crucial in determining the morphology of glycolipid membranes with oligolactose head groups. This dominate effect of the hydrophilic/hydrophobic balance can be attributed to the small sterical mismatch between the alkyl chains and the linear, cylindrical oligolactose head groups.

Presented in Chapter 4.1.3 are the studies of the mechanical properties of the same glycolipid monolayers at air/water interface using a quantitative interfacial stress rheometer (ISR) under well-defined thermodynamic conditions (temperature, area per molecule, surface pressure). The hydrophobic/hydrophilic balance was found to significantly influence the viscoelastic properties of glycolipid monolayers. For the lipid with trilactose head group, a rheological transition (from viscous to elastic) due to the exclusion of the hydrating water and the formation of a physical network of hydrogen bonds could be observed. Lipids with shorter oligolactose head groups did not display this rheological transition, revealing the critical role of the number of hydrogen bonding sites on network formation (cooperative effect). This approach was extended for the examination of another glycolipid with the same monosaccharide composition as lactose but different glucosidic bond. The results demonstrated the strong influence of steric (i.e. entropic) contributions from the carbohydrate head group on the viscoelasticity of the monolayer (Chapter 4.2.1). Furthermore, lipids with the asymmetric head group Lewis X, displayed an isotropic-to-nematic transition of their lipid head groups (Chapter 4.2.2), which could not be resolved in Langmuir isotherm experiments.

In an additional model system, micro-domains of glycolipids with specific functions (e.g. blood group antigens sialyl-Lewis-X) were designed by introduction of

partially fluorinated lipid anchors (F-alkyl chains). These lipids demonstrate strong de-mixing with alkyl chain lipids, which were used as the matrix system. Initial studies examined the thermodynamic properties of the pure F-alkyl lipid monolayer (Chapter 4.3.1). Fluorescence microscopy revealed a stripe like phase which can be explained theoretically as a consequence of the strong dipole moment of the terminal $-CF_3$ group observed by surface potential measurements. The unique phase behavior of partially fluorinated lipid anchors, which results in a strong de-mixing with matrix phospholipids, was utilized to confine functional carbohydrate ligands within micro-domains (Chapter 4.3.2). Fluorescence microscopy and laser scanning confocal microscopy showed that it is possible to self-assemble so-called “artificial lipid rafts” both in monolayers and in giant lipid vesicles. Additionally, dynamic flow chamber experiments demonstrated that the size and distribution of functional rafts can strongly influence the dynamic cell adhesion under shear flow.

2 Introduction

Biological membranes maintain the essential differences between the cytosol and the extracellular environment and between the contents of each cell organelle and the cytosol. The general structure common to all biological membranes is a very thin film (approximately 5 nm) of lipids and proteins, held together primarily by noncovalent interactions. The proteins stick in the lipid membrane or protrude through it and have a huge variety of different functions, ranging from the transport of specific molecules, sensory functions and cell signalling to their actions as catalysts in membrane-associated reactions, such as ATP synthesis, or work as

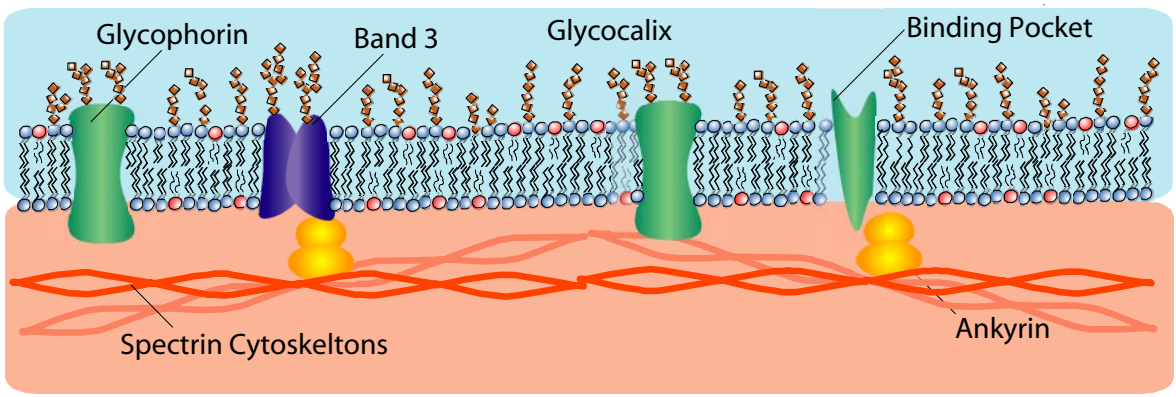

Figure 2-1 Cross section of an erythrocyte plasma membrane.

structural links that connect the cytoskeleton through the lipid bilayer to the extracellular matrix or adjacent cells. Figure 2-1 shows a sketch of a cross section of the plasma membrane of an erythrocyte. The fluid crystalline nature of the lipid bilayer and the fact that it is a multiparticle system with collective phenomena, e.g. self assembling, is very appealing from a physical perspective. As a consequence of this property, the membrane exhibits some very unique features, which are of basic importance to life. An example of this versatility is the ability of biological membranes to effectively form organelle compartments within the cytosol while at the same time maintaining the form variability of the outer cell membrane to fit into and through biological tissue. Due to its fluid crystalline character, the lipid membrane can be described using the thermodynamics of 2 D liquids. Such fluid crystals can appear in a variety of different phase states, such as isotropic, nematic, solid etc., displaying entirely different physical properties (optical, electrical, mechanical etc.). This structure-function relationship and the related phase diagram may lead to new applications in areas such as modern material science or biotechnology. In addition new developments in drug delivery systems, artificial implants or artificial membranes as drug testing kits can be envisaged. Moreover, the chiral character of lipids can introduce very unique physical properties, such as the piezoelectrical-like effect found for smectic C liquid crystals (Brand and Pleiner 1984). With respect to biomembranes, it is known that the physical state of the membrane can be coupled to the function of enzymes or proteins. One example of this is the activity of the enzyme phospholipase A2

which is increased when the membrane is found in the phase transition region (Burack, Yuan et al. 1993). Another example is the protein kinase C which becomes more active when the membrane forms a cubic phase (Giorgione, Huang et al. 1998). If this is an equilibrium process, thermodynamics predicts that, in the same way as the membrane state influences the enzyme activity, the enzyme activity can change the membrane's phase state. As a result the morphology and thermodynamics of membranes is a field of intense study (Schneider, Marsh et al., 1999).

The present work examines in particular the influence of the glycocalyx on these properties. The glycocalyx is a major part of the outer cell membrane consisting of lipids with carbohydrates as hydrophilic head groups (glycolipids), whose distribution is extremely asymmetric (Figure 2-1 and electron micrograph in Figure 2-2). Essentially all glycolipids are found on the extracellular side of the membrane and can interact and self assemble by means of van der Waals forces between their hydrophobic tails as well as hydrogen bonds between their head groups. The glycocalyx plays fundamental and essential roles in cell-cell and cell-matrix interactions. It serves not only as a soft cushion between cells due to its unique swelling behavior, but also contains specific recognition sites for counterpart lectins and cell adhesion receptors (Curatolo 1987; Hakomori 1991; Geyer, Gege et al. 1999; Schneider, Mathe et al. 2001). In addition to carbohydrate-protein interactions, it has been demonstrated, that cell surface carbohydrates can selectively bind to complimentary carbohydrates of other cells (Hakomori 1991). Furthermore, these carbohydrates stabilize the outer leaflet of the plasma membrane of animal cells via a combination of various physical forces (e.g. electrostatic, van der Waals, hydrogen bonding etc.) (Gabius and Gabius 1997). Although such phenomena have already been studied, the physical basis of glycocalyx function, as well as the interaction mechanisms on a molecular level was not understood.

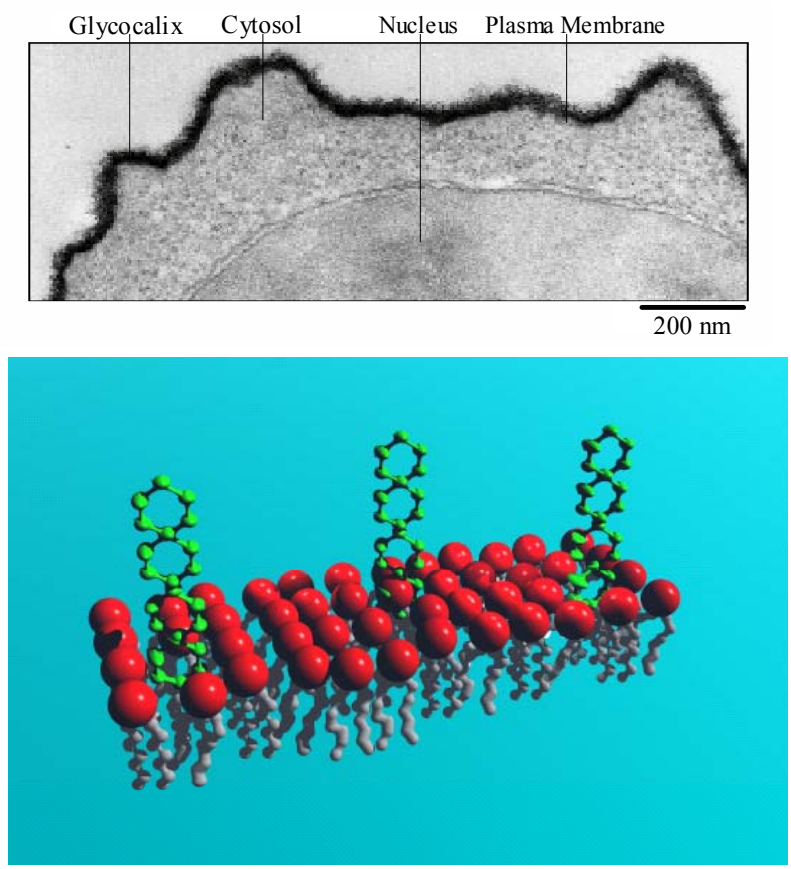

Figure 2-2 (Upper graph) Electron micrograph of a lymphocyte (taken from (Alberts, Bray et al. 1994)) showing the carbohydrate layer (black). (Lower graph) 3D sketch of the outer lipid monolayer including some glycolipids (green).

This was partially due to the lack of a systematically varied set of synthetic glycolipids until recently. Since the interaction between sugars change dramatically with size, bond angle and charge, it is difficult to draw any unambiguous conclusion from the experiments on just one glycolipid. Therefore, in order to mimic the cell surface glycocalyx, phospholipids with poly(ethylene glycol) chains (PEG lipids) have been widely applied (Harris 1992). These are believed to avoid non-specific adhesion on lipid vesicles or protein adsorption onto solid supports. However, it is shown in the present work, that the complex behavior of glycolipids and glycolipid films often depends on subtle changes in length and orientation of their head groups. The fact that this complex behavior is not found in lipopolymer membranes, clearly emphasizes the need for a more suitable glycocalyx model to mimic its biologically relevant functions. Moreover, for the understanding of the physics of the glycocalyx one has to examine both the

microscopic as well as the macroscopic properties to find the relationship between physical properties (and hence function) and structure. Structural changes were observed by x-ray scattering experiments and changes in physical properties (e.g. response functions) by means of Differential Scanning Calorimetry (DSC), film balance and viscoelastic measurements. As a result of these studies, insight into the nature and strength of the forces acting perpendicular to, as well as in the membrane plane was gained.

Another important role of glycolipids is their ability to form and stabilize laterally organized functional lipid microdomains (e.g. rafts), which can be thought of as a transient phase separation into condensed domains of lipids inside the fluid bilayer. As a result of this condensation, the domains are slightly thicker than the fluid matrix surrounding them, allowing the communication between the outer and inner monolayer, which usually move independent from each other, and enabling the accommodation of certain proteins and binding sites important for cell adhesion (Simons and Ikonen 1997; Jacobson and Dietrich 1999). The binding interaction can exist in the form of protein – protein, protein - glycolipid or glycolipid – glycolipid. Examples for the latter two are the selectin-sLeX and the homolytic LeX-LeX binding, both of which were shown to be cooperative (multivalent binding) [Rosenberg, 1997 #1342; Varki, 1997 #1388; Welply, 1994 #1401] (Geyer, Gege et al. 1999; Geyer, Gege et al. 2000) [Hernaiz, 2002 #51; de La Fuente, 2001 #1127; Tromas, 2001 #1384]. Although studies clearly demonstrated that clustering of glycolipids (e.g. sLeX) appears to be an essential prerequisite for the cell contact to take place (Vogel, Bendas et al. 1998), the number of reports on adhesion and rolling kinetics are still few. Taking this into account raft-like domains were reconstituted in lipid vesicles [Ahmed, 1997 #1073; Brown, 1998 #1103; Schroeder, 1994 #1358] and in solid supported membranes (Dietrich, Bagatolli et al. 2001; Dietrich, Volovyk et al. 2001) . However, this allowed only little control of size and distribution of the functional domains. The strategy developed and applied here not only overcomes these problems, but also allows for the first time, the study of the effect of dynamic accumulation of lipids into clusters on membrane contact (adhesion) formation. A fluorinated lipid tail plays the key role in this approach.

Fluorinated lipids are believed to be potential candidates for a variety of applications, e.g. drug delivery systems, microdomains etc.. This is due to the high electronegativity of fluorine (especially with respect to hydrogen), which causes strong dipole-dipole repulsion when oriented parallel, and because of its hydro- and lipophobicity (Riess and Greiner 2000; Riess 2002), which builds the basis for the design of small lipid domains when mixed with hydrocarbon chains. In the last chapter of this thesis (4.3) several studies on different lipids with partially fluorinated anchors (F-alkyl chains) used as a single component system as well as mixed with alkylated matrix lipids are presented. Phase separation in lipid monolayers and vesicles was investigated by film balance experiments and different types of fluorescence microscopy (epifluorescence, inverted and Laser Scanning Confocal Microscopy). The microdomains designed at the air/water interface were transferred onto a hydrophobized solid support and were subjected to a flow of cells in flow chamber experiments, where dynamic adhesion could be confirmed.

3 Material and Methods

To measure forces, thermodynamics and structure of glycolipids in two and three dimensions, the following set of methods was used.

3.1 Film balance and Langmuir-Blodgett-Technique

In order to study the macroscopic as well as the microscopic two dimensional phase behavior of monomolecular thin films, the film balance technique according

to Wilhelmy in combination with a Langmuir trough (Gaines 1966) was used.

3.1.1 Physical principles of the film balance technique

Using a film balance the lateral pressure π as a function of area per molecule *A* is measured in order to characterize the surfactant monolayer. π is measured as the difference in surface tension in the absence (γ_0) and presence (γ_1) of surfactant at the surface (Gaines 1966)

$$\pi = \gamma_0 - \gamma_1 . \qquad \text{Eq. 3.1}$$

It terms of energy, the surface tension is the surface free energy necessary to create the air/surfactant monolayer. Measuring π versus *A,* the so-called pressure-area isotherms, one can determine the isothermal compressibility κ_T by building the differential expression

$$\kappa_T := -\frac{1}{A}\left(\frac{\partial A}{\partial \pi}\right)_T . \qquad \text{Eq. 3.2}$$

Using the same setup, the isobaric thermal expansivity can by determined from the area/temperature experiments

$$\alpha_\pi := \frac{1}{A}\left(\frac{\partial A}{\partial T}\right)_\pi . \qquad \text{Eq. 3.3}$$

The isothermal compressibility can be related to the surface free energy by

$$\kappa_T = \frac{1}{A}\left(\frac{\partial^2 F}{\partial A^2}\right)_T^{-1} . \qquad \text{Eq. 3.4}$$

I.e. in all cases one measures derivatives of the free energy. Changes in the slope of the π-*A* isotherms indicate phase transitions of first (horizontal) and second order (kink). Whereas jumps in the compressibility give information about the symmetry of the second order phase transition (Albrecht, Gruler et al. 1978), the Clausius-Clapeyron- equation allows for the calculation of the heat of transition in first order transitions

$$\Delta Q_T = T \cdot \left(\frac{d\pi_T}{dT} \right) \cdot \left(A_{LE} - A_{LC} \right). \qquad \text{Eq. 3.5}$$

Where A_{LE} and A_{LC} are the area per molecule in the liquid-expanded and liquid-condensed phase respectively, and π_T the lateral pressure in the coexistence region.

3.1.2 The design of the trough with Wilhelmy plate

In Figure 3-1 the overall design of a film balance is shown. After the film is spread on the surface and is equilibrated, the barrier is moved to compress the film. The Wilhelmy- Plate is then dragged by the surface tension of water towards the air/water interface. The elongation of the spring in the Wilhelmy-System is measured by inductivity. Knowing the spring constant and the geometry of the plate the surface tension can be calculated. Besides surface tension there is also buoyancy and gravity acting on the plate.

$$F(\pi) = mg + \pi 2(a+b)\cos\alpha - \rho ghab \qquad \text{Eq. 3.6}$$

α is the contact angle formed by the water film with the plate, *b* the width and a the thickness of the Wilhelmy-Plate, h the height of the plate covered with water and ρ the density of water. When amphiphilic molecules acting at the air/water interface, the surface tension is reduced and hence the lateral pressure increased. Since all measurements are taken with respect to the free water surface, the exact

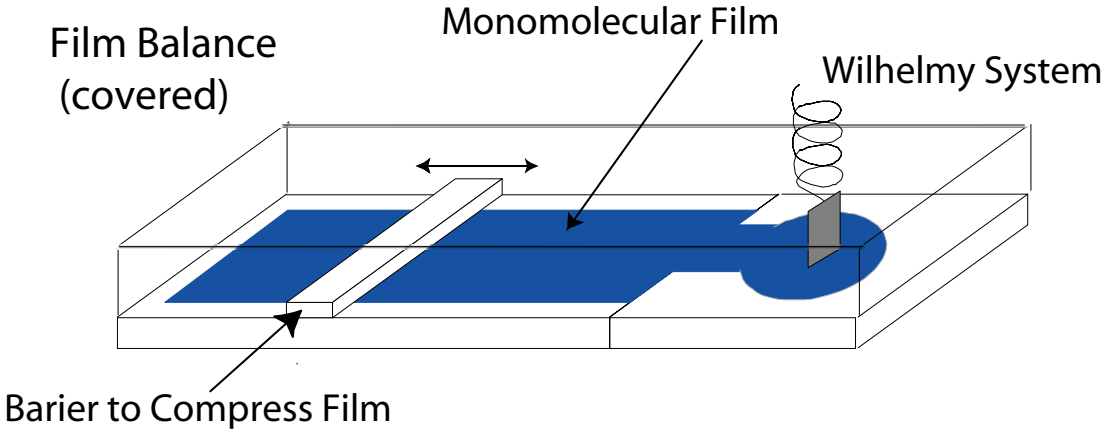

Figure 3-1 *Design of the Langmuir-Trough used. The surface tension was measured using a Wilhelmy plate. Compressing speeds vary between 20 – 100 μm/s.*

amount of subphase volume is not of crucial importance for π-A isotherms. To control the temperature, a coil heater connected to a heating bath (Julabo, Seelbach, Germany) was imbedded in the Teflon block, at the bottom of the trough. Furthermore, the whole setup was kept under a flow box to avoid dust adsorbing at the air/water interface.

3.1.3 Fluorescence Film balance

To get a close look at the phase behavior of two dimensional thin films, a fluorescence film balance was used similar to the one developed by Lösche et al [Lösche, 1983 #383]. A fluorescent dye used as a probe was incorporated into the film and the lateral dye distribution was measured from the fluorescent pictures. In these studies, the contrast in fluorescence signal was obtained by using dyes with different solubility for liquid expanded and liquid condensed phases. These two phases are separated by a first order phase transition. Furthermore, there is a first order gas to liquid transition which can not be resolved in the π-A-isotherms described in the last paragraph. The dyes used are presented in Figure 3-17. In Figure 3-2, a schematic picture of the epifluorescence setup is shown. The monolayer was illuminated from the top with monochromatic light (λ = 546 nm) from a mercury lamp using a 40x LDW plan (Olympus, Hamburg, Germany) objective. The light emitted by the fluorescence probe was registered by a SIT camera (Hamamatsu, Herrsching, Germany) and recorded by a VCR. To digitalize the recorded film, we used the open source software NIH image (NIH, USA).

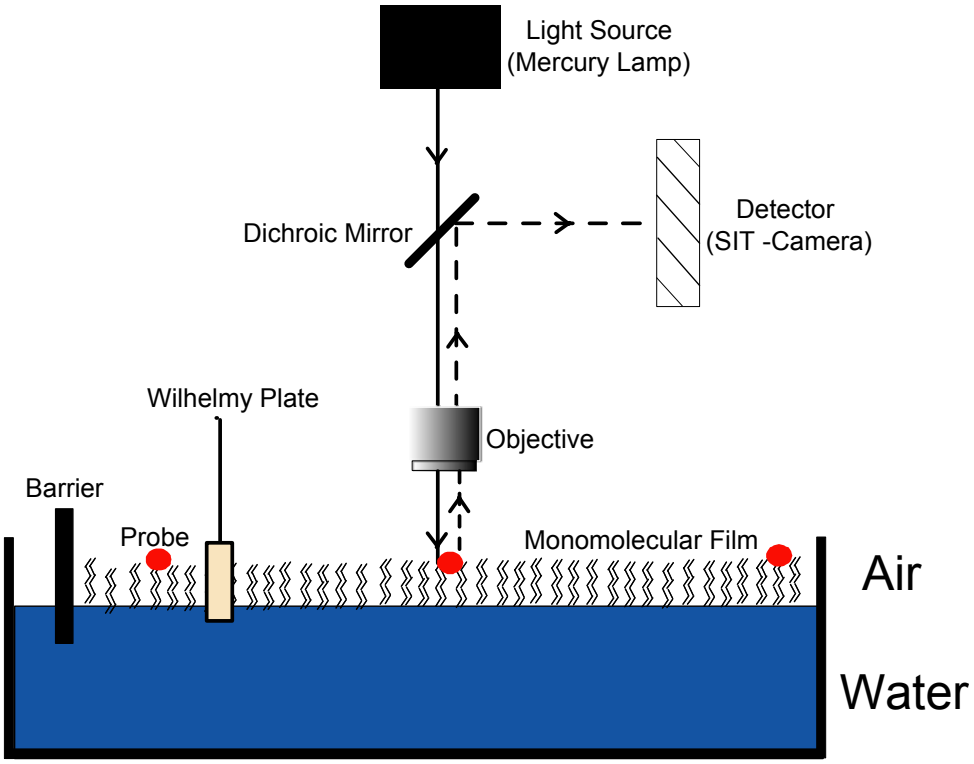

Figure 3-2 *Schematic overview of the fluorescence film balance used. Green light from a mercury lamp is used to excite the fluorescence probes (filled circles) at the air water interface and the emitted light is detected by a SIT camera. The good solubility of the probes in liquid domains allows for the optical contrast between different domains.*

3.1.4 Film Preparation and Langmuir-Blodgett transfer

The mixture of lipid, and when necessary the fluorescence probe (ratio 1000/1), was dissolved in a chloroform/methanol/water (65/25/4 vol%) solution, and spread directly onto the air-water interface. After evaporation of the solvent (30 min.) the film was compressed at a rate of approximately 1 $Å^2$/sec and molecule.

Using the Langmuir-Blodgett-Technique, monolayers of amphiphilic molecules can be transferred onto solid substrates (solid supported membranes) (Gaines 1966). In Figure 3-3 the transfer process is sketched for the case of a hydrophilic substrate. After the monolayer is compressed to a certain pressure, the substrate is slowly lifted while the pressure is kept constant and the transferred area is monitored. The result is a monomolecular film of lipids with their hydrophilic head groups facing the substrate. With the same technique a hydrophobic substrate can be used, resulting in a monolayer with the head groups facing the air. Prior to

transfer, the substrate was cleaned in a solution of hydrogen peroxide and sulfuric acid (piranha) for one hour and rinsed intensively afterwards.

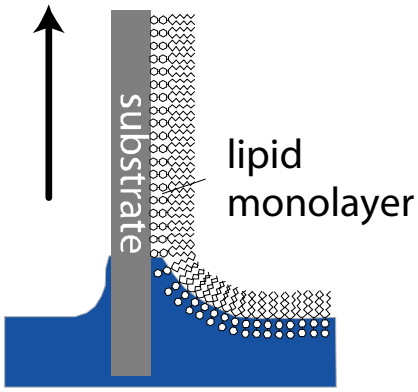

Figure 3-3 The Langmuir-Blodgett technique. After compression the substrate is lifted up at constant pressure. The hydrophilic head groups get physisorbed on the surface.

3.2 Ellipsometry

To study the forces acting perpendicular to the membrane surface the swelling behaviour of transferred glycolipid monolayer is investigated at controlled humidity conditions, using ellipsometry.

Ellipsometry is an optical non-invasive technique suited for the study of the structure and the swelling behavior of soft interfaces. With this technique the change in elliptical polarization of the light reflected from the sample can be measured.

Theory of Ellipsometry

Measuring near the Brewster angle, which is around 70° for our Si/SiO_2/lipid system, leads to the best thickness resolution. With the two ellipsometric parameters, Δ and Ψ, it is possible to determine the layer thickness or refractive index of the deposited film. The obtained measurement is an average over the illuminated area of the substrate (1-2 mm^2). Thus, it is feasible to measure statistical systems such as lipid films. Figure 3-4 shows the measurement principle

of the PCSA ellipsometer (Polarizer-Compensator-Sample-Analyzer) used in this study. A monochromatic, collimated light beam passes a polarizer of well-defined orientation, hits the multi layer structure at an angle Φ, and is reflected at the same angle. Then, the reflected light is detected by a rotating analyzer.

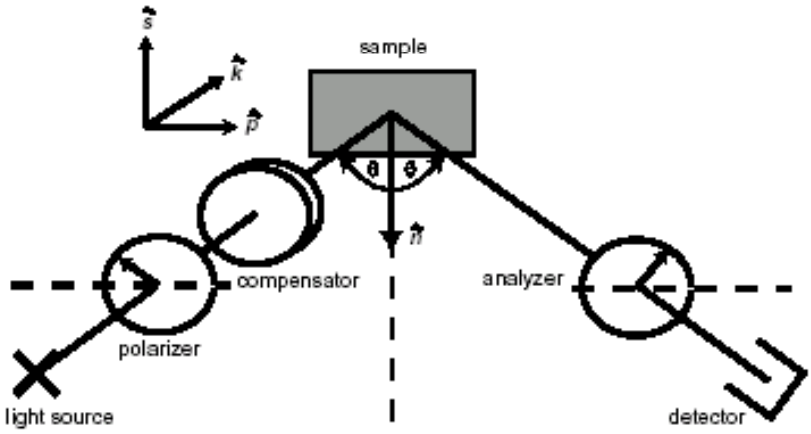

Figure 3-4 Principle of the PCSA ellipsometer

According to the Fresnel reflection equations, the incoming light is reflected at each interface as illustrated in Figure 3-5, depending on the state of polarization, angle of incidence and refractive indices of the layers. With the total Fresnel reflection coefficients R_p and R_s, the fundamental equation of ellipsometry (Eq. 3.7) which expresses the two ellipsometric angles Δ and Ψ in relation to R_p and R_s [Azzam, 1977 #384] , and can be derived:

$$\frac{R_P}{R_S} = \tan\psi \exp(-i\Delta) \qquad \text{Eq. 3.7}$$

The Δ values can vary from 0° to 360° and Ψ from 0° to 90°. From the equation (Eq. 3.7) one can calculate Ψ directly.

$$\tan\Psi = \sqrt{\frac{R_p R_p^*}{R_s R_s^*}} \qquad \text{Eq. 3.8}$$

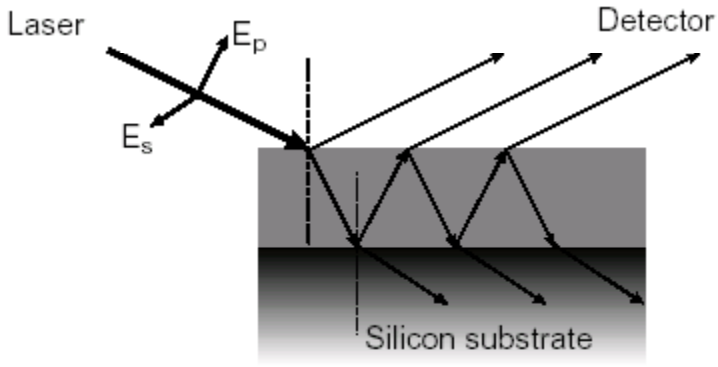

Figure 3-5 Reflection of the laser beam at the interfaces of the multi layer structure. E_p and E_s are the wave vectors parallel and perpendicular to the plane of incidence, which contains the beam and the surface normal.

For the determination of Δ two equations are necessary:

$$\cos\Delta = \frac{\mathrm{Re}\, R_p R_s^*}{\sqrt{R_p R_p^* R_s R_s^*}} \qquad \text{Eq. 3.9}$$

and

$$\sin\Delta = \frac{\mathrm{Im}\, R_p R_s^*}{\sqrt{R_p R_p^* R_s R_s^*}} \qquad \text{Eq. 3.10}$$

Among the two major classes of ellipsometers, the nulling ellipsometer and the photometric ellipsometer, the one with a rotating analyzer (rA) used in this study belongs to the second category. In this setup the intensity of the reflected light is monitored according to the position of the analyzer. The polarity of Δ can be determined by two measurement cycles, one with the $\lambda/4$ - plate as compensator and one without.

The detailed calculation of Δ and Ψ from the measured intensity is computed by a Fourier transformation as described in the literature [Azzam, 1977 #384]. For the bulk silicon, a complex refractive index of n = 3.868 - i0.024 for the wavelength of λ = 632.8 nm was assumed. The thickness and the refractive index of successive layers were fitted from the measured Δ and Ψ values using the ”Fitpaket” program

[Neumaier, 1999 #385].

The Experimental Setup

The experimental setup of the PCSA ellipsometer (Plasmos GmbH Prozeßortechnik, München, Germany) combined with the climate chamber is shown schematically in Figure 3-6. To adjust the angular position, a rotation stage can be moved in x, y direction. With an autocollimator the laser light path is adjusted to sample and detector. The film lift enables the control of the vertical position of the substrate. Three points were measured for each sample (at 8.8 cm, 9.3 cm, 9.8 cm in the readout of the film lift control) to measure mean values for the background data and the initial film thickness.

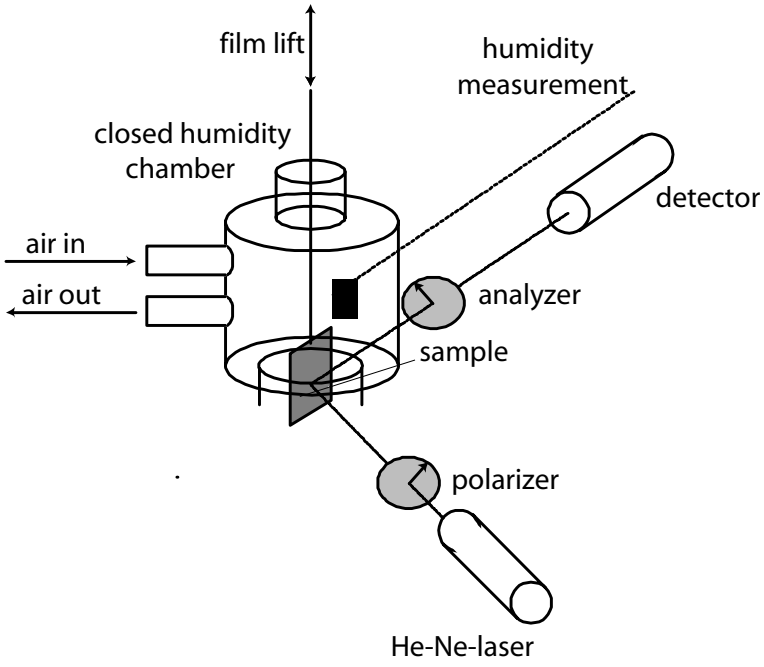

Figure 3-6 Ellipsometer with humidity chamber and film lift.

The conventional method for controling the relative humidity of the atmosphere is to put a salt solution with well defined concentration in a closed chamber. However, this requires up to 24 h to reach the equilibrium state and constant environmental conditions (temperature, humidity and pressure) are essential. Therefore, in this study a constant flow of air was applied. The pressurized air was

filtered and dried through a prefilter and an active carbon filter (Filter system G3XA, Zander, Essen, Germany), saturated with humidity in two water baths, then cooled through a Liebig-cooler to obtain the desired humidity inside the chamber. The relative humidity in the measurement cell was monitored by a digital hygrometer (Type MP100A, Rotronic, Ettlingen, Germany) in the vicinity of the sample. This experimental setup enables the control of the relative humidity from about 5% up to 98% [Elender, 1996 #386].

Static Swelling

Throughout the static swelling experiments, the equilibrium thickness of the lipid was measured about 10 min after the adjustment of the humidity condition in order to ensure thermodynamic equilibrium between the lipid film and the surrounding atmosphere. The refractive index of the swelling polymer was adjusted by applying the Garnet formula [Garnet., 1904 #387] (Eq. 3.11).

$$n_F = n_M \sqrt{1 + \frac{3\Phi}{(\frac{n_0^2 + 2n_M^2}{n_0^2 - n_M^2}) - \Phi}} \qquad \text{Eq. 3.11}$$

n_M and n_0 are the refractive indices for the pure solvent (here: water, n = 1.33) and the solute (lipid) and Φ the volume fraction of the solute (i.e. reciprocal value of the swelling ratio). By starting from n_0, the refractive index corresponding to the initial (dry) thickness d_0 of the polymer, the apparent thickness was calculated. The modified refractive index of the lipid head groups n_F can be estimated by applying Garnet's formula successively until the thickness and refractive index n_F are self-consistent. Absolute values of the disjoining pressure can be given as a function of relative humidity for equal chemical potentials according to van't Hoffs law [Landau, 1987 #388] (Eq. 3.12).

$$p = \frac{-RT}{V} \ln X \approx -1.4 * 10^8 \ln X \left[\frac{N}{m^2}\right] \qquad \text{Eq. 3.12}$$

T represents the temperature and R is the gas constant. V_m is the molar volume of the solvent (water), and X denotes the relative humidity. The change in thickness due to the water uptake can be normalized to the swelling ratio d/d_0. The obtained

equilibrium thickness as a function of relative humidity was analyzed in terms of the disjoining pressure - swelling ratio relationship, i.e. a force-distance curve with the effective force acting perpendicular to the lipid monolayer.

3.3 Interfacial Rheology

In order to study forces in the plane of a two dimensional monolayer an interfacial shear rheometer (ISR) developed in the laboratory of Prof. G.G. Fuller (Stanford University) was used. Rheometric measurements give insight in the side-by-side interactions between molecules restricted to two dimensions. This is in contrast to the out of plane forces measured in a swelling experiment in the last subsection.

3.3.1 Theory of Surface Rheology and measuring principle

In order to learn about the surface rheology of such delicate thin films like glycolipid monolayer it is important to decouple the drag of the probe on the surface from the subphase. The surface sensitivity is expressed as the Boussinesq number

$$B = \frac{SurfaceDrag}{SubphaseDrag} = \frac{\mu_s \frac{v}{l_s} P}{\mu \frac{v}{l} A} \qquad \text{Eq. 3.13}$$

Where μ, μ_s are the subphase and surface viscosity, v is a characteristic velocity, l, l_s are the length scales in which the velocity decays in the subphase and surface and P and A are the contact diameter and area respectively (Brooks, Fuller et al. 1999). Gain sensitivity towards the surface rheology requires B >> 1. The simplest parameter to vary experimentally is the geometry of the probe, hence the ratio P/A. It is minimized for the rotating disc and optimal for edge probes, since for them P/A ~ (edge thickness)$^{-1}$. For the magnetic rod used in our studies (30mm long, 0.450 mm in diameter) B becomes 2.8 mm^{-1} and we conclude that the main contribution of our detected signal results from the viscoelastic properties of the

surface.

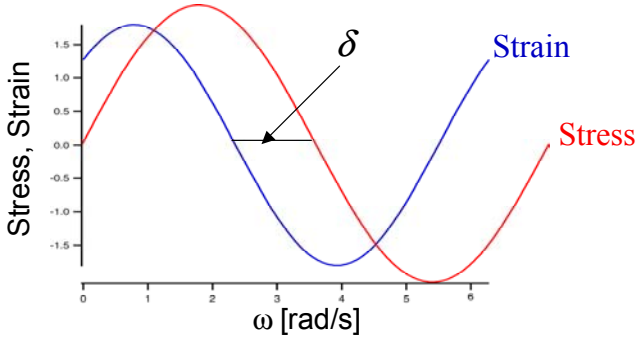

Figure 3-7 Stress, Strain relationship with phase shift r during one oscillation.

Applying a sinusoidal stress σ to a viscoelastic system results in a sinusoidal strain response α with different amplitude α_0 and a certain phase shift δ (Figure 3-7). This signal response can be split up into two components. The one in phase (real part) represents the stored energy (elastic properties) of the system while the one with a $\pi/2$ phase shift (imaginary part) takes the part of the lost energy (viscous properties). To summarize the two contributions into one elastic constant the complex dynamic surface module G^* is introduced

$$G_s^*(\omega) = \frac{\sigma_0}{\alpha_0} e^{i\delta(\omega)} = G_s'(\omega) + iG_s''(\omega). \qquad \text{Eq. 3.14}$$

Here, σ_0 is the stress amplitude, G' the so called storage modulus and G'' the loss modulus. From the phase shift δ, the relationship between G' and G'' can be derived

$$\tan\delta = \frac{G''}{G'} \qquad \text{Eq. 3.15}$$

By necessity G'' becomes 0 for an entirely elastic or hookean system (no phase shift) while $G' = 0$ for a purely vicious or Newtonian system ($\pi/2$ phase shift).

3.3.2 Experimental Setup

A sketch of the experimental setup used to measure two dimensional

viscoelasticity is shown in Figure 3-8 and Figure 3-9. The self-built ISR is coupled to a Langmuir film balance (KSV Instruments, Helsinki). A magnetized rod (length L = 30 mm, diameter ϕ = 450 µm) resides at the air/water interface, and is confined in a narrow channel (channel width W = 2.0 cm). By the nature of the geometry of the channel (Figure 3-9) applied force and displacement are related with the stress and strain amplitude as follows

$$\sigma_0 = \frac{\hat{F}}{2L},\ \alpha_0 = \frac{\hat{x}}{w/2}$$

A sinusoidal magnetic field gradient created by a pair of Helmholz coils was applied to elongate the rod at a certain frequency ω, and the displacement of the rod was monitored by a photodiode array. The translation of the rod causes a

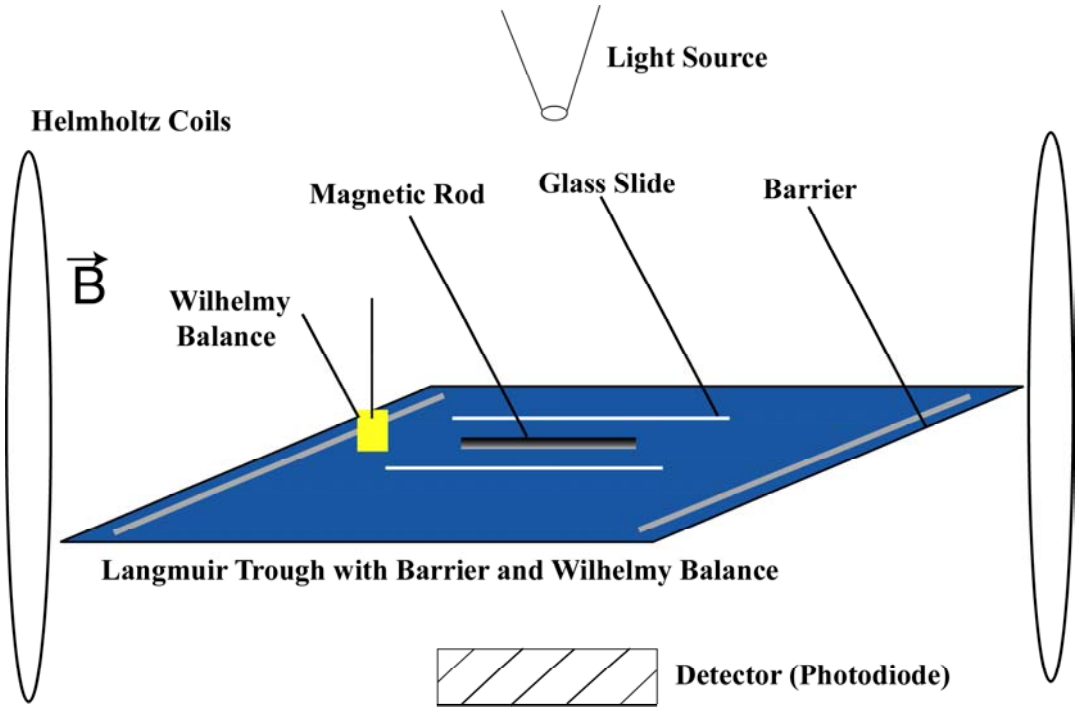

Figure 3-8 Schematic overview of the interfacial stress rheometer (ISR).

simple shear flow to occur at the interface. The measurements were carried out at 20ºC, and the frequency of the oscillation was set constant at 1 rad/s, if not stated otherwise. Lateral pressure or area per molecule respectively, were varied to study the effect of surface concentration on the viscoelasticity of the glycolipid

monolayer.

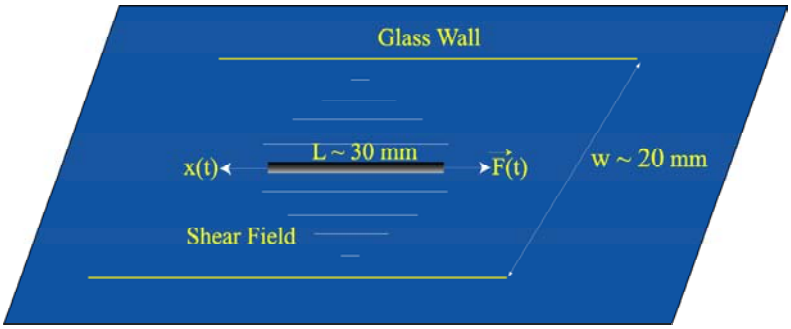

Figure 3-9 Close up of the ISR from the top.

3.4 Differential Scanning Calorimetry (DSC)

To build the bridge between the thermodynamic behavior of glycolipids in two (film balance) and three dimensions calorimetry experiments were performed. The film balance described above was used to study phase transitions in two dimensions and the calorimeter was applied to search for temperature induced phase transitions in lipid vesicles, lamellar stacks of membranes etc.

3.4.1 Theory of Calorimetry

Using calorimetry the heat capacity c_p of a substance or dispersions can be determined. Since phase transitions show remarking behavior in their response functions, calorimetry is suitable for the study of phase transitions in lipid membranes. The heat capacity is defined as

$$c_p = \left.\frac{\partial Q}{\partial T}\right|_p \qquad \text{Eq. 3.16}$$

Where the derivative of the heat of transition Q has to be taken at constant pressure. At constant pressure however

$$\Delta Q = \Delta H \qquad \text{Eq. 3.17}$$

and therefore,

$$c_p = \left.\frac{\partial H}{\partial T}\right|_p \qquad \text{Eq. 3.18}$$

At the melting transition $\Delta G = 0$ and since $\Delta G = \Delta H - T\Delta S$,

$$T_m = \frac{\Delta H}{\Delta S} \qquad \text{Eq. 3.19}$$

i.e. from integrating the heat capacity both the heat as well as the change in entropy accompanied with the phase transition can be calculated, by determine T_m.

Lipid membranes are known to be polymorphic systems dependent on temperature and concentration [Seddon, 1995 #389]. Although all basic thermodynamic quantities can be concluded from the DSC experiment the exact structure of the corresponding phase remains unclear; this is why x-ray scattering experiments are necessary. The relating theory and experimental setup used is explained in subsection 3.5.

3.4.2 Experimental Setup

In Figure 3-10 a schematic drawing of the DSC used (VP-DSC, Microcal, USA) is shown. An electronical circuit equals the temperature of both Tantal cells (sample (1) and reference (2)) by controlling the heating (or cooling) rate. A crystal sensor (3) measures the temperature difference between the two cells. Accordingly, the PC (5) switchess power to the heating coils (4) to account for temperature differences.

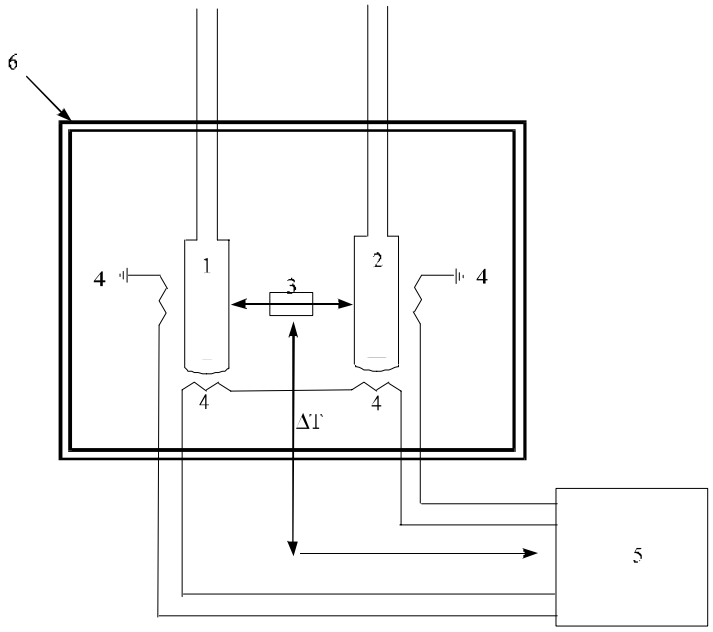

Figure 3-10 Schematic drawing of the DSC. Explanation in text.

The power difference multiplied by the time interval equals the heat ΔQ of Eq. 3.20. Therefore, the heat capacity for a certain time interval can be calculated by

$$c_P(T_i) = \frac{\Delta Q}{\Delta T} = \frac{\frac{1}{2}(\Delta P_i + \Delta P_{i-1})(t_i - t_{i-1})}{T_i - T_{i-1}} \qquad \text{Eq. 3.20}$$

3.5 X-Ray Scattering

X-ray scattering is one of the most powerful techniques used to determine the periodic structure of liquid crystals in the range of a few angstroms. The small angle region identifies the symmetry and long range order of the phase, whereas the wide angles give information on the molecular packing, or short range order of the phase. The changes in lattice spacing and symmetry which take place during phase transition, can therefore be resolved and combined to the thermodynamical properties acquired by DSC.

3.5.1 Physical Principles of X-Ray Scattering

According to Hyugens the outgoing wave scattered at some obstacle can be described by a wave of spherical shape. Assuming a plane wave coming in (Figure 3-11)

$$\vec{E}(\vec{r}) = \vec{A}_0 e^{-i(\vec{q}_0\vec{r}-\omega t)}$$

a fraction *f* gets scattered and gives the amplitude at the point $\vec{R}_0$ at a distance $\vec{R}$ from the scattering center

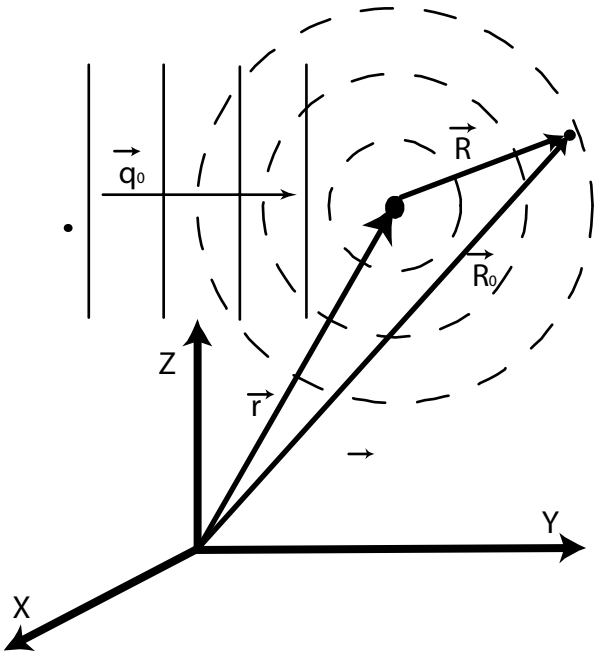

Figure 3-11 *Huygens principle. The planar and coherent incident wave $\vec{q}_0$ is scattered at $\vec{r}$. This results in an outgoing spherical wave.*

$$\vec{A}(R_0) = f\frac{\vec{E}(r)}{R}e^{i\vec{q}\vec{R}} = f\frac{\vec{A}_0}{R}e^{i\vec{q}\vec{R}_0}e^{i(\vec{q}-\vec{q}_0)\vec{r}}e^{-i\omega t}$$

Considering a lattice with *N* scattering centers the total amplitude becomes

$$A(q) = C\sum_{n=1}^{N} f_n e^{i\Delta\vec{q}\vec{r}_n} .$$

Where $C = \frac{A_0}{R}e^{i(\vec{q}\vec{R}_0-\omega t)}$ and $\Delta\vec{q} = \vec{q}_0 - \vec{q}$ is the difference between the incoming and

outgoing wave vector. If the scattering center consist of *i* units (atoms, molecules etc.) and every atom scatters a fraction f_i, then

$$A(q) = C\sum_i f_i e^{i\Delta\vec{q}\vec{r}_i} \sum_n e^{i\Delta\vec{q}\vec{r}_n} = C(F)(SF).$$

The form factor (F) resulting from the sum over *i* depends on the conformation and scattering properties of the atoms (or molecules) inside the unit cell. However, the structure factor (SF) resulting from the sum over all scattering centers n, represents the symmetry (Bravais-Lattice) of the liquid crystal. Since the measured intensity in a scattering experiment is the square of the total amplitude the information about the phase gets lost.

$$I(q) \propto |A(q)|^2 = |F(q)|^2 |SF|^2$$

In mathematical terms SF is the Fourier transformation of the real lattice with its Bragg-Peaks being the lattice point of the reciprocal lattice (h,k,l). From this peaks the distance between neighboring planes can be calculated using

$$d_{hkl} = \frac{2\pi}{|q_{hkl}|} = \frac{2\pi}{\sqrt{(ha^*)^2 + (kb^*)^2 + (lc^*)^2}}.$$

Where a^*, b^*, c^* are the vectors spanning the reciprocal lattice. This represents the fact that the reciprocal lattice vectors are perpendicular with respect to their planes in real lattice. From the form factor F the electron density profile can be calculated by inverse Fourier transformation. Going from the sum to the integral representation

$$F = \int \rho(z) e^{-i\vec{q}\vec{x}} dV$$

With $\rho(z)$ being the electron density at the point *x* in the volume dV. The Fourier transformation gives

$$\rho(z) = \int_V F(q)\cos(qz)dV \approx \sum_{h=1}^{h\max} \pm F_h \cos\left(\frac{2\pi hz}{d}\right) \qquad \text{Eq. 3.21}$$

h represents the order of the reflection, F_h the respective form factor and d the

lamellar spacing. Here centrosymmetry of the crystal was assumed, as found in stacks of lamellar bilayers. As a consequence, the unknown phases are either 0° (+) or 180° (-). From all the possible phase shift combinations the most likely is picked to reconstruct the electron density profile.

3.5.2 Experimental Setup

Figure 3-12 shows a schematic drawing of the setup used. Wheresa the resolution of the SAXS data is around 4 – 10 nm which therefore resolves the lattice spacing, the WAXS data are suited for the investigation of in plane correlation in the range of a few nm down to 1 Å. The suspensions with the concentration of 20 wt% water were filled into quartz capillaries (Hilgenberg, Malsfeld, Germany). The experiments were performed at three different beamlines. SAXS data were measured at the synchrotron beamline ID2A of European Synchrotron Radiation Facility (ESRF, Grenoble), with a resolution better than $\Delta q = 0.0015$ Å^{-1}. WAXS data were taken at the beamline D43 of Laboratoire pour l'Utilisation du Rayonnement Electromagnétique (LURE, Paris). In this case the resolution was $\Delta q = 0.0055$ Å^{-1}. Furthermore SAXS and WAXS experiments were done at the beamline A2 (HASY-Lab) at DESY (Deutsches Elektronen Synchrotron) in Hamburg. In all cases, SAXS and WAXS, the observation of isotropic Debye-Scherrer rings indicated that all the samples consisted of perfect powders. The radial integration of the two dimensional data recorded using the local CCD camera at ID2A, was carried out by the standard routines of ESRF. At LURE, data was collected using Fuji image plates in combination with homemade data processing software on the basis of Igor PRO (Wave Metrics Inc., USA).

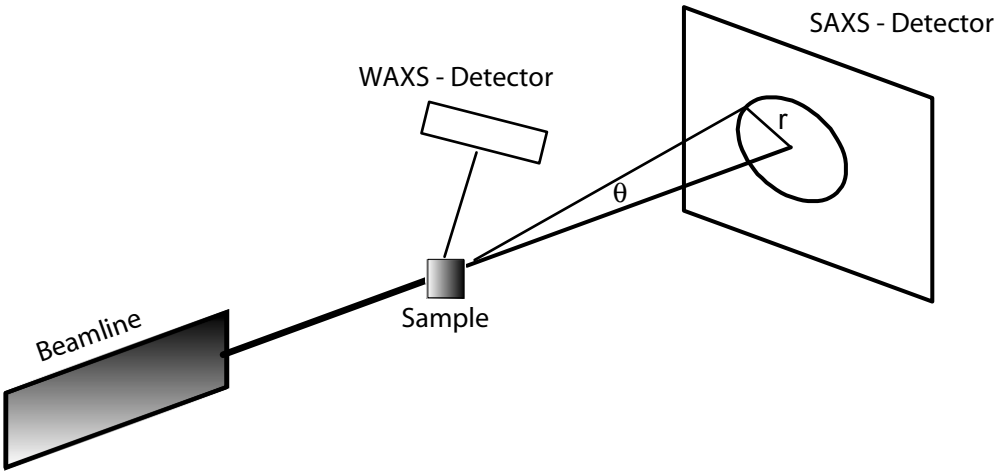

Figure 3-12 The scattered wave of a monochromatic, coherent incident wave, appears under an angle Θ at the detector.

3.6 Chemicals and Chemical Structures

Unless otherwise specified, all lipids (including labelled) were dissolved in a chloroform/ethanol/water (65/25/4) solution (called "magic"). All lipids used were synthesized by C. Gege in the laboratories of Prof. R. R. Schmidt at the Universität Konstanz, Germany. Glycolipids with both linear and branched head groups were used. The samples with linear head group were named Lac N, corresponding to the number of lactose units, N = 0, 1, 2, and 3 (Figure 3-13). Details of the synthesis have been reported elsewhere (Schneider, Mathe et al. 2001).

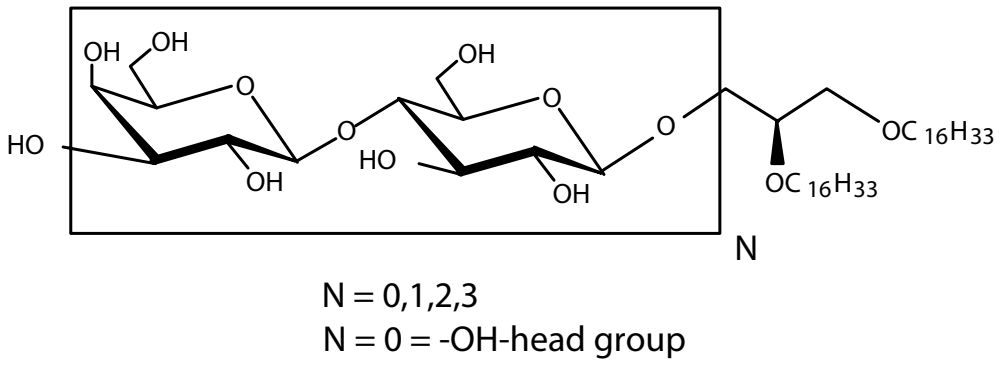

Figure 3-13 Chemical structure of the synthetic glycolipids with oligolactose head groups, Lac N (N=1-3).

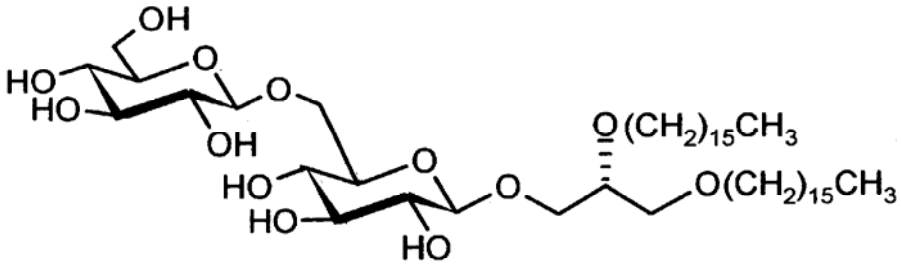

Figure 3-14 Chemical structure of the synthetic glycolipid with the disaccharide head group gentiobiose.

The branched (bent) glycolipids studied all have the same hydrophobic tails and glycerol junction however, the head group were either the disaccharide gentiobiose and the trisaccharide Lewis X (plus lactose spacer) as shown in

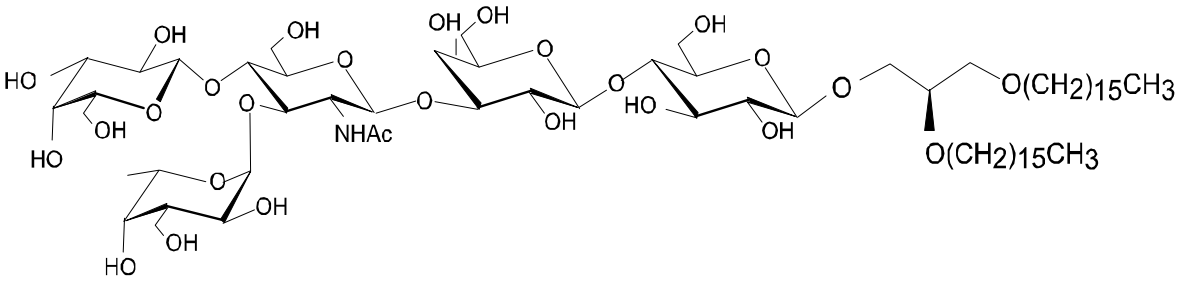

Figure 3-15 Chemical structure of the synthetic glycolipid with the Lewis X head group and lactose spacer.

Figure 3-14 and Figure 3-15.

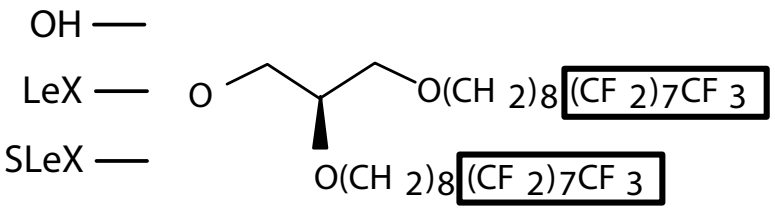

Figure 3-16 Chemical structure of the per fluorinated lipid with the three different head groups used in this study.

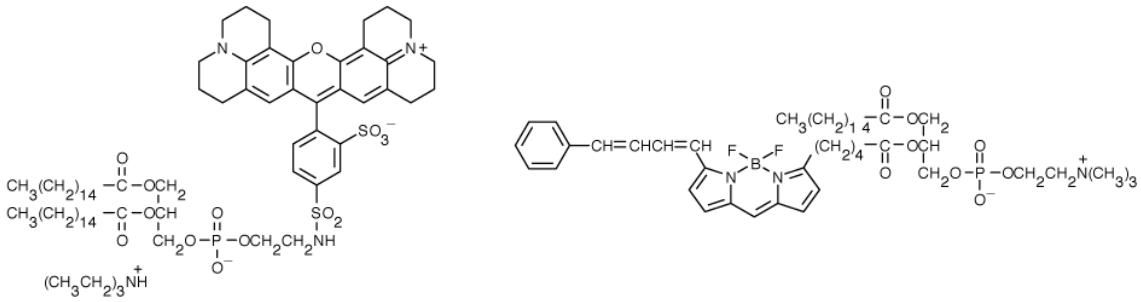

Figure 3-17 Chemical structure of the fluorescence probes used. (Left) T-Red. (Right) Bodipy.

4 Results and Discussion

In the following subsections the results for a variety of glycolipids are presented and discussed. The complete set of complementary experiments gives a good phenomenological explanation for the enormous differences in viscoelasticity, thermodynamics and structure found for these glycolipid membranes in two and three dimensions.

In the last subsection novel compounds of fluorinated lipids are presented. The appearance of modulated phases is discussed, in terms of dipolar forces according to the theoretical work by D. Andelman (Andelman, Brochard et al. 1987), and their unique properties for the design of artificial lipid microdomains are discussed.

4.1 Glycolipids with Linear Head group Conformation (Lac1-3)

4.1.1 Pressure Area Isotherms

For each glycolipid (the number of lactose units, N = 1, 2, 3), the pressure-area isotherms were measured at several different temperature conditions between 283 K and 308 K. In order to eliminate hysteresis effects, the isotherms were monitored during expansion as well as during compression.

The Langmuir isotherms of the *Lac 1* lipid are shown in Figure 4-1. At $T \leq 298$ K, the isotherms exhibited no liquid expanded phase, and were dominated by the condensation of the dihexadecyl chains from a gas phase to a liquid condensed

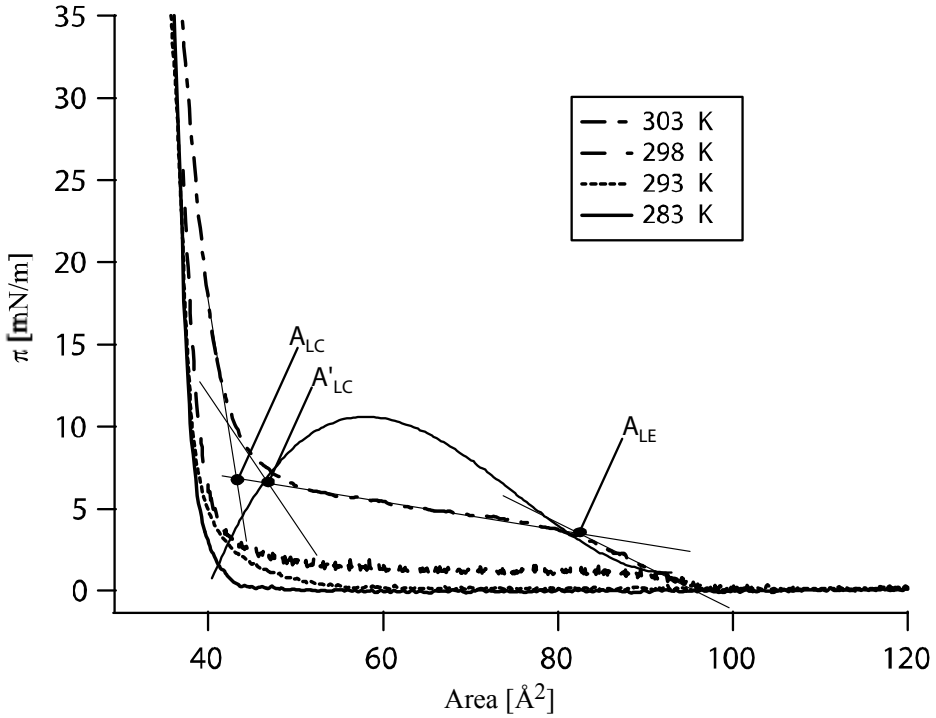

Figure 4-1 *Langmuir isotherms of the Lac 1 monolayer at different temperatures. The liquid-expanded (LE), liquid-condensed (LC) coexistence line was fitted by a polynomial of 4th order. The linear extrapolated lines were taken to define onset and endpoint of the phase transition A_{LE}, A_{LC}. To estimate the deviation in area several points were taken (A_{LC}, $A_{LC''}$).*

phase. Such behaviour can be explained by the stiffness of the short, fully hydrated, and stretched “rod-like” lactose moieties. At T = 303 K, an onset of a plateau-like regime was observed, corresponding to a first order phase transition from the liquid expanded to the liquid condensed state. Further rise in temperature led to an increase in the transition pressure and a decrease in the coexistence region. Such a systematic tendency coincides with the approach to a critical, or as will be explained later rather tricritical point, which is well known from the previous studies on ordinary phospholipids monolayers (Albrecht, Gruler et al. 1978; Möhwald 1995).

As presented in Figure 4-2 a and b, qualitatively similar isotherms were observed for the monolayers of *Lac 2* and *Lac 3*. In accordance with the increase in lactose units, a systematic increase in the transition pressure, p_K, and a clear decrease in the phase transition temperature was observed (Figure 4-2 a and b). The obtained results suggest that the steric interactions between neighbouring lipid molecules were dominated by the strong repulsion between the head groups. However, the qualitative shape of the coexistence region was still dominated by the lateral packing density of the alkyl chains, and not by the “polymer-like” effects of the head groups. A similar tendency was observed in the previous study for the monolayers of PEG-lipids with shorter chains (Mathe, Gege et al. 2000).

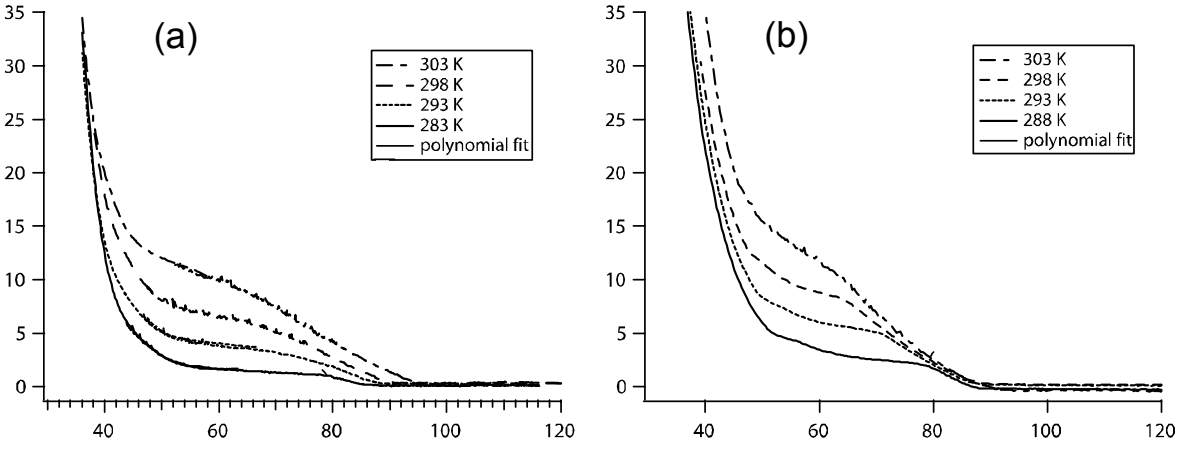

Figure 4-2 Langmuir isotherms of a, Lac 2 and b, Lac 3 monolayers at different temperatures. Onset and endpoint of the phase transition area was defined as in Figure 4-1.

It should be noted, that the slope of the isotherms in the coexistence region

increases respectively with the increase in the size of the lactose head groups. Such a slope in the Langmuir isotherms can be generally explained by the stabilization of domains due to; i) small amounts of impurities (≥ 0.2 mol %) (Pallas and Pethica 1985; Miller and Mohwald 1987), ii) 'intermediate' states of the alkyl chains (Mouritsen 1983), or iii) the strong interaction between the head groups (Scott 1975). The first two approaches are based on non-equilibrium effects, which do not follow the Gibbs phase rule, however, the third interpretation explains this slope by the continuous compression of the head groups. By applying the Clausius-Clapeyron equation

$$\frac{dp_K}{dT} = \frac{\Delta s}{(A_{LE} - A_{LC})} = \frac{\Delta q}{T(A_{LE} - A_{LC})} \qquad \text{Eq. 4.1}$$

thermodynamic quantities such as the molar latent heat, q, or the molar transition entropy, $s = q/T$, can be derived from the variation of the transition pressure with

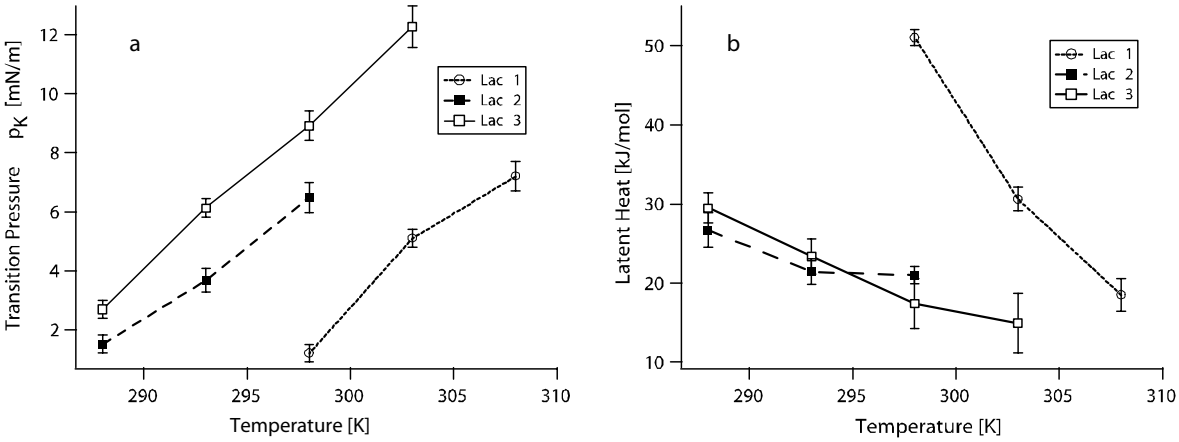

Figure 4-3 *(a) Transition pressure* p_k *and (b) molar latent heat* q *of the phase transition plotted as a function of temperature* T *for Lac 1 (open circle), Lac 2 (closed square), and Lac 3 (open square).*

absolute temperature, dp_k/dT. Figure 4-3b shows the temperature dependence of the latent heat, q, whose error bars are mainly due difficulties in defining the onset and the end point of the transition, A_{LE} - A_{LC}. Latent heat is inversely correlated to lactose moiety length this can be explained by the lower degree of cooperativity due to the larger head groups.

The increase in p_K as well as the decrease in A_{LE} - A_{LC} can be explained by the

approach towards a tricritical point (Albrecht, Gruler et al. 1978) where the first order phase transition between the liquid expanded and liquid condensed phase transforms into a second order phase transition of phases with different orientation. This can be understood within the framework of the Landau-De Gennes theory with a symmetrical Landau free energy of the form (Landau and Lifschitz 1987)

$$\Phi - \Phi_0 = \frac{1}{2} A\eta^2 + \frac{1}{4} C\eta^4 + \frac{1}{6} E\eta^6 . \qquad \text{Eq. 4.2}$$

Where A, C, E are function of temperature and pressure and basically free to choose, while the order parameter η is determined from the equilibrium conditions of the system (minimization of Φ). Since this is a system of two order parameters (orientation and density) coupled by the fact that the volume of a lipid stays constant during inclination, multicritical points are possible. It turns out that the coefficient C can change its sign as a function of temperature and area per molecule. At $C = 0$ the critical behaviour abruptly changes from first to second order, hence a tricritical point. As for the fluid-gas transition in the van der Waals gas model, in the close vicinity of the tricritical point, the coexistence line can be represented by a parabola whose vertex coincides with the (tri-) critical point. In this regime, A_{LE} - A_{LC} in the Clausius-Clapeyron equation disappears and both the transition entropy and the latent heat become zero (Möhwald 1995). The critical temperature T_C can be calculated by

$$\frac{A - A_C}{A_C} = 2\left(\frac{T_C - T}{T_C}\right)^{1/2} . \qquad \text{Eq. 4.3}$$

Where A_C is the middle point between A_{LE} and A_{LC} (Goldenfeld 1992). From the approximately linear relation of Δq *vs.* T_k (Figure 4-3b) another estimation of the (tri-) critical temperature, T_C can be performed ($\Delta q = 0$) and the two T_C *'s* can be compared to each other. The results are in good agreement and finally give a (tri-) critical pressure of p_C = 9 - 16 mN/m and a (tri-) critical temperature of T_c = 313 - 316 K, respectively, which are comparable to those of phospholipids with dihexadecyl chains. Since the lateral pressure expected in lipid vesicles is above

25 mN/m, these bilayers would not be expected to be in any critical state. It should be mentioned that the coupling of order parameters does not necessarily require a tricritical point, because a critical endpoint can exist instead. Since it is not possible to distinguish between these two phenomena with the technics applied, mainly due to the fact that the film loses it's stability at higher temperatures, the prefix tri- is put in brackets.

4.1.2 Swelling Behaviour of glycolipid monolayer

4.1.2.1 Theoretical Concepts

The measured swelling curves were analyzed by applying two different physical concepts; (i) the scaling theory by Alexander and de Gennes [De Gennes, 1976 #393] (Alexander 1977)[De Gennes, 1980 #395][Daoud, 1977 #396] and (ii) the mean field approach (also called self consistent field SCF) by Milner [Milner, 1988 #391] [Milner, 1988 #391]. Although our experimental systems do not fulfil a symmetrically planar situation with the polymers confined between two parallel plates, all the equations discussed in the following chapter were applicable to the experimental data by multiplying all theoretical expressions by a factor of unity.

Scaling Theory

A general expression for the free energy *F* of grafted polymers on the surface is given by de Gennes, Alexander, and Daoud [De Gennes, 1976 #393; De Gennes, 1980 #395][Daoud, 1977 #396; Alexander, 1977 #394]

$$F \approx kTN\left(\frac{a}{D}\right)^{5/3} - \delta\left(\frac{Na}{D}\right) + \delta\left(\frac{Na^3}{\sigma D}\right)^{5/4} + kT\left(\frac{D}{a}\right)^2\left(\frac{\xi}{a}\right)^{-1/3} N^{-1} + kT\ln\sigma . \qquad \text{Eq. 4.4}$$

N is the number of monomer segments with length *a*, and *D* is the thickness of the polymer layer. δ represents the surface adsorption energy per monomer in units of *kT*, while σ and ξ are the mean area per polymer and the blob diameter, respectively [De Gennes, 1980 #395]. The first term describes the energy necessary to confine a polymer molecule, behaving as an ideal chain inside a blob. The second term stands for the adsorption energy of a chain on the surface, while the third term represents the repulsion between overlapped polymer chains.

The fourth term describes the so-called “brush” regime and the last term represents the translational entropy of the polymers, which can be neglected by assuming that the alkyl chains are immobilized on the surface.

In the case of higher grafting density where the grafting distance is less than the Flory radius, $d_p < R_F$, the polymer chain takes a “brush” conformation with the blob diameter of ξ. The equilibrium thickness D_{brush}^{st} can be described as $D_{brush}^{st} \approx aNd_p^{-2/3}$. The interaction potential of the polymer V_{brush}^{st} is given by

$$V_{brush} \approx \frac{kT}{d_p^3} D_{brush}^{st} \left[\frac{4}{5} \left(\frac{D_{brush}^{st}}{D} \right)^{5/4} + \frac{4}{7} \left(\frac{D}{D_{brush}^{st}} \right)^{7/4} \right] \quad \text{Eq. 4.5}$$

yielding the resulting pressure of

$$P_{brush}^{st} \approx \frac{kT}{d_p^3} \left[\left(\frac{D_{brush}^{st}}{D} \right)^{9/4} - \left(\frac{D}{D_{brush}^{st}} \right)^{3/4} \right]. \quad \text{Eq. 4.6}$$

Mean Field Theory

The mean field approach of Milner et al. [Milner, 1988 #391; Milner, 1988 #392] is based on the terminally fixed linear chains exhibiting a high grafting density. In contrast to the scaling approach, the quality of the solvent is not so crucial in this treatment. When the film is compressed from the equilibrium thickness D_{brush}^{scf} the interaction energy per unit area can be described as

$$V_{brush}^{scf} \approx -\left(\frac{\pi^2}{12} \right) N(\sigma w)^{2/3} \left[\frac{D_{brush}^{scf}}{2D} + \frac{1}{2} \left(\frac{D}{D_{brush}^{scf}} \right)^2 - \frac{1}{10} \left(\frac{D}{D_{brush}^{scf}} \right)^5 \right] \quad \text{Eq. 4.7}$$

and the resulting interfacial pressure is given by

$$P_{brush}^{scf} \approx \left(\frac{\pi^2}{12} \right) N(\sigma w)^{2/3} \frac{1}{D_{brush}^{scf}} \left[-\frac{1}{2} \left(\frac{D_{brush}^{scf}}{D} \right)^2 + \frac{D}{D_{brush}^{scf}} - \frac{1}{2} \left(\frac{D}{D_{brush}^{scf}} \right)^4 \right] \quad \text{Eq. 4.8}$$

$\sigma = d_p^{-2}$ is the grafting density, and *w* stands for the "excluded volume".

4.1.2.2 Results

The glycolipid monolayers were transferred onto the substrate at *T* = 293 K and at a lateral pressure of p = 25 mN/m. The grafting densities were 37 Å^2 (*Lac 1*), 37 Å^2 (*Lac 2*) and 40 Å^2 (*Lac 3*), respectively. In this regime, the glycolipids are in the liquid condensed phase, where the alkyl chains orient nearly perpendicular to the surface. The relative humidity was varied between 30 % and 98 %, corresponding to a change of the disjoining pressure (cf. 4.1.2.1) between 1.69 x 10^8 and 2.83 x 10^6 Pa. In Figure 4-4 a - c, the disjoining pressure is plotted versus the absolute thickness of the swollen lactose layer. In each plot, both the experimental data (open squares) and the two theoretical fits are presented based on the scaling approach and the mean field model. To expose a possible power law dependence between the disjoining pressure and thickness, all results are presented as *log-log* plots. The swelling behaviour of *Lac 1* could hardly be interpreted as "brushes" neither by the scaling approach nor by mean field theory, even though the swelling ratio of ~ 2.0 in the low-pressure regime (~ 10^7 Pa) is still in a plausible range as is known from the corresponding ratios of dextran (~ 2.0) and hyaluronic acid (~ 2.7) (Mathe, Albersdorfer et al. 1999). This observation suggests that the very short head groups behave like "rigid-rods" but not like "polymer chains", similar to what has been observed for the PEG-lipid monolayers with shorter chains (Mathe, Gege et al. 2000). This is also in good agreement with the Langmuir isotherms of *Lac 1*, showing the qualitatively similar characteristics to phospholipid monolayers. At high disjoining pressures from 2 x 10^8 to 7 x 10^7 Pa a power law $p \propto (d/d_0)^n$ was fitted to the disjoining pressure curves, yielding an exponent of $n \approx -9$ (Figure 4-5). In this high disjoining pressure regime, typical intermolecular distances, *r*, are comparable to the Bohr radius (~ 0.5 Å), and the swelling is expected to be mainly dominated by short-range repulsive interactions caused by the overlapping of molecular orbitals. The hard core repulsion of the Lennard-Jones potential scales as r^{-12}. This exponent corresponds to a scaling law of $p \propto (d/d_0)^{-9}$ [Israelachvili, 1992 #390], that agrees with the power law obtained from our experiments. Similar

power law dependencies in the high disjoining pressure regime could be also

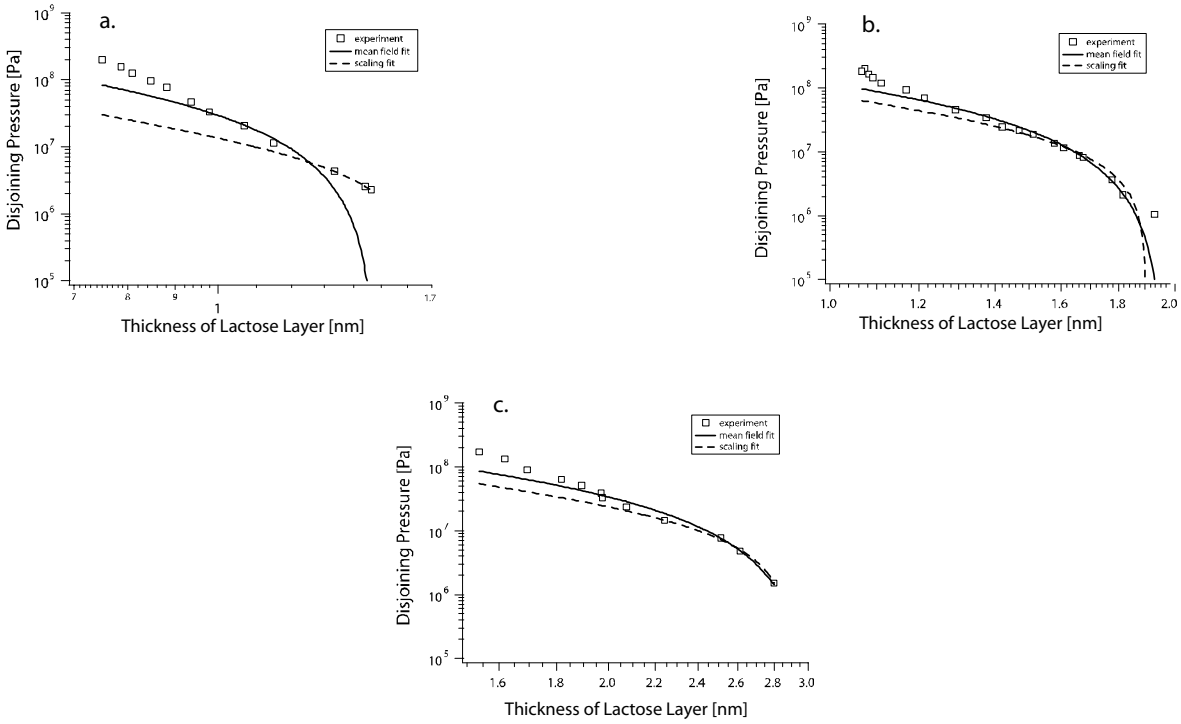

Figure 4-4 *Absolute disjoining pressure versus thickness of the lactose layers: (a),* Lac 1*; (b),* Lac 2*; and (c),* Lac 3*. The measured values (open circles) were compared with the theoretical predictions based on the self-consistent-field approach (solid lines) and the scaling theory (broken lines). The swelling behavior of Lac* 2 *and* Lac 3 *could be well explained by both of the "brush" models.*

observed for *Lac 2* and *Lac 3*.

In Figure 4-4 b and c, the swelling behaviours of *Lac 2* and *Lac* 3 were compared with theoretical predictions for "polymer brushes" based on the scaling approach and the mean field theory. Both of the "brush" models fit very well to the measured disjoining pressure curves. We were not able to fit these curves by the "mushroom" model (not shown), where lower surface coverage is assumed, which is in agreement with the conditions of our preparations (i.e. high transfer pressure, relatively short head groups). In addition, it should be noted that the thickness of the lactose layers (≤ 3 nm) still remains far away from the basic statistical condition, N » 1. These results also showed a good agreement with results for PEG-lipids with longer chains (Mathe, Gege et al. 2000).

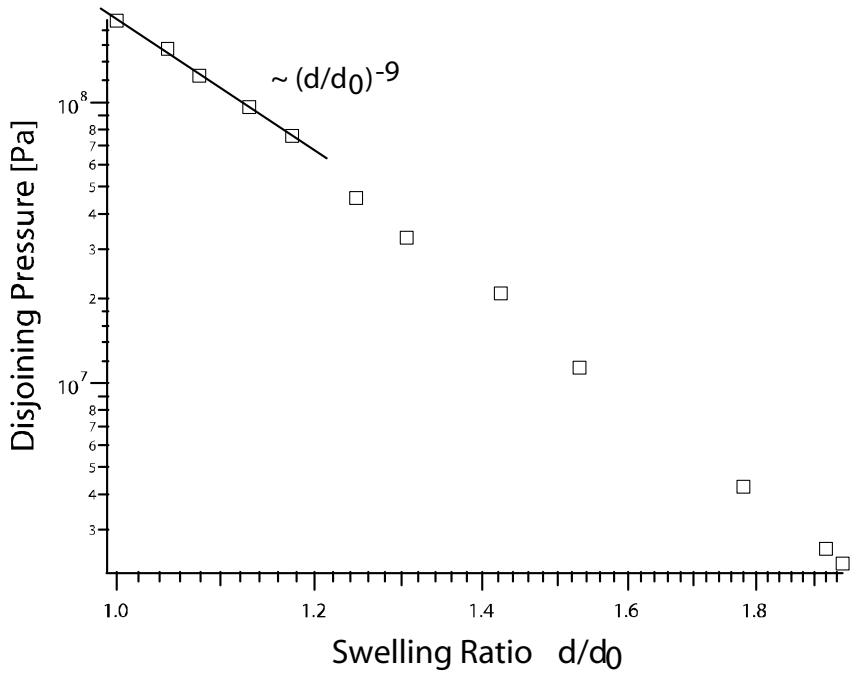

Figure 4-5 *Absolute disjoining pressure as a function of relative swelling ratio of* Lac 1, d/d_0, *normalized to the thickness of "dry" layer. At high disjoining pressures from 2 x* 10^8 *to 7 x* 10^7 *Pa, a power law* $p \sim (d/d_0)^n$ *was fitted to the disjoining pressure curves, yielding an exponent of* $n \approx -9$.

The difference between the swelling behaviour of *Lac 1* and that of *Lac 2* and *Lac 3* can be explained in the same way as the influence of the head groups on the phase transition of the glycolipid monolayers. Actually, the Langmuir isotherms of *Lac 1* were dominated by the condensation of the alkyl chains at $T \leq 298$ K (Figure 4-1). In accordance with the increase in the lactose units, the head groups gained conformational entropy. The steric interaction between the neighbouring lipids is strongly influenced by the repulsion between the head groups. Thus, the swelling curves can be well explained by the "brush like" behaviour of the lactose groups.

4.1.3 Rheology at the Air/Water Interface (Schneider, Lim et al. 2002)

To reveal insight on the forces acting in the monolayer plane rather then perpendicular to it (cf. previous chapter), viscoelasticity measurements on glycolipid monolayers were performed and are reported in the present chapter.

To ensure that all experiments were done in the linear viscoelastic regime, an amplitude sweep was performed prior to every experiment. The amplitudes found ranged between 20 and 100 μm. If not otherwise specified the frequency was set to 1 rad/s (approx. 0.16 Hz). Figure 4-6 presents the storage modulus *G'* and the loss modulus *G''* of the Lac 1 monolayer, plotted as a function of area per molecule. Even at a large area per molecule, the monolayer was already quite viscoelastic. Both the storage and loss moduli of the monolayer showed a sharp increase when compressed from the liquid expanded to the liquid condensed phase. The increase in surface viscosity across the phase transition of the alkyl chains was also found in previous studies

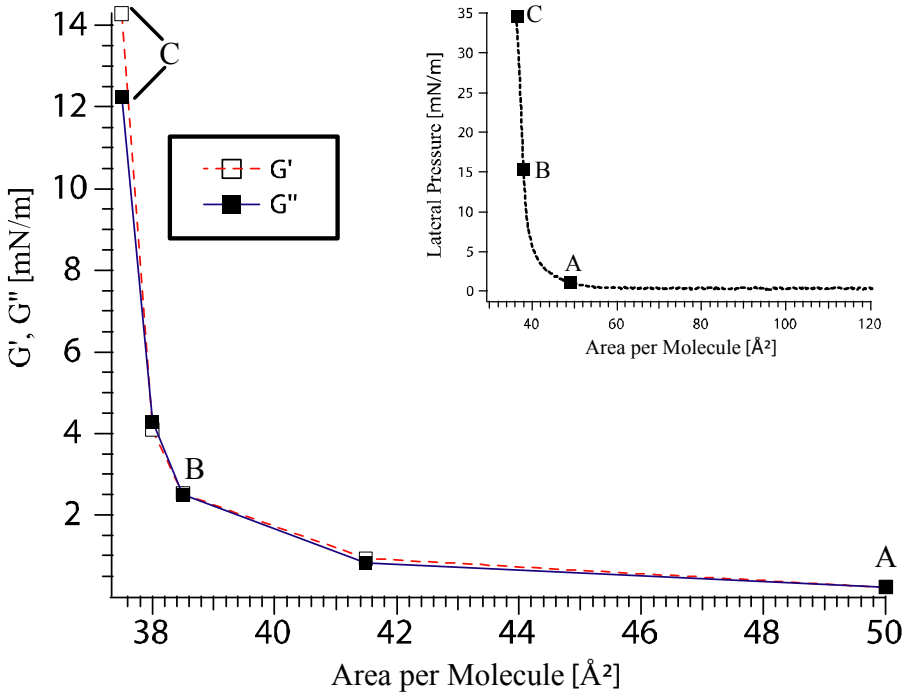

Figure 4-6 *The storage modulus G' and the loss modulus G'' of the Lac 1 monolayer, measured at T = 20°C. The oscillation frequency was set constant, ω = 1 rad/s. The Langmuir compression isotherm of the monolayer was given in inset, and the correspondence between the dynamic moduli and the isotherm is indicated.*

of phospholipid monolayers (Kraegel, Kretzschmar et al. 1996; Naumann, Brooks et al. 1999). This observation can be attributed to strong chain-chain interactions that arise from film condensation, and dominate the in-plane correlation. The surface storage and loss moduli of the Lac 2 monolayer are plotted versus area per molecule in Figure 4-7. Similar to the results obtained for the Lac 1 monolayer, G'' was larger than G' over a wide range of surface pressures. Nevertheless, both G' and G'' values were remarkably smaller, by almost an order of magnitude, in comparison to those of the Lac 1 monolayer, suggesting that the film is rather fluid. This can be interpreted qualitatively in terms of the hydrophilic/hydrophobic balance between the head group and the alkyl chains. When this balance is shifted towards greater hydrophilicity, the cooperativity between the alkyl chains is reduced (cf. chapter 4.1) and the head groups are more hydrated, resulting in a rather fluid-like film. This can also be concluded from the linear behaviour of G'' in Figure 4-9, where the loss moduli of Lac2 (square symbols) and Lac3 (triangular symbols) are plotted as a function of frequency. This fluid like character was observed over a wide range of surface pressures. It should be noted that the "fluidization" observed here is not due to the relaxation of the lateral packing, because the area per molecule of the Lac N in the liquid condensed phase (π = 25 mN/m) is almost independent of the number of lactose units, A = 37 ~ 40 Å^2 (Schneider, Mathe et al. 2001). In fact, recent NMR studies and molecular dynamic simulation have also shown that a linear tetrasaccharide resembling the Lac 2 head group (lacto-N-neotetraose) takes a uniaxial, cylindrical conformation in dilute liquid crystalline media such as phospholipid dispersions (Rundlöf, Landersjö et al. 1998; Landersjö, Höög et al. 2000) and therefore does not significantly affect the lateral packing of the hydrophobic chains. Furthermore, the dynamic moduli of the Lac 0 (dihexadecylglycerol without saccharide head groups) monolayer were too large to obtain any quantitative data, since strong correlations between saturated alkyl chains are dominant. These results suggest a continuous reduction in the chain-chain correlation with increases in the number of saccharide units.

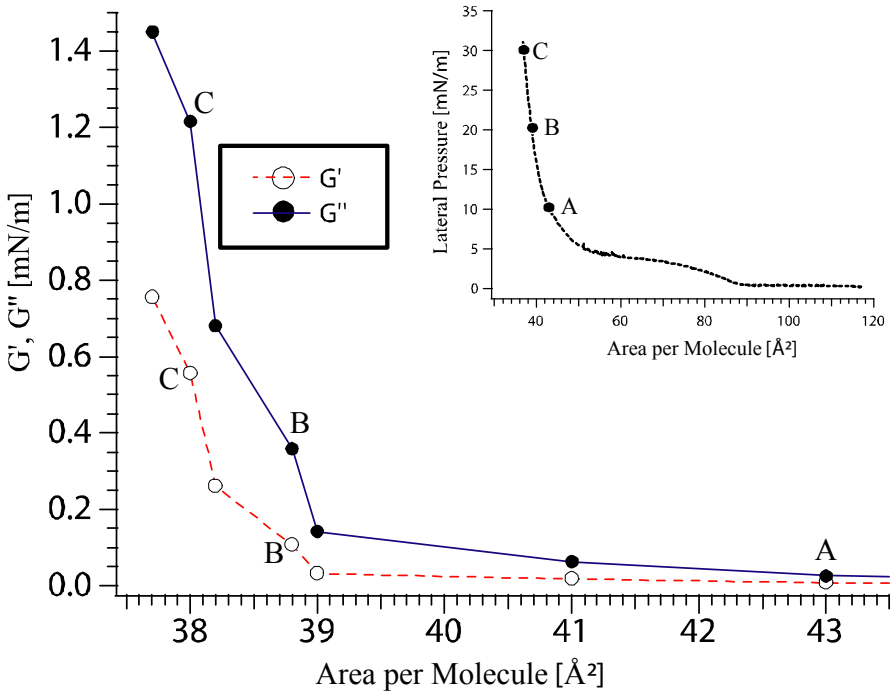

Figure 4-7 The dynamic moduli of the Lac 2 monolayer, measured at the same conditions as in Fig. 2 (T = 20°C, ω = 1 rad/s). Both G' and G'' are smaller by almost an order of magnitude than those of the Lac 1 monolayer.

In comparison to the other examined monolayers, the viscoelastic properties of the Lac 3 monolayer were strikingly different. As presented in Figure 4-8, the monolayer became elastic at surface areas below 50 Å^2, where the storage modulus *G'* became larger than the loss modulus *G''*. This molecular area corresponds to the surface pressure of around 6 ~ 8 mN/m in the Langmuir isotherm (inset of Figure 4-8). The Lac 3 monolayer was viscous (*G'' > G'*) when the surface pressure was less than this transition pressure (Figure 4-10). Above this transition pressure, however, the elastic contribution became dominant (*G' > G''*). Such a crossover point where *G' = G''* is referred to as a rheological transition point. If one considers the short (the stretched length of Lac 3 head group is still less than 4 nm) and cylindrical head group of Lac 3, this transition can obviously not be caused by a physical entanglement of the oligosaccharide head groups, which would be in contradiction to the swelling behaviour studied in chapter 4.1, but rather by the formation of a physical network of hydrogen bonds. Interestingly, the surface pressure at which the rheological transition of the Lac 3

monolayer takes place (π = 6 ~ 8 mN/m) corresponds to the end point of the coexistence of the liquid expanded and the liquid condensed phase (inset of Figure 4-8). As described in chapter 4.1, compared to the isotherm of the Lac 2 monolayer (inset of Figure 4-7), the slope of the isotherm in the coexistence region is apparently larger, indicating a decrease in the effective interaction between alkyl chains. When the Lac 3 monolayer is compressed to the liquid condensed phase (e.g. at π = 10 mN/m), the elastic contribution becomes dominant (G' > G''). In fact, as seen in Figure 4-9 the measured G'' values are almost independent of the oscillation frequency at π = 25 mN/m. In this regime, the hydrating water is excluded and hydrogen bonding "bridges" the Lac 3 head groups during lateral compression to higher pressures. The coupling between thermodynamic (alkyl chain density) and rheological (head group cross-linking) transition is illustrated in Figure 4-11. As the condensation of the hydrophobic chains takes place the water is partially released from the interface, which enables the formation of a hydrogen network with predominantly elastic properties. This is in contrast to the monolayers of Lac 1 and Lac 2, where the phase transition to the liquid condensed phase results in a significant increase in the film viscosity.

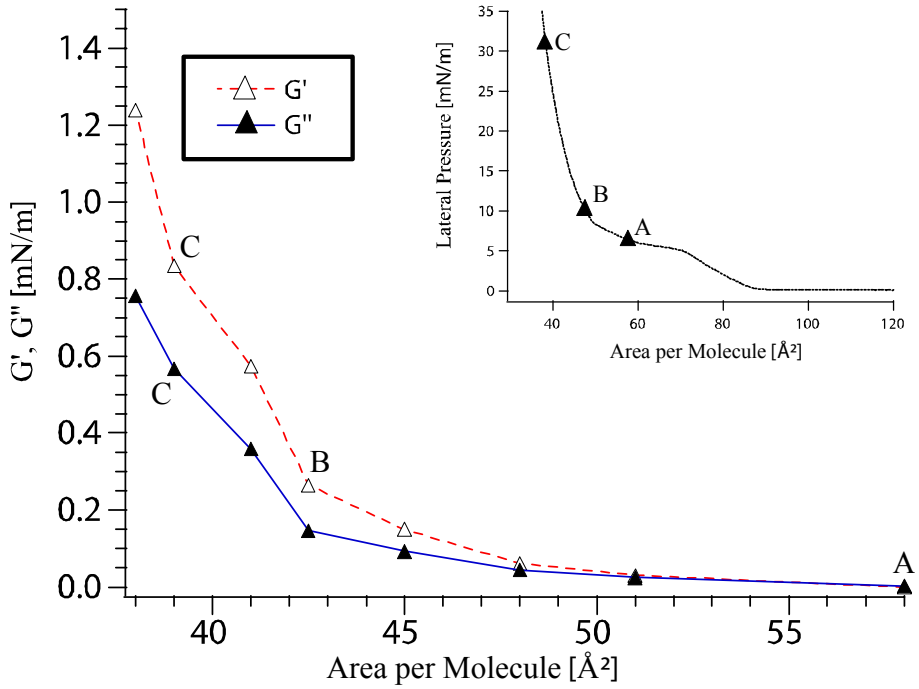

Figure 4-8 The dynamic moduli of the Lac 3 monolayer. The measurement conditions were the same as in the previous figures (T = 20°C, ω = 1 rad/s). The monolayer became elastic (G' > G'') at surface areas below 50 Å^2.

Thus, it can be concluded that the rheological transition of the Lac 3 monolayer is not caused by the correlation between the condensed alkyl chains, but by the strong coupling between the linear hexasaccharide (Lac 3) head groups. These results are in good agreement with our recent X-ray scattering experiments on Lac N lipid dispersions, demonstrating that the strong correlation between Lac 3 head groups actually prohibits the endothermic transition of the alkyl chains, which will be discussed in the following subsections in detail (Schneider, Zantl et al. 2002). Such strong carbohydrate-carbohydrate attractions between linear oligo- and polysaccharides have also been reported for other glycolipids with cellooligosaccharides (Hato and Minamikawa 1996; Tamada, Minamikawa et al. 1996) and cellulose (Brandrup and Immergut 1975; Hato and Minamikawa 1996; Tamada, Minamikawa et al. 1996).

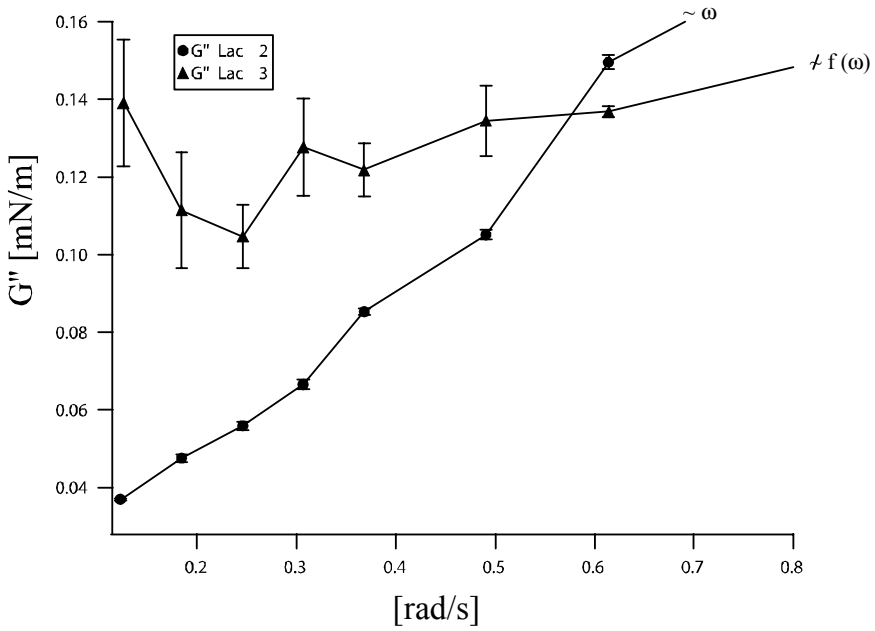

Figure 4-9 The loss modulus G'' of Lac 2 (square symbols) and that of Lac 3 (triangular symbols) at π = 25 mN/m, plotted as a function of oscillation frequency.

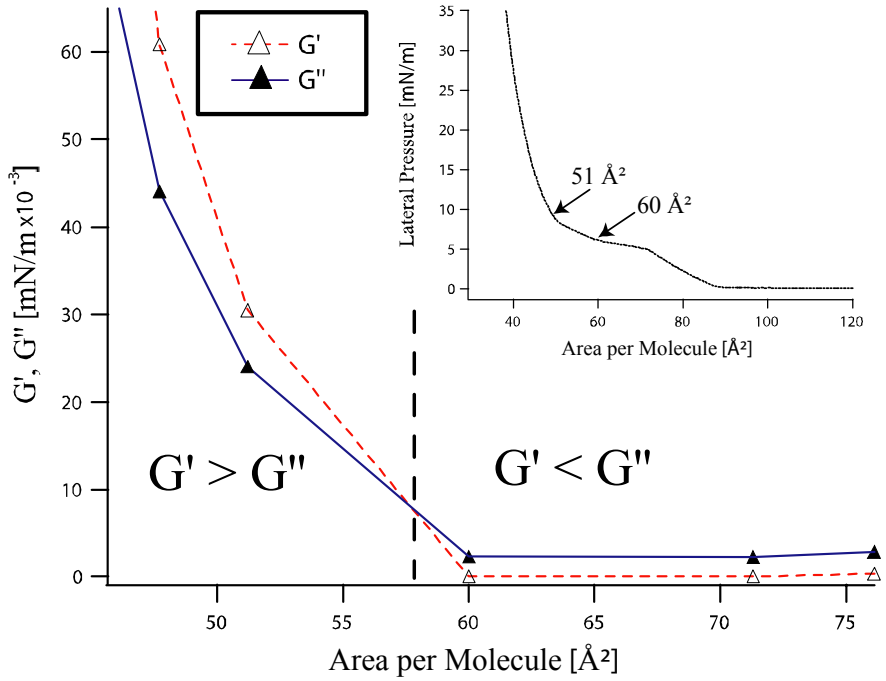

Figure 4-10 *The dynamic moduli of the Lac 3 monolayer. The measurement conditions were the same as in the previous figures (T = 20°C, ω = 1 rad/s). The monolayer became elastic (G' > G'') at surface areas below 51 Å².*

Upon compression, the viscoelasticity of glycolipids with the shorter head groups (Lac 1 and Lac 2) exhibited a continuous increase through the condensation of alkyl chains. Even the Lac 3 monolayer, where a clear rheological transition was observed, revealed a continuous change in the dynamic moduli when the film was compressed. This is in contrast to the studies by Naumann et al. (Naumann, Brooks et al. 1999) who found a discontinuous change in the dynamic moduli related to a "high-pressure rheological transition", i.e. a crossing between G' and G'' at high surface pressures π. A recent study of Ahrens et al. (Ahrens, Bækmark et al. 2000) demonstrated that this "high pressure transition" resulted in the formation of hydrophilic/hydrophobic nano-stripes with weakly ordered alkyl chains and polymer head groups. Considering the longer, flexible head groups of PEG-lipids (N = 44, 112), the rheological transition of lipopolymer monolayers seems to follow a different mechanism (e.g. the in-plane interaction between these nano-domains). In addition, the viscoelasticity of PEG 3, 6 and 9 lipopolymers (Appendix) show a continuous decrease in G' and G'' with increasing length. This clearly suggests the use of glycolipids as they were studied here rather than

lipopolymers for future studies on artificial glycocalyx models as used for example in adhesion studies.

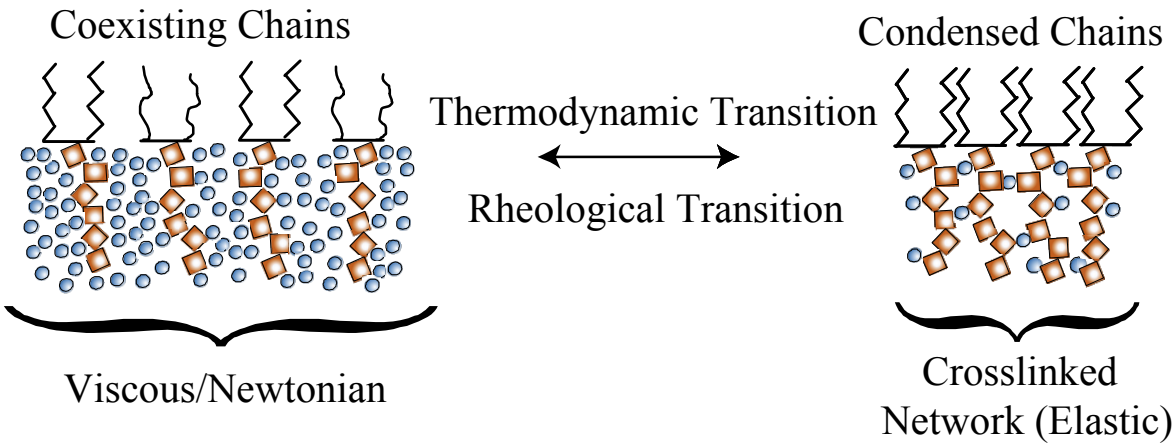

Figure 4-11 *Illustration of the coupling between thermodynamical and rheological transition. The phase transition related condensation of the chains, helps to squeeze out the water between neighbouring head groups and therefore facilitates the formation of a physical network of hydrogen bonds with a higher elastic modulus.*

4.1.4 Calorimetry and X-Ray Scattering on Glycolipid Dispersions

To study the morphology and corresponding phase behaviour of glycolipid membranes in the lamellar phase a systematic combination of differential scanning calorimetry (DSC) and small- and wide angle X-ray scattering experiments (SAXS and WAXS) was performed.

All the measured DSC data (transition temperature and enthalpy) and the diffraction peaks obtained by SAXS and WAXS experiments are summarized in Table 1, and the details are described for each lipid in the following sub-sections.

Lac1

The heat capacity trace of Lac 1 is given in Figure 4-12 (upper graph), exhibiting a

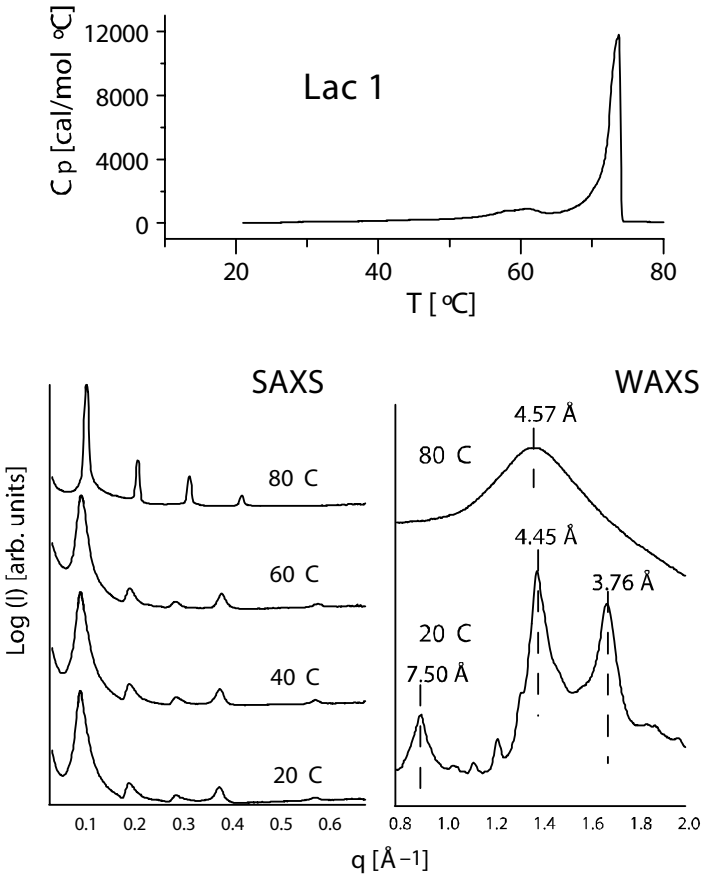

Figure 4-12 (Upper) Differential heat capacity scan of the Lac 1 dispersion (1 mg/mL) recorded at the heating rate of 20 °C/h, exhibiting a sharp transition at T_t *= 74 ˚C and the phase transition enthalpy of* ΔH *= 30 kcal/mol. (Lower) Powder-averaged small angle X-ray scattering (SAXS) data of the lamellar dispersion of Lac 1 at T = 20, 40, 60, and 80 °C). The lamellar spacing showed a transition between 60 °C (*d_{SAXS} *= 68 Å) and 80 °C (*d_{SAXS} *= 60 Å). Wide angle X-ray scattering (WAXS) data suggested the transition between the crystalline* L_C *phase and the fluid* $L\alpha$ *phase (lower right).*

sharp transition at T_t = 74 ˚C and a phase transition enthalpy of ΔH = 30 kcal/mol. A distinct and broad pre-transition peak was also observed at around T = 60 ˚C. The powder-averaged small angle X-ray scattering data at T = 20, 40, 60, and 80 ˚C are summarized in Figure 4-12 (lower graph), indicating periodic 3D lamellar structures. Across the main transition at T_t = 74 ˚C, the periodicity of the low angle spacing was changed from 68 Å (below) to 60 Å (above), suggesting the “melting” of the dihexadecyl chains. As shown in Figure 4-12 (lower graph), the wide angle patterns at $T < T_t$ (T = 20 ˚C) can be characterized with three pronounced

scatterings at 3.76, 4.45, and 7.50 Å. The scattering peak at 4.45 Å corresponds to the alkyl chains in the lamellar crystalline (L_C) phase with a triclinic packing mode (Larrson 1988). On the other hand, the peaks at 7.50 and 3.76 Å can be interpreted as the first- and the second order peaks due to the strong correlation between dehydrated head groups (Seddon, Cevc et al. 1984; Caffrey 1987; Hinz, Kuttenreich et al. 1991; Köberl, Hinz et al. 1998). At T > T_t (T = 80 ˚C), a broad band at about 4.57 Å could be observed, suggesting the fluid Lα phase of the alkyl chains. Furthermore, the scattering peaks from the head group correlation disappeared because the lactose groups were hydrated. Thus it has been demonstrated that the Lac 1 lamellar has a transition between the crystalline L_C phase and the fluid Lα phase. However the corresponding phase transition temperature of 74°C is apparently higher than that of other lipids with dihexadecyl chains, such as DPPC (T_m = 41.4 ºC) and the obtained transition enthalpy (ΔH = 30 kcal/mol) is larger in comparison to the sum of transition enthalpies of DPPC from L_C phase to L_α phase (i.e., L_C . $L_{ß'}$. $P_{ß'}$. L_α), ΔH = 15 kcal/mol (Cevc 1993), respectively. Alkyl chains of Lac 1 are strongly correlated by the very strong van der Waals interaction, which even enable them to form crystalline-like tight packing with almost no tilting. The additional enthalpic contribution may be due to the hydrogen bonding between the Lac 1 head groups that are free from dipoles, in contrast to phospholipids with P–N dipoles (Cevc 1993). Nevertheless, further structural characterizations are necessary to understand the small satellite peaks observed in the L_C phase, which indicate in-plane correlations.

Table 1		*The measured phase transition temperatures (T_t, T_p), phase transition enthalpy (ΔH) as determined by DSC, and the low- and wide-angle spacing (d_{SAXS}, d_{WAXS}) with their identified phases for Lac 1 -3 are summarized.*			
			Lac 1	Lac 2	Lac 3
DSC		T_t / T_p [°C]	74 / 60	50 / 40	--*
		ΔH[kcal/mol]	30	9.2	--
Phase	L_c, $L_{c'}$	d_{SAXS} [Å]	68	--	108
		d_{WAXS} [Å]	3.76, 4.45, 7.50#	--	4.19, 4.46, 7.61#
	$L_{\beta'}$	d_{SAXS} [Å]	--	87	--
		d_{WAXS} [Å]	--	4.17	--
	L_α	d_{SAXS} [Å]	60	78	--
		d_{WAXS} [Å]	4.57	4.45	--

* no phase transition was observed until T=80°.

The diffraction peak corresponds to the head group correlation.

Lac 2

Figure 4-13 (upper graph) shows the DSC scan of Lac 2. In comparison to that of Lac 1, the main transition peak was broadened and the T_t was reduced to T_t = 50 °C. The phase transition enthalpy was also clearly reduced to *D*H = 9.2 kcal/mol. A broad enthalpic peak was still observed at around T_p = 40 °C, does not however correspond to any changes in lamellar spacing or chain packing. The small angle X-ray scattering data at T = 20, 40, 60, and 80 °C (Figure 4-13, lower graph) showed periodic lamellar structures. Across T_t = 50 ºC, the low angle spacing was changed from 87 Å at T < T_t to 78 Å at T > T_t, respectively. The reproducibility of the SAXS data was checked by the measurement of a different sample at LURE. Here, the wide angle patterns at T < T_t (T = 20 °C) can be characterized with only

one sharp scattering peak at 4.17 Å, which corresponds to the gel ($L_ß$) phase. The absence of a pronounced shoulder denotes that the alkyl chains have nearly no tilt (Hinz, Kuttenreich et al. 1991; Köberl, Hinz et al. 1998). No correlation between the lactose head groups could be seen, indicating that the head groups are already hydrated in this phase. At T > T_t (T = 80 °C), a broad band at about 4.45 Å could be observed, which is consistent with the fluid L_α phase without any head group correlation. The number of the equi-distanced peaks in the small angle scattering were smaller at T > T_t.

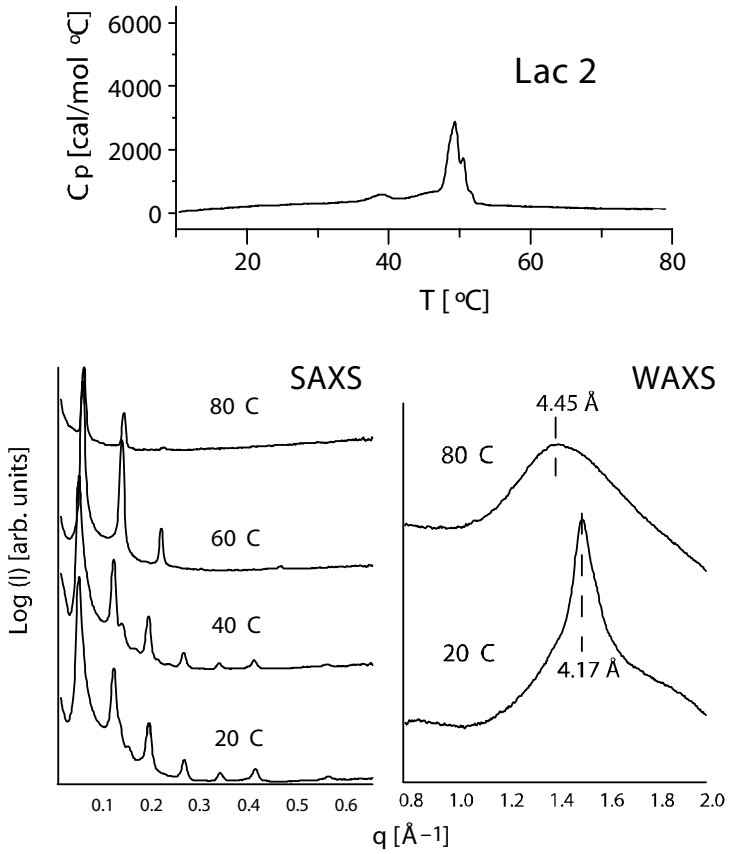

Figure 4-13 *(Upper) Heat capacity trace of the Lac 2 dispersion (1 mg/mL), showing a broadened transition peak at T_t = 50 ˚C and a distinct pre-transition at around T = 40 ˚C. The phase transition enthalpy was also clearly reduced to ΔH = 9.2 kcal/mol. (Lower) SAXS diffraction patterns of the lamellar dispersion of Lac 2 at T = 20, 40, 60, and 80 ºC (left). The lamellar spacing showed a transition between 40 ºC (d_{SAXS} = 87 Å) and 60 ºC (d_{SAXS} = 78 Å). WAXS peaks suggested the transition between the gel phase and the fluid phase.*

Here can be concluded that the Lac 2 lamellar has a transition between the gel

phase and the fluid L_α phase caused by a shift of the hydrophobic/hydrophilic balance between the head groups and the alkyl chains. This shift towards the hydrophilic side reduces the cooperativity between the alkyl chains, resulting in the decrease in the transition temperature and the phase transition enthalpy. The strongly crystallized alkyl chain packing modulates to the gel phase, which allows for the hydration of the head groups.

The change in the Gibbs free energy between the two phases can be expressed as

$$\Delta G = \Delta H - T\Delta S . \qquad \text{Eq. 4.9}$$

At the phase transition temperature T_t, DG = 0 and therefore

$$\Delta S = \Delta H / T_t . \qquad \text{Eq. 4.10}$$

The transition enthalpy and temperature could be measured experimentally; the entropy can be calculated by Eq. 4.10. This leads to a change in phase transition entropy:

$$\Delta(\Delta S) = \Delta S_{Lac2} - \Delta S_{Lac1} = -59 kcal / molK \qquad \text{Eq. 4.11}$$

The decrease in transition entropy from Lac 1 to Lac 2 agrees well with the morphology suggested by X-ray diffraction. Below the phase transition temperature, Lac 1 is in the highly ordered crystalline L_C phase, while Lac 2 takes the gel ($L_ß$) phase due to the hydration of the head groups. Thus, the higher degree of order in the crystalline phase can be related directly to the difference in the phase transition entropy.

Lac3

In contrast to Lac 1 and Lac 2, the phase behaviour was significantly changed when the number of lactose units was increased to N = 3. The DSC traces (upper graph Figure 4-14) showed much less remarkable peaks until T = 80 ºC, which is close to the highest operating temperature for aqueous dispersion. The SAXS data (lower graph Figure 4-14) exhibited more than 10 equi-distanced peaks, suggesting a highly ordered lamellar structure, which remained constant at 108 Å

between 20 ºC and 80 ºC. For the sample with a concentration of 50 wt%, the SAXS data measured at LURE confirmed the reproducibility. The wide angle scattering patterns (lower graph Figure 4-14) suggested no transition, exhibiting three sharp scattering peaks at 4.19, 4.46, and 7.61 Å. These results clearly indicate that the Lac 3 lamellar has no chain melting. The sharp peak at 7.61 Å can be attributed to the strong head group correlation between the dehydrated head groups. Judging from the peaks at 4.19 and 4.46 Å, dihexadecyl chains of Lac 3 take a highly packed crystalline-like phase with a slight tilt or defects. Moreover, it is also confirmed that the very weak enthalpic peaks around 25 ºC and 55 ºC do not induce any morphological transition.

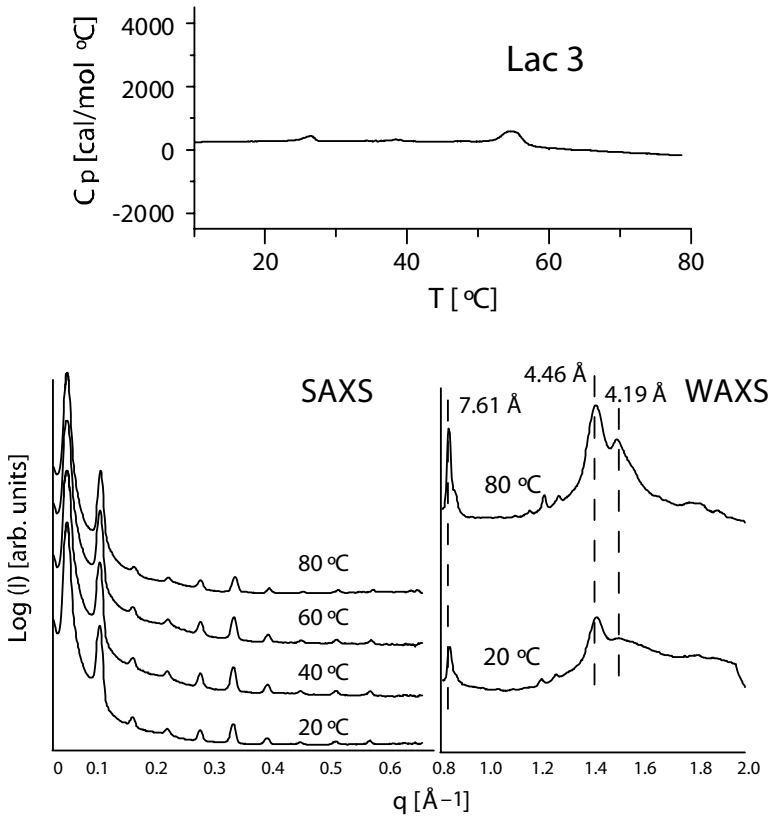

Figure 4-14 *(Upper) DSC trace of the Lac 3 dispersion (1 mg/mL), showing no evidential endothermic peaks. (Lower) SAXS diffraction patterns of the Lac 3 lamellar dispersion at T = 20, 40, 60, and 80 ºC (lower left). The lamellar spacing showed no transition at all measurement conditions,* d_{SAXS} *= 108 Å. WAXS peaks suggested that the Lac 3 lamellar takes crystalline-like phase and no chain melting takes place.*

The very strong correlation between the hexasaccharide head groups obviously forced the alkyl chain to take the tight, crystalline-like packing, which is different from the ideal hexagonal lattice. Since the attractive interaction between the head groups is strong, hydration can no longer take place.

"Hydrophobic" appearance of linear oligo- and polysaccharides has been well known for cellooligosaccharides and cellulose. For example, Sano et al. reported that cellooligosaccharides are mono-molecularly soluble in water when the monosaccharide unit number was N = 1 ~ 4, whereas they can only be dissolved in an aggregate state when N = 5 (Sano, Sasaki et al. 1991). Hato et al. reported a similar phase for a lipid with two dodecanoyl chains and cellooligosaccharides with N = 5, to which they gave the name "hydrated crystal" (Hato and Minamikawa 1996). But, the interpretation of this phase behaviour remained difficult. Indeed, cellulose is insoluble in most solvents as well as in water (Brandrup and Immergut 1975). It has recently been shown, that the water uptake ability of the highly ordered cellulose films is obviously poorer (Rehfeldt) compared to that of dextran films (Mathe, Albersdorfer et al. 1999). We tentatively understand this Lc' phase of Lac 3 in terms of a "frozen" bilayer, which can appear either at very low temperature conditions or at very high surface pressures (Lipowsky 1991; Sackmann 1996). The WAXS peak positions can be related to the chain tilting, in-plane defects, or the buckling induced by the strong head group correlation.

Electron density Profiles of Some Representative Phases

Structural analyses of several representative phases were attempted by reconstruction of the electron density profiles (Harper, Mannock et al. 2001). The measured SAXS data were fitted with Gaussians after subtraction of background scattering. A Lorentz correction was applied by multiplying each peak intensity (peak area) with its corresponding wave vector q (Warren 1969). Finally, the square root of the corrected peak intensity was used to determine the constant form factor F of each respective reflection. The electron density profile relative to the constant electron density profile of water was calculated by the Fourier synthesis according to Eq. 3.21. For centrosymmetric crystals such as lamellar stacks of lipid bilayers, the electron density can be presented as a Fourier series

of cosines, therefore, the unknown phases are either 0 º (+) or 180 º (–). In the following consideration, the origin was set to the center of the methyl dip of the hydrophobic chains by fixing the phase of the first order reflection to "–". All peak-fittings and further calculations were carried out with the software package Origin 5.0 (Microcal Software, Northampton, U.S.A.).

Firstly, the SAXS data of Lac 1 at 80 °C and Lac 2 at 60 °C (L_α phase) were analyzed. Each, four strong reflections h = 1, 2, 3, 4 of Lac 1 and h = 1, 2, 3, 6 of Lac 2 were considered for the Fourier synthesis. Out of the possible 2^4 = 16 combinations, we chose 8 combinations that were centred in the middle of the bilayers "– – – –, – – – +, – – + –, – – + +, – + – –, – + – +, – + + –, – + + +", corresponding to the terminal methyl dip (–). The most plausible phasing "– – + –" shows a good similarity in the hydrocarbon chains region to the very well studied L_α phase of dipalmitoylphosphatidylethanolamine (DPPE) (Pabst, Rappolt et al. 2000), and displays the appropriate head group size: about 10 Å for Lac 1 and 20 Å for Lac 2, respectively. All the remaining combinations lead to inappropriate structural features, such as too large hydrocarbon core, missing methyl dip, or too small head group size. By assuming that the maximum of each electron density profile in Figure 4-15 (left) displays the midpoint of head groups, thickness of the alkyl chains d_{al} can be estimated to be 15 - 17 Å, for both Lac 1 and Lac 2. This is in good agreement with the corresponding value reported for DPPE of 15.4 Å at 74 °C. From the obtained d_{al} value, the thickness of the water layer between two bilayers was calculated to be 6 - 8 Å. SAXS diffraction pattern of the crystalline-like phase of Lac 3 (at 20 °C) displays 10 diffraction orders (Figure 4-15 right), which results in 2^9 = 512

Table 2 Summary of the Fourier coefficients F_h, which have been used to determine the electron density maps of Figure 4-15.

h	F_h (Lac 1 at 80°C)	F_h (Lac 2 at 60°C)	F_h (Lac 1 at 20°C)	F_h (Lac 3 at 20°C)
1	-1	-1	-1	-1
2	+0.22	+0.58	+0.11	-0.28
3	-0.18	-0.15	-0.07	-0.03
4	-0.10	----	-0.17	+0.04
5	---	----	---	-0.05
6	---	-0.04	-0.10	-0.08
7	---	---	---	-0.05
8	---	---	---	+0.03
9	---	---	---	-0.04
10	---	---	---	-0.03

different possible phase combinations. The simple approach to choose the most reasonable matching from all possible results obviously fails in this case. Therefore, we have developed a simple three strip model for the L_c phase of Lac 3 (Figure 4-15 right (bottom)), based on the lactose head group, the hydrocarbon, and the mid-plane region. Here, the water layer was not taken into account because strong head group correlation in the crystalline phase of Lac 1 and Lac 3 suggested that there should be no bulk water between the bilayers. The electron density of the head group was estimated from the density of lactose of 1.525 g/cm3 and its molar mass of 342.0 g to be about 0.48 e/Å^3.

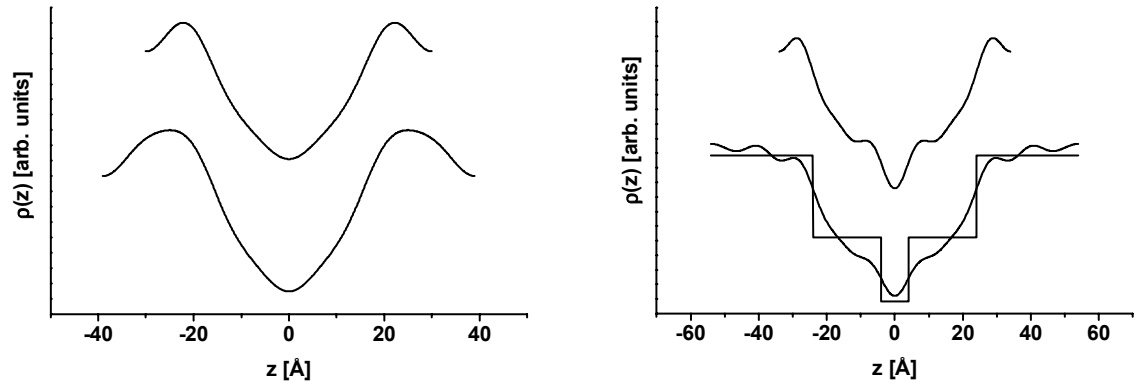

Figure 4-15 *(Left) Electron density profiles calculated from SAXS diffraction patterns of Lac 1 at 80 °C (top), and that of Lac 2 at 60 °C (bottom). Under these conditions, the glycolipids are in fluid L_α phase. (Right) Electron density profile of crystalline-like Lac 1 at 20 °C calculated from h = 1, 2, 3, 4, 6 (top) and that of Lac 3 at 20 °C obtained from a simple three-strip model (bottom).*

The electron density of the hydrocarbon region, 0.30 e/Å^3, and the terminal methyls, of 0.16 e/Å^3, were taken from the work of Harper et al. (Harper, Mannock et al. 2001). Width of the head group region was set to 30 Å by assuming a cylindrical conformation, while that of the methyl trough was assumed to be 8 Å (Wiener, Suter et al. 1989). The phasing that results in the electron density plot with the smallest mean absolute deviation to the simple three-strip model is given in Table 2. The final electron density profile is superimposed to the model shown in Figure 4-15 right (bottom). It is noteworthy that the given resolution enables one to distinguish each lactose unit at the positions of about z = +/– 29, +/– 40 and +/– 52 Å. SAXS data of Lac 1 at 20 °C, corresponding to crystalline phase, was analyzed by taking the reflections h = 1, 2, 3, 4, 6 into account. Among the 16 possible solutions 4 reasonable candidates were found "– – – – –, – + – – –, – – + – –, – + + – –" to be consistent with typical lipid bilayer features. Here, we chose "– + – – –" as the final solution (Figure 4-15, right, upper) since the corresponding electron density profile shows the best similarity in the hydrocarbon chains region with that of Lac 3 at 20 °C. The head group centre at z = +/– 29 Å almost coincides with the first lactose position of Lac 3, and the alkyl chain length d_{al} is about 24 Å in both crystalline phases. Here we refrained from determining the electron density profile of Lac 2 at 20 °C (gel phase), because the sub peak between the h = 2 and

3 could not be explained.

4.1.5 Summary

Phase behaviour, forces and morphology of three different glycolipids, Lac 1 -3, with linear head group conformation were studied in monomolecular films and dispersions. When the length of the head group is increased, the phase transition pressure rises and the monolayer swelling behaviour (*"out of plane elasticity"*) becomes more polymer-like. This is understood in terms of stronger sterical interactions between head groups due to a higher number of monomer (carbohydrate units) unit. Quite different, the *"in plane viscoelasticity"* does not change continuously with the length of the head group. For short head groups the hydrophobic chain-chain interactions are dominant and addition of carbohydrate dimers disturbs these interactions causing a decrease in viscoelasticity with the monolayer being predominately viscous. For 3 carbohydrate dimers (Lac 3) however, the head group interactions dominate the system resulting in an increase in G' and G'' and a rather elastic monomolecular film. In addition, for Lac 3 a coupling between thermodynamic (1st order) and rheological transition by the formation of physical network of hydrogen bonds has been observed. Both DSC and especially X-Ray scattering experiments are in excellent agreement with the molecular picture outlined above, suggesting the hydrophobic/hydrophilic balance between chains and head groups being the driving mechanism for the *"in plane viscoelasticity"* of the three glycolipid monolayers studied in this section. For short head groups the strong chain chain correlations found in SAXS combined with the DSC profile propose the chains being in a crystalline phase, which even causes the head groups to dehydrate (concluded from the sharp head group correlation peak). As the head group length is increased their correlation peak disappears caused by the hydration of the sugar moiety. This in turn reduces the strong correlations between the hydrophobic chains causing a shift from crystalline to gel phase. The DSC and X-ray scattering experiments of Lac 3 strongly suggest the idea of a "frozen" bilayer. No clear phase transition could be observed. The WAXS data propose the head groups being dehydrated, which supports the picture of a strong network of hydrogen bonds. This behavior of a type of "critical length" of the

head groups in order to shift the balance from hydrophobic to hydrophilic interactions is similar to the results by Sano (Sano, Sasaki et al. 1991) who found that cellooligosaccharides are soluble in water up to a number of 5 monomers. Above 5 monomers, these molecules form aggregates. All this shows the enormous importance of understanding the interactions between carbohydrates (especially hydrogen bonding) in order to correctly judge their role for membrane mechanic and stability.

4.2 Glycolipids with Branched or Bent Head Group Conformation (Lewis X, Gentiobiose)

The experiments presented in the last section can explained to a significant degree by the formation of hydrogen bonds between neighbouring carbohydrates. This formation is strongly influenced by the sterical alignment of these sugars. Therefore, two glycolipids one, with branched and one with a bent carbohydrate head group, as opposed to linear (cylindrical), were studied. The first one, gentiobiose lipid, is believed to be involved in the toxicity of lipoteichoic acid (LTA) in gram positive bacteria, similar to the well known lipid A anchor of the

lipopolysaccharide (LPS) layer in gram negative bacterias (Morath, Stadelmaier et al. 2002). Chemically, it is almost identical to Lac 1 with the only difference being a junction between the glucose and galactose (compare Figure 3-13 and Figure 3-14) causing a slight bend. The second one, Lewis X lipid, partakes in the adhesion process of leucocytes in cell rolling events (Figure 3-15).

4.2.1 Monomolecular Films of Gentiobiose Lipids.

Langmuir isotherms

To characterize the phase behaviour of gentiobiose lipid films Langmuir isotherms were taken at different temperatures (Figure 4-16). Tentatively, the same behaviour was found as for the three Lac lipids, although the phase transition pressure is about 5 *mN/m* higher at otherwise identical conditions. Following the concept outlined in section 3.1.1 a tricritical pressure around 18 *mN/m* at an area per molecule of about 64 $Å^2$ can be calculated. The latent heat decreases linearly from approximately 80 *kJ/mol* at *T*= 283 *K* to 40 *kJ/mol* at 302 *K*, which is slightly lower than that for Lac 1 due to the decreased cooperativity of hydrophobic chain – chain interactions.

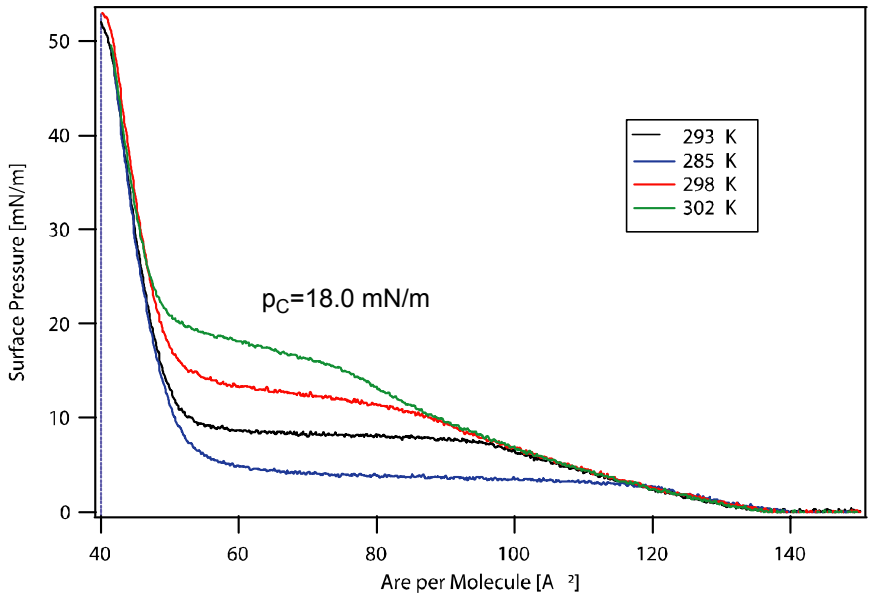

Figure 4-16 Langmuir isotherms of the Gentiobiose Lipid monolayers at different temperatures. The thermodynamic evaluation was done in the way described in section 2.1.1.

ISR Experiments

After the linear viscoelastic regime was found to be around 100 μm, the amplitude was set and fixed at that number. The frequency was fixed to 0.92 rad/s, where no strain rate induced structural changes were found in the frequency sweeps done

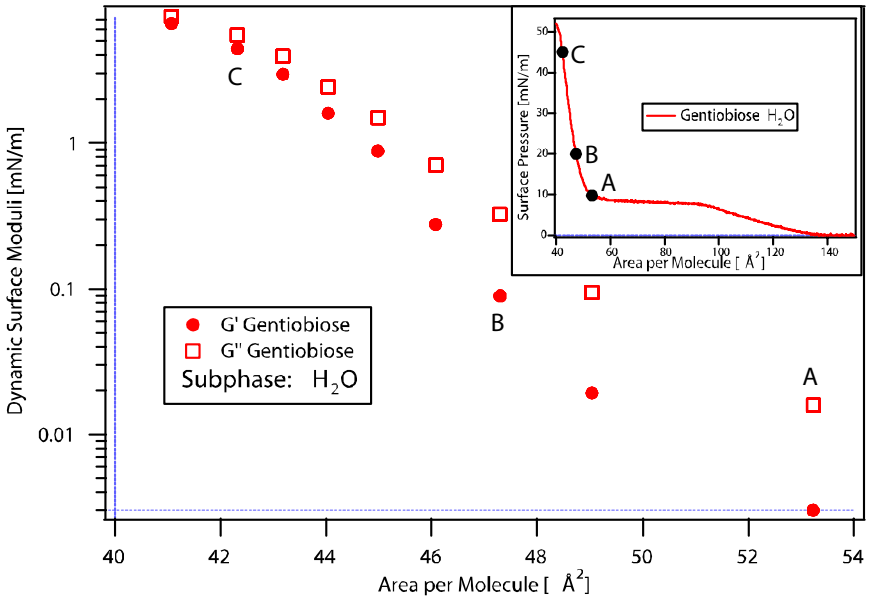

Figure 4-17 *Dynamic moduli of a gentiobiose monolayer on H_2O as a function of area per molecule. Correspondence between dynamic moduli and the Langmuir isotherm (given in the inset) is indicated. The strain amplitude was kept in the linear response regime (100 μm) throughout the experiments. T = 20°C, f = 0,92 rad/s.*

prior to every experiment. In Figure 4-17 the rheological numbers of a gentiobiose lipid monolayer are shown.

As the film was compressed below the liquid expanded – liquid condensed phase transition (marker A in Figure 4-17), the viscoelasticity shows a drastic increase, followed by a continuous one. This is similar to the behavior found for Lac 2 in the last section (Figure 4-7). At an area of 41Å^2 , which corresponds to a surface pressure of 50 mN/m, the film reached its collapse pressure with G'=6.6 mN/m and G''=7.4 mN/m. Over the whole range of surface pressure the film behaved more viscous than elastic (G'>G''), although the ratio between G'' and G' decreased from 6 (marker A) to a factor of almost 1 at marker C. The enormous decrease in viscoelasticity, with respect to the Lac 1 monolayer, is again explained in terms of hydrophobic/hydrophilic balance. The branched conformation of the gentiobiose lipid causes a better hydration of their head groups which in turn decreases the hydrophobic chain-chain interactions. The balance is shifted towards the hydrophilic head group. However, as was shown for Lac 3, the viscoelasticity of these monomolecular films of glycolipids do not only increase due to stronger hydrophobic interactions or weaker hydrophilic disturbance, but also due to an enforced network of hydrogen bonds. To manipulate these hydrogen bonds

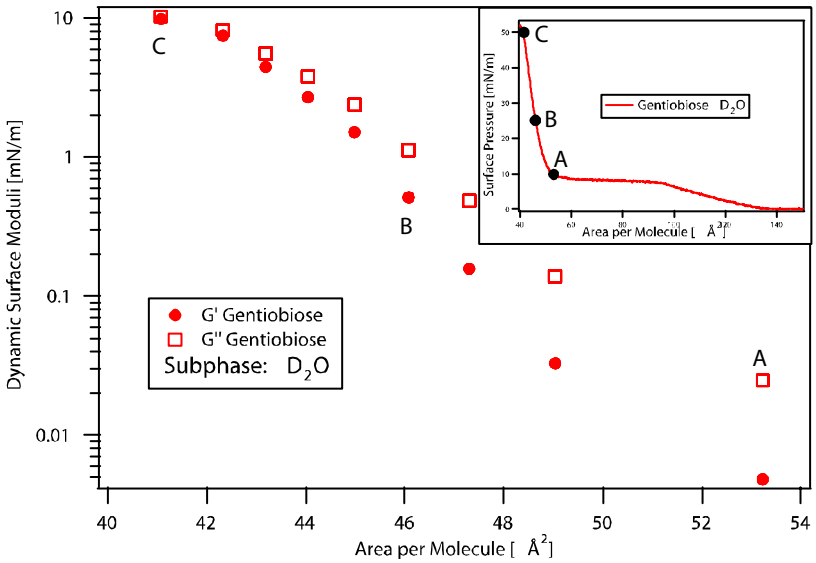

Figure 4-18 Dynamic moduli of a gentiobiose monolayer on D_2O as a function of area per molecule measured at a strain amplitude of 100 µm. Correspondence between dynamic moduli and the Langmuir isotherm is indicated (given in the inset). T = 20°C, f = 0,92 rad/s.

between the head group for identical molecules, we replaced the subphase water by D_2O. In Figure 4-18 the experiments on this subphase are presented. Even

though no change in the isotherms was observed, a clear shift in G' and G'' can be seen. Obviously, the D_2O causes a stronger network of hydrogen bonds between the polar head groups of the gentiobiose lipid. This effect is in accordance with the stronger dipole moment of D_2O and was also found on thin polymer films (Naumann, Brooks et al. 1999). Again it was nicely demonstrated that the viscoelastic behavior of glycolipid films is determined by the balance between hydrophilic and hydrophobic interactions. Furthermore, from the comparison between isotherm and ISR experiments it can be stated that new insight into the viscoelastic properties of glycolipid monolayers was gained from these in plane rheology experiments.

X-Ray and DSC

The interpretation of our experiments is strongly supported by DSC and x-ray scattering experiments (HASY Lab, Hamburg, Germany), which showed prominent indications of a L_β to L_α phase transition of hydrated bilayers (or lamellar stacks of bilayers), i.e. no dehydrated crystalline phase with strong head group correlations, as in the case of *Lac 1*, was observed. This is obvious from the shift in lamellar spacing from 6.8 nm to 6.1 nm (Figure 4-20 left), as followed by SAXS as well as

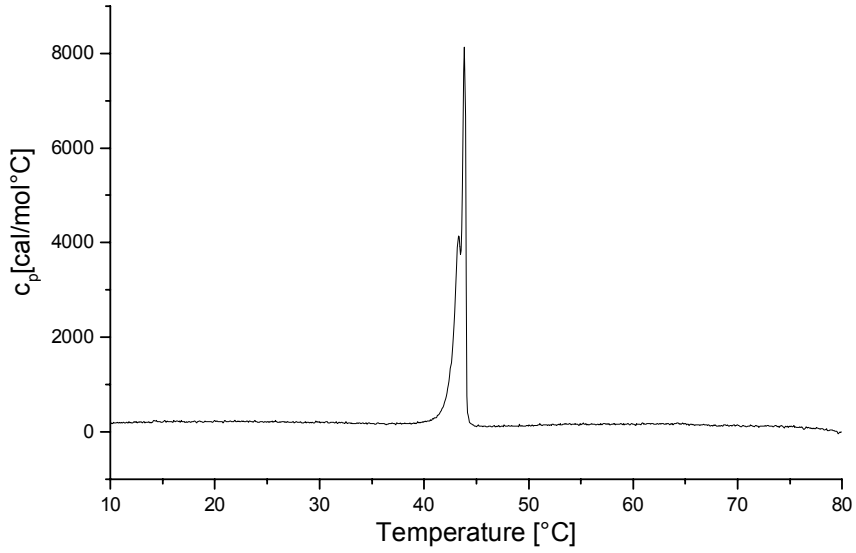

Figure 4-19 DSC data of Gentiobiose lipid vesicles. The phase transition enthalpy was calculated to be about 8 kcal/mol, similar to the Lβ to Lα transition of DPPC or Lac 2.

from the WAXS peak at 4.2 Å (Figure 4-20 right), which clearly correlates with the melting transition observed in the DSC experiment (Figure 4-19). The change in the SAXS peak position between 45 and 50 °C can be partially attributed to the thermal expansion coefficient of the lipids, which were calculated to be approximately -2.2*10^{-3} 1/K, which is comparable to the one for DPPC (-3*10^{-3} 1/K) (Sackmann 1996). This shows once more, that the hydrophilic interactions for these lipids are not strong enough to dominate the physical behaviour of the system. Also, already during preparation of the dispersions a very good solubility of the lipid vesicles in water was obtained, which is in accordance with the smooth change in the c_p trace and results from the good hydration of the head groups. Furthermore, no hysteresis for subsequent scans was detected.

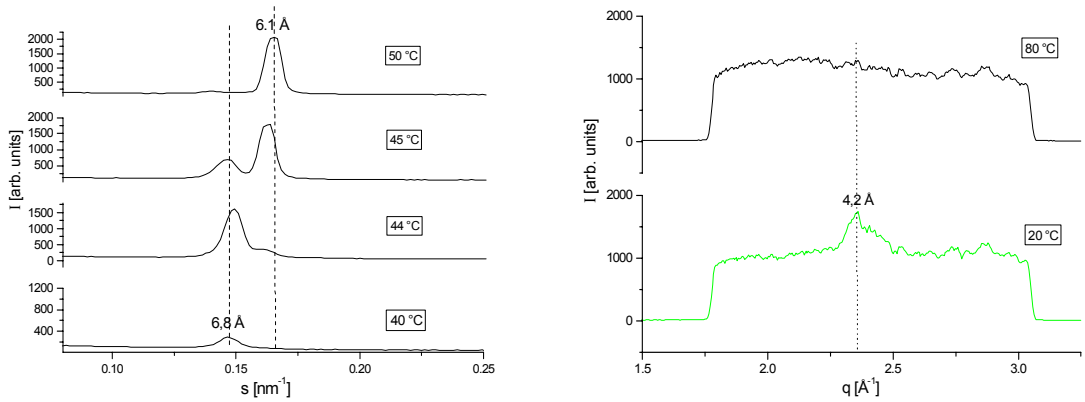

Figure 4-20 SAXS (left) and WAXS (right) data of lamellar dispersions (50 wt% water) of Gentiobiose lipid bilayers. Both indicate a phase transition. The WAXS peak (right) at 4.2 Å suggests a Lβ phase.

4.2.2 Monomolecular Films of Lewis X Lipids.

In this subsection, the physical behaviour of thin films of Lewis X lipids will be discussed. The Lewis X head group is known to take part in the cell rolling process during leukocyte adhesion. Concerning the conformation of the head group, it's important to notice that they take a branched rather than linear conformation.

Langmuir Isotherms

Langmuir isotherms taken at four different temperatures are shown in Figure 4-21.

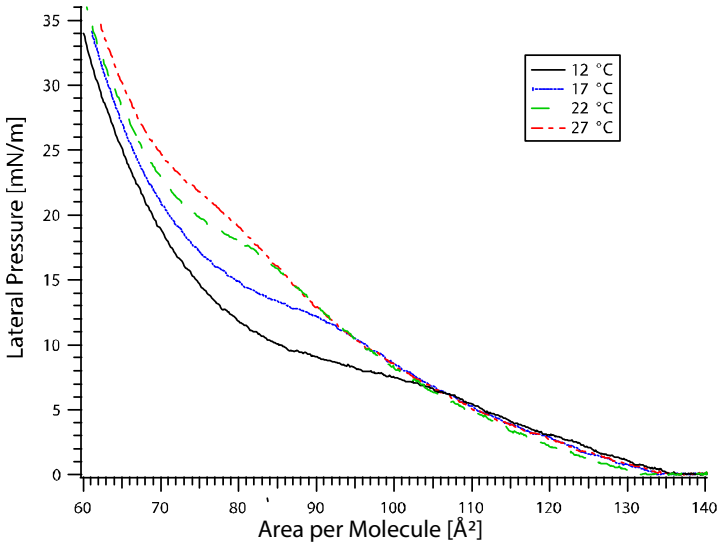

Figure 4-21 Isotherms of Lewis X at four different temperatures. Heat of transition were extracted as described in Figure 4-1

Again (cf. Figure 4-1 and Figure 4-2), a continuous (linear) increase in phase transition pressure p_k and decrease in phase transition enthalpy (calculated following Eq. 4.1) can be observed. For 17°C (290 K) the heat of transition is approx 15 kJ/mol, which is only about 50% of that observed for Lac 2 and Lac 3 (Figure 4-3). Following the same arguments as above, this can be attributed to the decrease in cooperativity between the hydrophobic alkyl chains caused by the disturbing influence of the bulky hydrophilic head group. Also the minimal area of approximately 65 $Å^2$ clearly demonstrates the strong influence of the head groups on the isotherms. Since the hydrophobic backbone has a minimal area of approximately 37 $Å^2$ (cf. Figure 4-1) and the cross section area of a sugar molecule is about 20 $Å^2$, the minimal area of approximately 60 $Å^2$ suggest a non perpendicular alignment of the trisaccharide Lewis X with respect to the air/water interface. This conformation is supported by recent x-ray crystallography experiments by Üerez and co-workers (Perez, Mouhous-Riou et al. 1996), who found a rod like conformation of the trisaccharide head group Lewis X in a highly hydrated environment.

ISR Experiments

As in all the other ISR experiments, the range of linear viscoelasticity first was determined. From this the frequency was set to 1 rad and the amplitude to 50 μm.

Completely different from the rheology of Lac 1 -3 and gentiobiose lipid, the viscoelasticity of Lewis x lipid showed a transient changes in *G'* and *G''* (Figure 4-22). As the film was compressed below 70 Å^2 , *G''* (the viscosity) increased until it reached a maximum of 0.4 mN/m at approx. 64 Å^2. Further compression decreased the viscoelasticity of the monolayer down to almost 0 mN/m at 58 Å^2. If the film was even further compressed below this area the viscoelasticity again started to rise, until the film collapsed. Subsequent expansion and compression of the film revealed the numbers for *G'* and *G''* with an error bar of about 10 %, accounting for the reversibility of this transient change. Obviously, a more complex mechanism, as believed for Lac 1 - 3 and gentiobiose lipid, determines the surprising rheological behavior of Lewis X lipid monolayers. The behavior found here might be explained by an isotropic – nematic transition as it is known from liquid crystals. For high areas per molecule, the system was in an isotropic phase. Compressing the film to lower areas per molecule eventually lead to a strong increase in molecular interaction between neighboring molecules and hence rise in the viscoelastic constants. This is visualized in Figure 4-23. Decreasing the area per molecule further lead to a reorientation of the rods which caused a drastic reduction in molecular interaction (higher rotational entropy). The following continuous increase in viscoelasticity until the collapse pressure is reached can be explained by an increase in molecular interaction due to an increase in lateral density. The rod like conformation parallel to the air/water interface and therefore an anisotropic two dimensional layer of molecules is supported by our isotherms as well as by x-ray crystallographic experiments ((Perez, Mouhous-Riou et al. 1996). The theory from Maffetone and coworkers predicts a transition from the isotropic to the nematic state for cL^2 = 2.1 – 2.4, where *c* is the surface concentration and *L* the length of the rod (Maffettone, Grosso et al. 1996). Taking *c* = 1/64 Å^2 from the isotherm and *L* = 12 Å from the mentioned x-ray experiments, we end up at cL^2 = 2.3 – 2.5, i.e. in excellent agreement with the theory. Therefore, the transition can be considered as an isotropic nematic transition of a two dimensional liquid crystal.

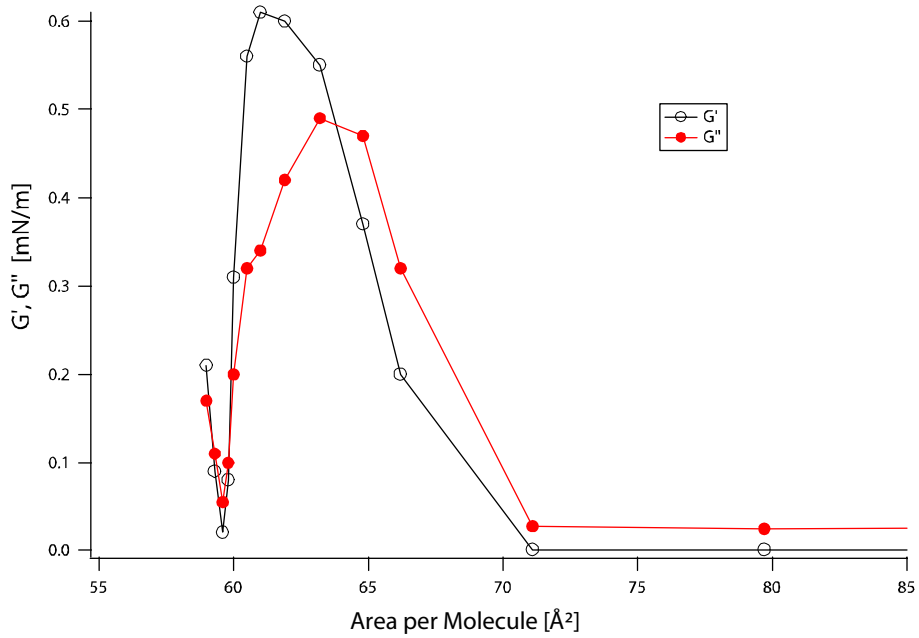

Figure 4-22 *G' and G'' of Lewis X as a function of area per molecule. Clearly, the transient change in G' and G'' can be seen.*

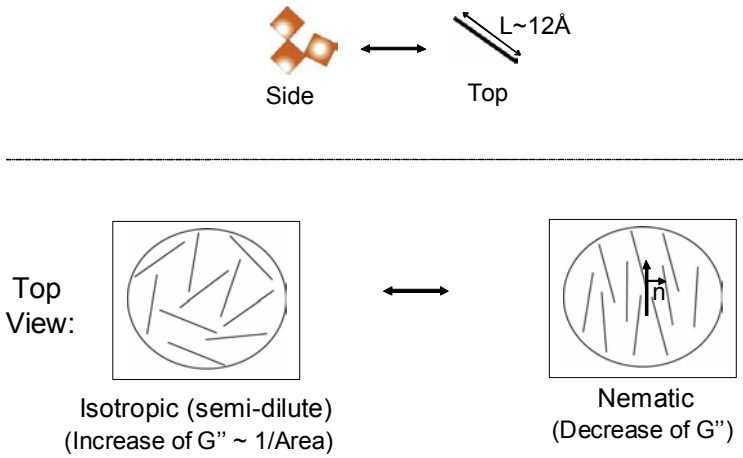

Figure 4-23 *Sketch of the projection of a Lewis X molecule on the surface (upper) and an isotropic nematic transition (lower).*

It is very important to note that no indication for such a transition was expected from the Langmuir isotherm (Figure 4-21), which again clearly shows that the ISR gives new insight in the physical properties monomolecular lipid films, which can not be extracted from Langmuir isotherms.

4.2.3 Summary

In this section the viscoelasticity of two synthesized glycolipids were studied by ISR. Prior to all experiments, the linearity of the stress-strain relationship was assured by amplitude sweeps. In addition, the absence of frequency induced changes in G' and G'' was certified around 0.15 Hz.

The gentiobiose lipid, which has identical chemical composition as *Lac* 1 but differs only in head group conformation (β 1, 4 junction), caused a drastic fluidization of the monolayer. Again, this was because of disturbed chain – chain interactions by the hydration of the head groups, which resulted in a shift of the hydrophobic/hydrophilic balance. This is also evident from the x-ray scattering experiments. The gentiobiose lipid showed a gel $L\beta$ to fluid $L\alpha$ phase transition, while for *Lac* 1 a crystalline L_c to fluid $L\alpha$ phase was observed. Furthermore, an increase in viscoelasticity could be achieved by exchanging the subphase with D_2O, clearly showing the importance of hydrogen bonds and hydrophilic/hydrophobic balance in viscoelasticity studies of membranes. The branched tetrasaccharide Lewis X head group revealed a fluid crystalline behavior. At a surface pressure of approximately 25 mN/m an isotropic to nematic phase transition took place, which manifested as a transient change in the viscosity. This was a result of the anisotropy of the Lewis X molecules, when aligned as little rods of about 12 Å parallel to the air/water interface. Above the transition, i.e. for high surface pressures, when all rods are aligned in the same direction and tightly packed together a continuous increase in viscosity was observed owing simply to the reduction in area per molecule.

It should again be emphasized that neither the viscoelastic behavior of gentiobiose nor the curious transition in Lewis X lipid monolayers could have been predicted or explained from Langmuir-isotherms. This is obvious, since *i)* the isotherms of gentiobiose lipid on D_2O and H_2O are identical and *ii)* absolutely no indication of a transition from isotropic to nematic can be extracted from the Lewis X lipid isotherm. Clearly, we have gained new insights into the physics of 2*D* monomolecular films of glycolipids.

4.3 Phase Behaviour of Fluorinated Lipids and Artificial Microdomains

Fluorinated lipids are promising candidates for a variety of applications, e.g. as drug delivery systems. This is due to the high electronegativity of fluorine

(especially with respect to hydrogen) which causes strong dipole-dipole repulsion when parallel oriented and because of its hydro- and lipophobicity. This builds the basis for the design of small lipid domains when mixed with hydrocarbon chains. Both in plane dipole – dipole interactions as well as microdomain formation will be explained in this section.

4.3.1 Stripe-like Phase Formation in Fluorinated Lipid Monolayer (Schneider, Andelman et al. 2003)

The shapes and shape transitions of domains in lipid membranes, accompanied by phase transitions, have been a subject of intensive research for many years. This arises from the interest in the formation process of lipid microdomains (e.g. rafts) in biomembranes as well as from fundamental questions about the self-assembling or pattern formation of lipid microstructures. In the following section the formation of a modulated stripe-like phase is discussed. It is shown for the first time that this formation is based on strong dipole-dipole interactions and not on reduced line tension as discussed previously (Keller, McConnell et al. 1986).

4.3.1.1 Experimental Observation

Figure 4-24 shows the fluorescence images taken at a mean molecular area of 90Å² per lipid molecule or 45 Å² per single chain. The thickness of the stripes

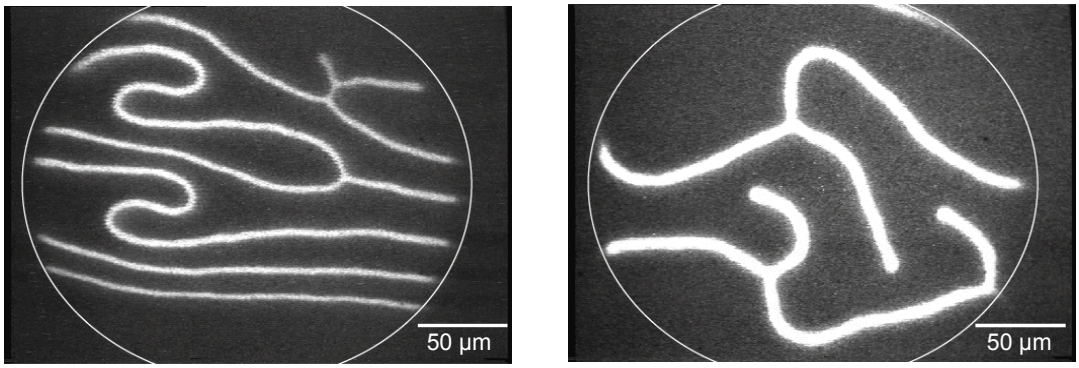

Figure 4-24 Fluorescence pictures of fluorinated lipid monolayer taken at 45 A² per lipid chain, where the film is in the gas-liquid coexistence phase. The fluorescence probe concentration was 0.1% and the line thickness measured from these pictures varies between 2 – 8 µm.

obtained from different images ranges between 2 – 8 μm. In the Langmuir isotherm (Figure 4-26) this means that the molecular area is close to the onset of the surface pressure increase, suggesting that it is close to the first order phase transition from gas to liquid-expanded. No fluorescence signal could be detected for mean molecular areas above 100 Å² as would be expected for the gas phase, while homogenous fluorescence images could be obtained for mean molecular areas below 80 Å², which is typical for liquid-expanded phases. Therefore, the picture in Figure 4-24 corresponds to the coexistence of liquid-expanded and gas phases. Surprisingly, the shape of the bright (i.e. fluid domains), appeared to be stripe-like rather than circular, as observed for other non fluorinated lipids (Figure 4-25) (Möhwald 1995). It is also of interest to note that the domains in Figure 4-24 do not merge with each other and have rather sharp domain walls. To eliminate kinetic effects arising from the finite compression speed, the monolayer was kept at constant area (90 Å² per molecule) for more then 30 min. Subsequent fluorescence images taken at 5 min intervals, showed no significant changes in shape or thickness of the domains. We conclude that the observed structures are thermodynamically stable. This is a necessary knowledge for the application of any theoretical assumptions on the nature of these interesting domain shapes. The shape and thickness of such domains is determined by two opposing forces (McConnell 1991). One of these two forces is the line tension, which reflects the energy needed to create a domain boundary between two phases. This energy is proportional to the length of the line surrounding the domain and favors circular shapes. The second force arises from the dipole moment of the lipid which tends to elongate the domains due to their electrostatic interaction.

The effective molecular dipole moment in the Langmuir monolayer can analytically

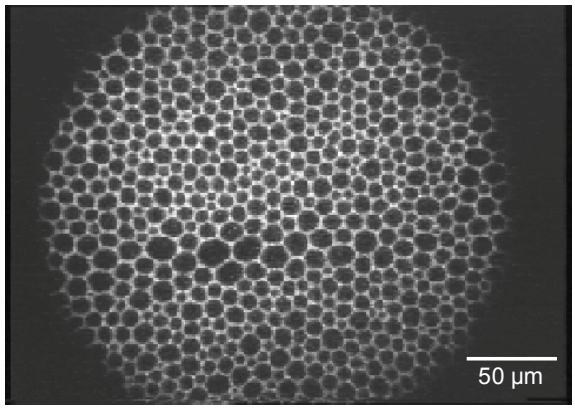

Figure 4-25 *Fluorescence pictures of non fluorinated lipids taken at 30 A² per lipid chain, where the film is in the gas-liquid coexistence phase. The fluorescence probe concentration was 0.1%. No stripe-like domains can be observed.*

be estimated by surface potential measurements (Brockman 1994) using the Helmholz equation,

$$V = \frac{\mu}{\varepsilon A} \qquad \text{Eq. 4.12}$$

where μ is the molecular dipole moment, A the area per moment and ε the local dielectric constant. In Figure 4-26 the surface potential of the fluorinated lipid studied is shown as a function of the area per fluorinated chain. This figure also

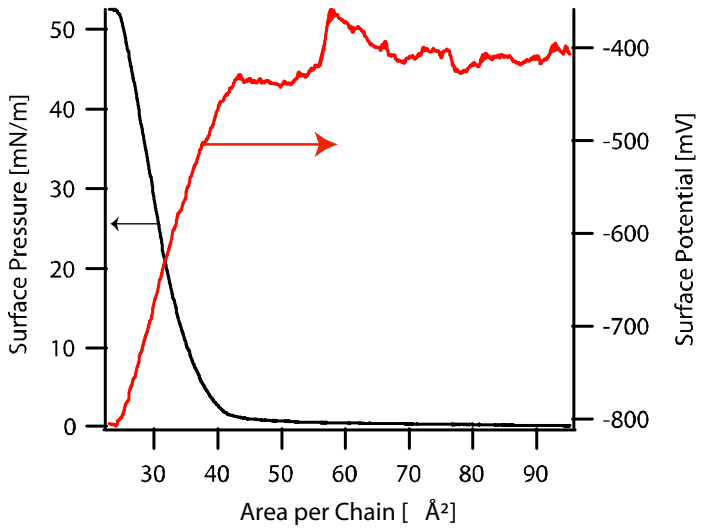

Figure 4-26 *Surface potential and pressure-area isotherms of the fluorinated lipid monolayer. The onset of the transition to the condensed phase correlates with the abrupt decrease in surface potential. An average surface potential in the gas-liquid coexistence region around – 430 mV ($\bar{A}$ = 45 A²) was found.*

includes the simultaneously measured pressure-area isotherm (area per chain instead of molecule). For relatively large areas per lipid chain the surface potential remains relatively constant and stripe like domains as shown in Figure 4-24 can be observed. Compression of the film eventually leads to a steep increase in surface pressure, indicating the end of the gas-liquid expanded coexistence. This sudden increase in surface pressure correlates with an abrupt decrease in surface potential. This can be attributed to an effective increase in the number of dipoles aligned perpendicular to the subphase as a result of the higher chain ordering. Figure 4-26 demonstrates two remarkable features of the surface potential which are in juxtaposition to those of ordinary fatty acids or phospholipids: i) the surface potential is negative and ii) compression results in much higher absolute values for small areas per chain. The potential of the fluorinated lipid monolayer at mean molecular areas of 45 Å² per lipid chain, where the monolayer is in the gas – fluid coexistence (Figure 4-24), ranged between -420 mV and -340 mV. Since the lipids used in this study are not charged, the measured surface potential should be dominated by the dipoles of the hydrophobic tails.

Three contributions are generally taken into account when examining the effective molecular dipole moments in Langmuir monolayer (Brockman 1994): (i) the contribution from the polar head group of the lipid, (ii) the influence of oriented (i.e. polarized) water adjacent to the head group and (iii) contributions of asymmetric chain termini. In the experimental system, the intermediate chain regions do not contribute to the net molecular dipole, because the successive dipoles of the groups along the chain cancel each other out as a result of their structural symmetry. The contributions from (i) and (ii) are basically identical for fluorinated and non fluorinated lipids (Smondyrev and Berkowitz 1999) therefore, the difference in dipole potential arises from the fluorinated chain termini. Because the surface potential of non fluorinated lipids in the gas or liquid-expanded phase is close to 0 V (Vogel and Mobius 1988; Oliveira Jr, Taylor et al. 1992), the molecular origin of the measured surface potential in the range of -420 mV to -340 mV can be entirely attributed to the terminal $–CF_3$ group. Thus, it is concluded that this strong dipole moment determines the formation of stripe-like domains in the two phase coexistence region.

The influence of line tension on the shape of stripe-like domains was studied by adding a small amount of cholesterol which is known to reduce line tension significantly (Weis and McConnell 1985). When 0.1 mol% of cholesterol was added to the fluorinated lipids, the average thickness of stripe domains was decreased to 1 – 2 μm (Figure 4-27). This can be understood as a result of the above outlined picture of opposing forces and is described theoretically in the next section.

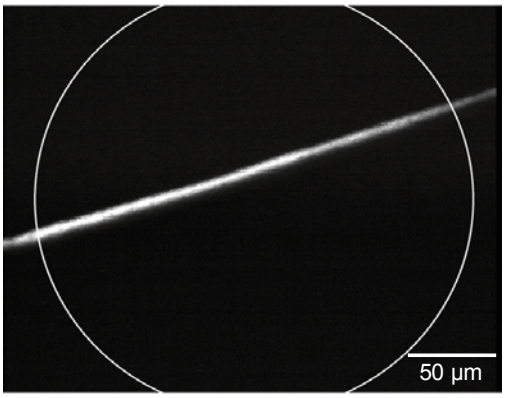

Figure 4-27 Fluorescence pictures taken at 45 A² per lipid chain with the film in the gas-liquid coexistence phase. The fluorescence probe concentration was 0.1% and in contrast to Figure 4-24 , the film contains 0.1 mol% cholesterol. The average line thickness found decreased with respect to Figure 4-24 down to 2 μm.

4.3.1.2 The Free Energy of a Patterned Field of Dipoles

A first-order phase transition between gas and liquid-expanded or liquid-expanded and liquid-condensed can be induced in a Langmuir trough by decreasing the mean molecular area of the film. The transition occurs as the attractive interaction between molecules starts to dominate over the entropy of mixing. The first-order coexistence curve in the temperature – density plane terminates with a critical point (Albrecht, Gruler et al. 1978). Electrostatic interactions alter the above mentioned gas-liquid expanded transition as a result of their tendency to stabilize phases with modulated density (Andelman, Brochard et al. 1987).

Starting from dipole–dipole interactions the electrostatic free energy of a stripe–like phase pattern following Keller (Keller, McConnell et al. 1986) and Andelman

(Andelman, Brochard et al. 1987) can be derived. A dipole μ at a distance r from another dipole sees the field created by the dipole and its image dipole μ'. The interaction energy between the two "real" dipoles located at a distance h above the air/water interface (Figure 4-28) is therefore

$$g(r) = \frac{\mu^2 \varepsilon}{2\pi r^3 \varepsilon_0 (\varepsilon + \varepsilon_0)}. \qquad \text{Eq. 4.13}$$

Where ε, ε_0 represent the local dielectric constants seen by the dipoles (water) and the dielectric constant of air respectively. This dipolar interaction energy is long range and repulsive, since all dipoles point in the same direction. Translating the dipoles from just above (air) to just below (water) the interface decreases the interaction energy by a factor of 6400 as a consequence of the high dielectric constant of water, illustrating the significance of this constant. Since the above discussed $-CF_3$ dipoles are not immersed in water, large contributions to the dipolar interaction energy can be expected, supporting the formation of modulated phases. Close to the critical point it is convenient to remain within the framework of the Landau expansion and to consider the contributions from electrostatics and line tension as additional spatial varying terms leading to a Landau-Ginzburg expansion. However, for lower temperatures where domains are assumed to have

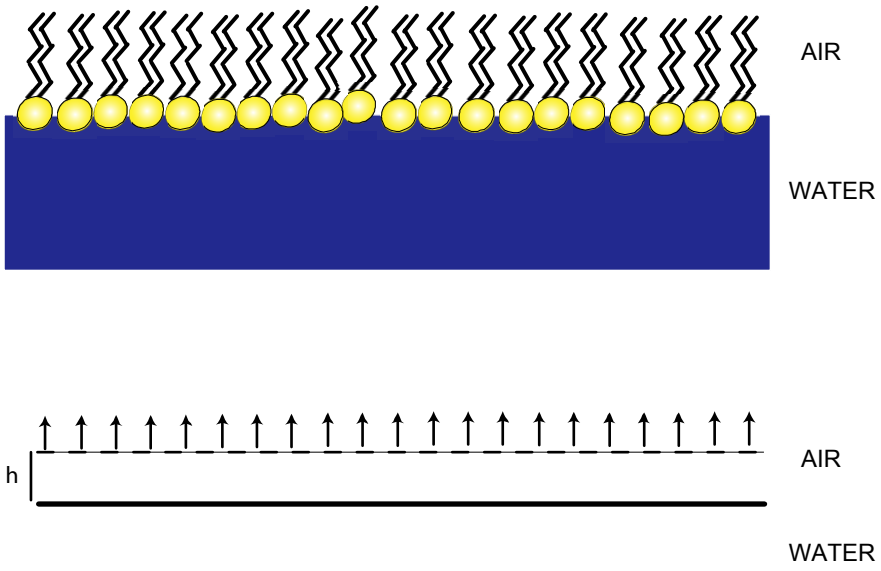

Figure 4-28 Sketch of monomolecular film at the air/water interface. The dipoles at a distance h above the interface are presented as little arrows (lower sketch). They are not immersed in water but "see" the dielectric constant of air and neighboring chains.

sharp walls, as found in our experiments (Figure 4-24), a low temperature (with respect to the critical point) calculation seems to be more convenient.

From Eq. 4.13 the interaction energy between one dipole and an infinite line of dipoles at distance *x* can be calculated:

$$U_{Line} = \frac{a^4 \mu^2 \varepsilon}{\varepsilon(\varepsilon + \varepsilon_0)} \int_{-\infty}^{\infty} \frac{1}{(x^2 + y^2)^{3/2}} \frac{dy}{a} = \frac{a^3 \mu^2 \varepsilon}{\varepsilon(\varepsilon + \varepsilon_0)} \frac{2}{x^2} . \qquad \text{Eq. 4.14}$$

Where *a=(area per dipole)*$^{0.5}$ is a microscopic cutoff length (distance between dipoles). The interaction between two lines of dipoles of length l is

$$U_{2\,Lines} = U_{Line} \frac{l}{a} = \frac{a^2 \mu^2 \varepsilon}{\varepsilon(\varepsilon + \varepsilon_0)} \frac{2l}{x^2} . \qquad \text{Eq. 4.15}$$

In one strip of width D_L, there are D_L / a lines (Figure 4-28b). This leads to an electrostatic energy of one single strip

$$F_{el} = \frac{2la^2 \mu^2 \varepsilon}{\varepsilon(\varepsilon + \varepsilon_0)} \sum_{n=1}^{D_L/\sqrt{a}} \left(\frac{D_L}{a} - n \right) \frac{1}{na} . \qquad \text{Eq. 4.16}$$

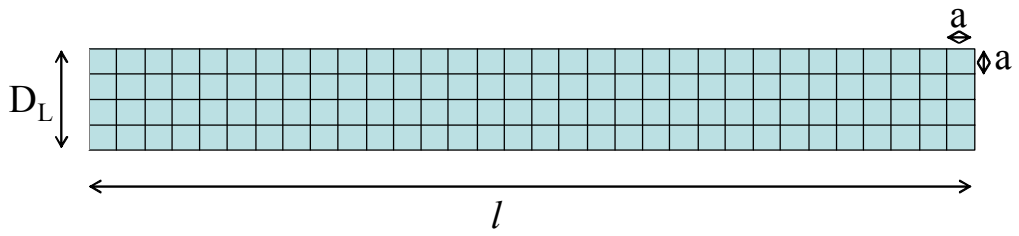

Figure 4-28b *Definition of one strip - One strip is made up of multiple lines of dipoles with the width a and length l. Its total width D_L can be extracted from the fluorescence pictures.*

The sum leads to the energy of one single strip of dipoles build of many lines of dipoles. Following the same concept the interactions between the stripes can be calculated. This eventually leads to

$$F_{el} = \frac{kTb^3}{\pi a}\left[x\phi_L^2 + (1-x)\phi_G^2\right] - \frac{b^3}{\pi D}(\phi_L - \phi_G)^2 \log\left(\frac{D\sin(\pi x)}{\pi a}\right) \quad \text{Eq. 4.17}$$

where $x = D_L/D = D_L / (D_L+D_G)$, $\phi = \frac{1}{A}$ and

$$b^3 = \frac{\mu^2 \varepsilon}{kT\varepsilon_0(\varepsilon_0 + \varepsilon)} \ .$$

The first two terms in Eq. 4.17 represent the overall average contribution to the electrostatic energy and are independent of the periodicity D. The third term is an exact summation of the inter-stripe electrostatic interactions (Keller, McConnell et al. 1986). The total free energy difference between the stripe and the homogenous phase is therefore

$$\Delta F = -\frac{kTb^3}{\pi D}(\phi_L - \phi_G)^2 \log\left(\frac{D\sin\pi x}{a\pi}\right) + \frac{2\gamma}{D}. \quad \text{Eq. 4.18}$$

Minimizing Eq. 4.18 with respect to *D*

$$D_{Equi} = a\left(\frac{\pi}{\sin(\pi x)}\right)\exp\beta \quad \text{Eq. 4.19}$$

where $\beta = \frac{2\pi\gamma}{kTb^3(\phi_L - \phi_G)^2} + 1$

This is the equilibrium thickness of the stripes and can be compared to the above observed patterns. Due to the exponential dependence of *D* on ε, the choice of ε is critical. Using $\varepsilon=2$ (approx. dielectric constant of fluorine media) decreases *D* by a factor of approximately 100. However, since the dielectric contributions from fluorine are already taken into account by their dipole-dipole interactions, e the dielectric constant of air surrounding the -CF3 dipoles were chosen. Using γ = $1.6*10^{-12}$ N [Benvegnu, 1992 #12] leads to a stripe thickness in the range of 1 μm for the measured surface potential, which is in excellent agreement with the numbers taken from the fluorescence pictures. Since the above theory is an equilibrium theory, the observed patterns can be considered as equilibrium

patterns rather than intermediate states as previously observed and theoretically described in many nucleation and growth processes. From Eq. 4.19 one would also expect that a decrease in line tension γ leads to a decrease in line thickness *D*. This is in agreement with the observation (Figure 4-27) that small traces of cholesterol (<0.1% mol) caused a decrease in the microscopically observed line thickness and thus further supports the idea that this are thermodynamically stable structures.

Finally, the phase diagram shall be constructed from the thermodynamic potential. From Eq. 4.18 and Eq. 4.19 follows

$$\Delta F = -\frac{kTb^3}{\pi a}(\phi - \phi_G)(\phi_L - \phi)\exp(-\beta). \qquad \text{Eq. 4.20}$$

This is the free energy of the stripe phase. The thermodynamic potential of the two isotropic phases (gas, fluid) close to their equilibrium order parameter can be approximated by parabolas

$$G_{Gas} = \frac{1}{2}k_{Gas}^{-1}(\phi - \phi_{Gas})^2 \qquad \text{Eq. 4.21}$$

$$G_{Fluid} = \frac{1}{2}k_{Fluid}^{-1}(\phi - \phi_{Fluid})^2.$$

Where k represents the compressibilities of the gas and the fluid phases, respectively. In Figure 4-29 the free energy (upper graph) and the phase diagram is shown. The double tangent construction yields the phase diagram (lower graph in Figure 4-29). Regions for pure gas, fluid (or liquid) and stripe–like phases are found, separated by two small regions of coexistence between modulated stripe-like and isotropic phases are found.

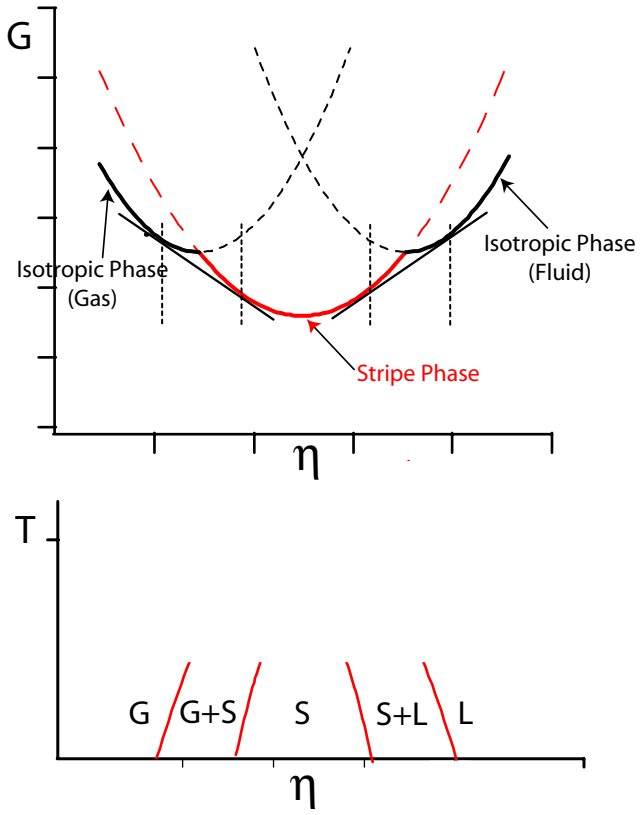

Figure 4-29

(Upper Graph) Thermodynamic potentials if isotropic and stripe phases as a function of surface concentration. Double tangent construction yields the coexistence region. (Lower Graph) Phase Diagram of gas (G), liquid (L) and stripe (S) phases. The coexistence regions are calculated from the upper graph.

4.3.2 Design of Artificial Glycolipid Microdomains by Fluorinated Lipids (Gege, Schneider, et al 2003)

In the following subsection the application of partially perfluorinated lipids with functionalized saccharide based head groups is demonstrated.

4.3.2.1 Mixing Behaviour in Monolayers

Perfluorinated lipids are known to take helical conformation (Bunn and Howells 1954). This is because of the high space requirement of the CF_2 groups as compared to CH_2 groups ($CF_2 \approx 1.5\ CH_2$), where the chains take a rather zig zag (trans or gauche) conformation. Instead of increasing the bond angle between two C Atoms to account for the higher VdW radius of Fluorine, the chain introduces a twist, hence a helical conformation arises. The different space requirements can be clearly resolved in the Langmuir isotherms (Figure 4-30), where the isotherms of two lipids with exact same head group, but different tails, one of them partially fluorinated, are shown.

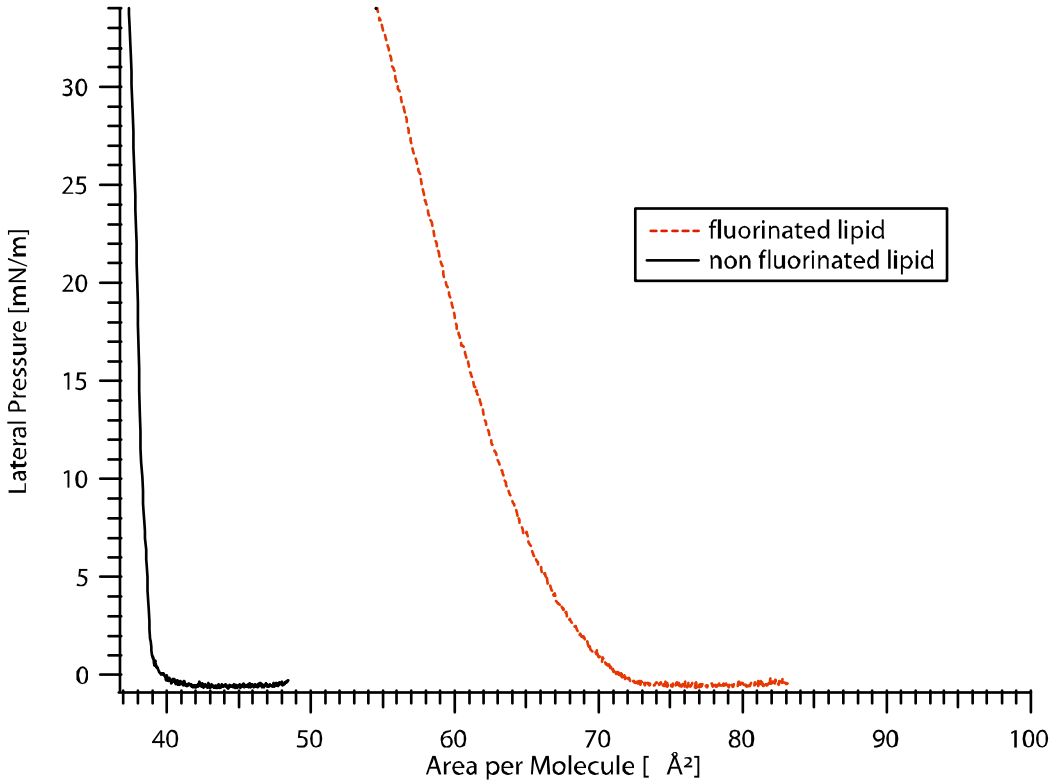

Figure 4-30 Langmuir isotherms of fluorinated and none fluorinated lipid monolayers.

This and the enormous difference in electronegativity between fluorine and hydrogen (cf. chapter 3.3.1) is believed to make the perfluorinated chains not only hydrophobic, but also lipophobic ((Shin, Collazo et al. 1993) and thus potential candidates for the design of microdomains in lipid membranes. The fluorinated lipids used in the present study are only partially fluorinated (Figure 3-16), i.e. only their eight terminal CH_2 and CH_3 groups are replaced by CF_2 and CF_3 groups, respectively. As illustrated in Figure 4-31, this should allow the remaining hydrocarbon chain to stay in their disordered configuration (of course not with respect to their diffusion properties) even in highly compressed films. Therefore the fluorescence marker T-Red, which only emits light in the vicinity of unordered chains stays visible even in high compressed fluorinated lipid monolayer (Figure 4-32 right), whereas a film of hydrocarbon chain based lipids appears almost completely black (Figure 4-32, left) (Möhwald 1995). This unique behaviour of partially fluorinated lipid chains enables us to visualize fluorine lipid domains even

for high compressed films. This is important, since only such films (highly compressed) can reliable be transferred to solid supports and therefore used for further studies.

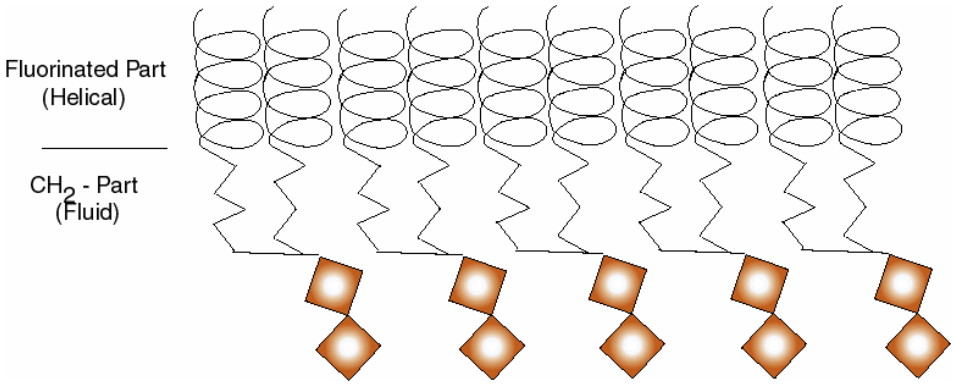

Figure 4-31 Sketch of the helical structure of fluorinated chains. The alkyl chains stay fluid due to the higher area uptake of the fluorinated chains.

The fact, that the partially fluorinated chains mix non ideal with hydrocarbon chains can be concluded from Figure 4-33. Obviously, at least for high surface pressure (25 *mN/m*), where the film is supposed to be transferred, the two lipids neither mix ideally nor completely demix, since both should result in an isotherm in the middle between the two pure systems for a 1/1 mixture ((Gaines 1966)).

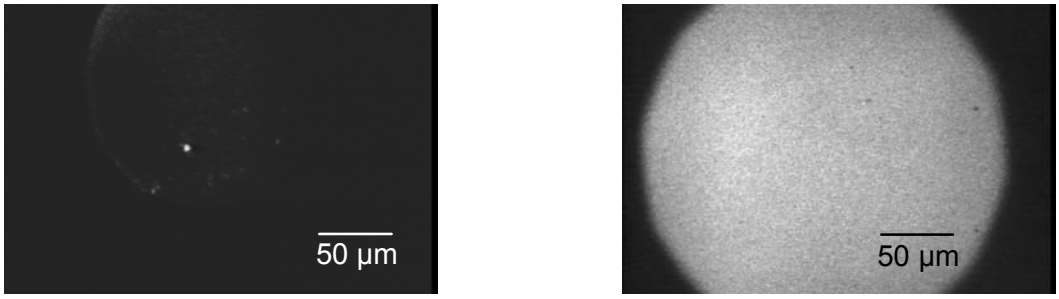

Figure 4-32 *(Left) Films of lipid monolayers with regular alkyl chains become dark at high lateral pressure. (Right) Perfluorinated lipid chains stay bright even at high compression.*

In Figure 4-34 the corresponding fluorescence images for a 10/90 mixture of fluorinated S-Lex lipid and DMPC are shown. At low surface pressures a fluid film with liquid-condensed domains of DMPC can be seen, while at higher pressures a few bright domains appear in an otherwise black lipid matrix. Since at high surface

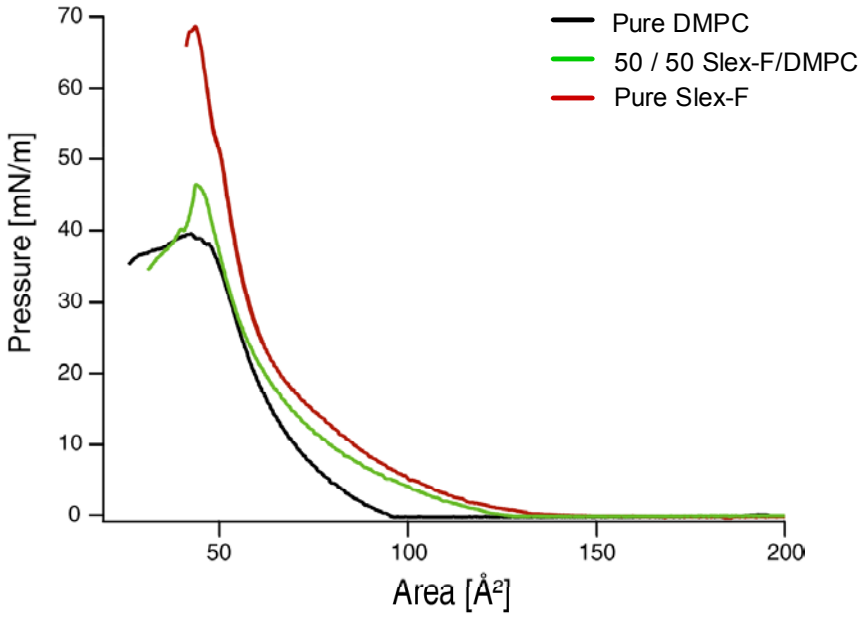

Figure 4-33 *Langmuir isotherms of DMPC, fluorinated lipids and mixtures. The non ideal mixing behaviour can be concluded from the isotherm of the mixture (green).*

pressures the dye is supposed to accumulate only in the disordered region of the fluorinated lipids, this bright spots can be addressed to be domains of such lipids. Thus it has been shown, that in fact small domains of a few micrometer with functionalized head groups can be designed.

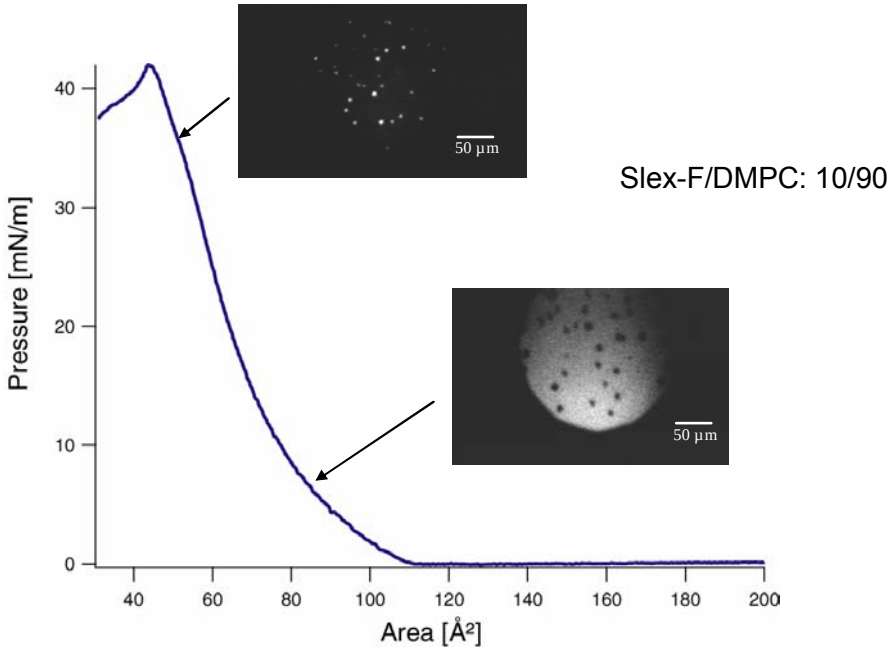

Figure 4-34 *The Langmuir isotherm and fluorescence images of the mixed S-LexF/DMPC monolayer (molar ratio: 10/90). As described in the text, the fluorescence lipids (Texas Red DHPE) accumulated in the domains of perfluorinated lipids. At high surface pressure (Π > 20 mN), fluorescent clusters of S-SlexF could be observed in the dark matrix of DMPC. Total diameter 250 μm*

The next step in testing about the general application of fluorinated lipids for the design of microdomains with functionalized head groups was to exclude the effect of the head group structure on the overall mechanism of the formation process. For that reason the mixing behaviour for two more head groups was studied. In Figure 4-35 the domains for LexF/DMPC (10/90) and S-LexF/DMPC (10/90) are compared. Even though somewhat different in size, the results are qualitatively the same. Systematic variations of the concentration ratio of fluorinated and none fluorinated chains (Figure 4-36) were done for mixtures between the lipid anchors (-OH head group). Again even though not identical in shape and size, a continuous increase of the bright domains with fluorinated anchor concentration

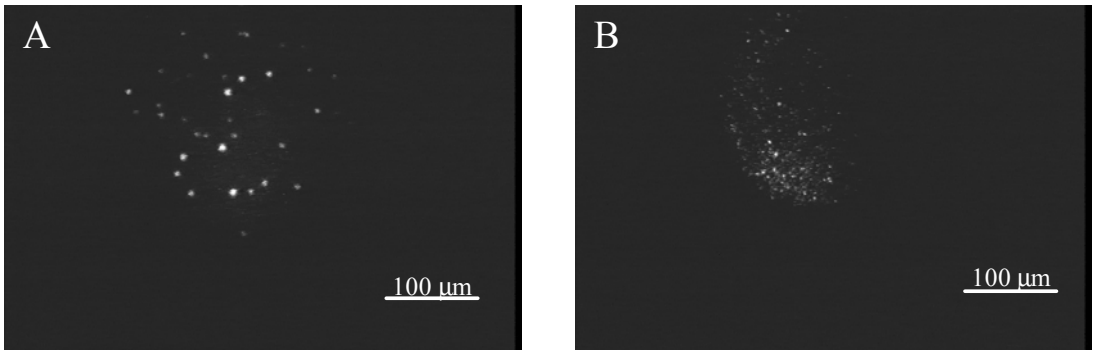

Figure 4-35 *Impact of the head group functions on the micro-domains: A) S-LexF/DMPC (10/90) monolayer at Π = 30 mN/m, and B) LexF/DMPC (10/90) monolayer at Π = 30 mN/m. Although the size of clusters appeared slightly different, the qualitative tendency strongly suggested that the hydrophobic mismatch between alkyl and F-alkyl chains plays a dominant role in formation of the micro-domains.*

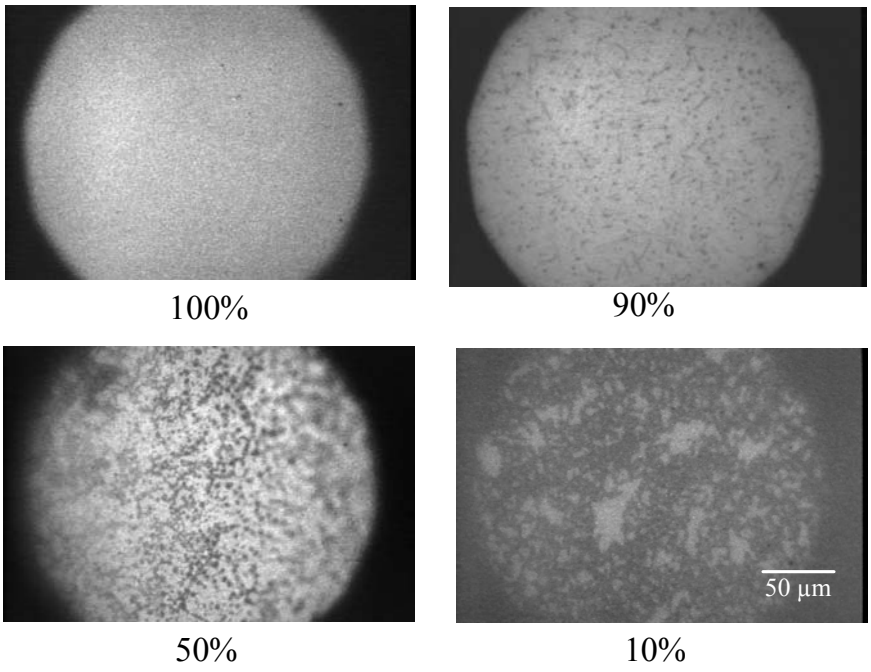

Figure 4-36 *Impact of the mixing ratio on the micro-domains. For simplicity, F-alkyl lipid anchors were mixed with the alkyl lipid anchors. According to the increase in F-alkyl lipids from 10 % to 100 % a continuous growth of the fluorescent domains of F-alkyl lipids could be observed. Total diameter 250 µm.*

could be observed. Thus, it can be concluded, that the formation of microdomains is independent from the head group structure of the lipids and is therefore obviously dominated by the mixing behaviour of the fluorinated lipid chains. It

should be noted that only the unique conformation of perfluorinated chains in correspondence with the emission behaviour of the fluorescence probe used, allowed for these important conclusions.

4.3.2.2 Mixing Behaviour in Bilayer (Vesicles)

To generalize and expand the concept of artificial microdomains giant lipid vesicles of SlexF/DMPC mixtures (15/85) were prepared (appendix). In Figure 4-37 a typical fluorescence image of two vesicles (a small one inside a larger one) is shown. The focus plane was set in the middle of the vesicle. All vesicles appeared to be circular with a diameter between 5 – 50 μm. The picture was chosen to illustrate the size distribution and similarities of domain appearance in a single picture. The existence of fluorinated domains can be clearly seen. This conclusion is drawn since, as shown in the last subsection, the fluorescence probe accumulates in the fluorinated domains. The fact that the lateral pressure *P* expected in lipid bilayer vesicles is above 25 mN/m, ((Möhwald 1995)) further excludes that the bright spots seen, can be attributed to fluid like DMPC domains, that reach the liquid-condensed phase around 5 – 10 mN/m. As a consequence the probe must be diluted in the fluorinated domains. Even though the fluorescence microscopy picture of Figure 4-37 clearly demonstrates the occurrence of microdomains in giant lipid vesicles, a clear image of the shape and size of the domains is lacking. Therefore, to gain the full 3D image of the vesicles, scanning confocal fluorescence microscopy experiments were performed. In Figure 4-38 a 3D reconstruction of a whole lipid vesicle from a stack of z-scans is shown. Impressively the phase separation between the fluorinated SlexF and DMPC domains as well as their size and shape on the vesicle surface is resolved. Qualitatively the same formation of domains as in the monolayer studies is found. Comparing the details of the domain shapes between the two systems seems difficult, since the lateral pressure *P* in the bilayer is not know and the effect of higher cooperativity in vesicles (additional cooperativity between the two monolayer) as compared to monolayers is hard to account for.

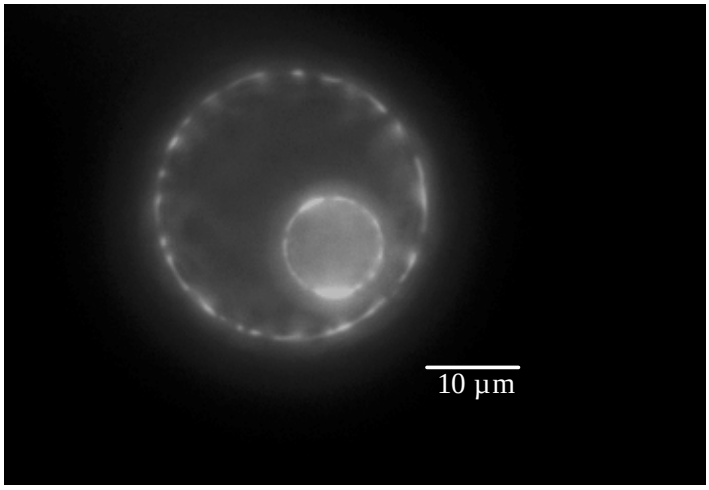

Figure 4-37 Fluorescence image of S-lexF lipid micro-domains (artificial lipid rafts) reconstituted in giant vesicles of DMPC (S-lexF/DMPC = 15/85).

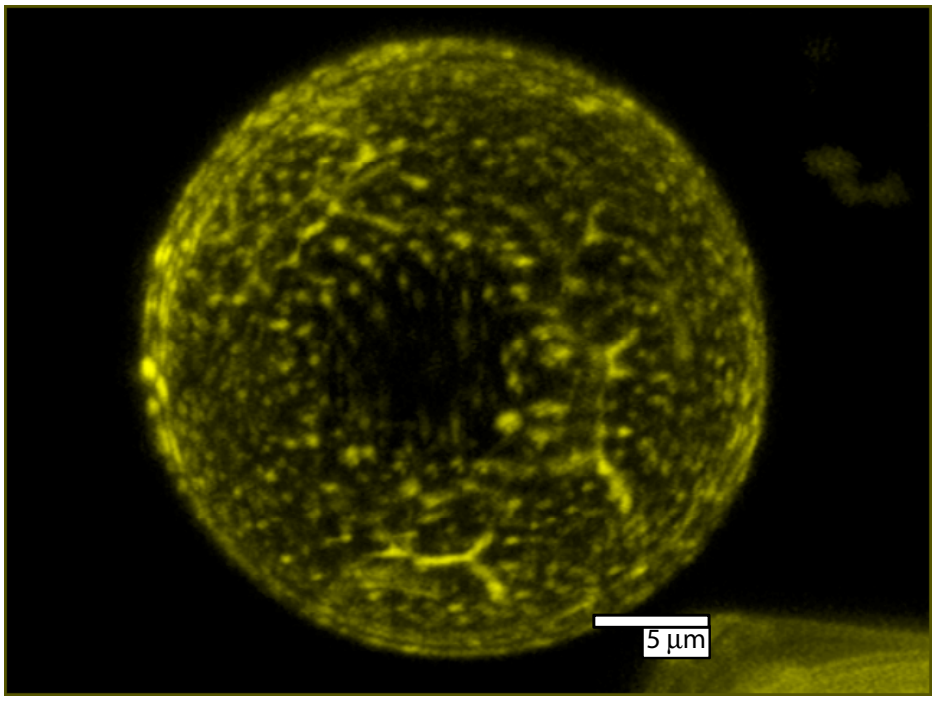

Figure 4-38 3D reconstruction of artificial rafts in a giant vesicle. It demonstrates that the F-alkyl lipids form self-assembled micro-domains in alkyl lipids both in monolayers at air/water interface as well as in vesicles with a single bilayer. Scale bar 5 µm.

4.3.3 Summary

The unique phase behaviour of fluorinated lipids and their mixing behaviour with hydrocarbon chain based lipids has been intensively studied by fluorescence microscopy and film balance experiments. For one component monolayers a stripe like phase in thermodynamic equilibrium was observed and described on the base of a theoretical model by D. Andelman (Andelman, Brochard et al. 1987). The origin of this modulated phase was identified to be the strong dipole contribution of the terminal CF_3 groups. Apart from this, their distinctive mixing behavior was shown to enable the controlled design of lipid microdomains not only in monolayers, but also in lipid bilayers. Since the demixing is dominated by the lipid chains, this holds in principle for every attached (especially functionalized) head group. These results build the basis to study not only the effect of size and concentration on cooperative binding events between membranes (ligand – receptor), but also the influence of domain shape on such and other events (e.g. enzymatic reactions).

5 Conclusions and Outlook

In the present study the physical properties of lipids with and without fluorinated tails and covalently attached carbohydrates (lactose oligomers, gentiobiose and (sialyl) Lewis X) were systematically studied by applying six experimental techniques. Thermodynamic and structural properties were obtained from film balance, calorimetry (DSC), fluorescence microscopy, and x-ray scattering experiments. Information about forces and viscoelastic properties within the plane

of the membrane and perpendicular to the surface (*"out of plane"*) was acquired with the use of interfacial stress rheometry (ISR) and ellipsometry under controlled and variable humidity conditions. It was found, that *"out of plane"* and *"in plane"* elasticity can behave differently. Namely, although the membrane becomes more *"soft"* perpendicular to the surface when increasing the number of carbohydrates, the lateral viscoelasticity increases when the number of monomers becomes N > 4, as a result of the non linear increase of hydrogen bonds between neighboring carbohydrates with N. This is completely different from the behavior of lipopolymers (e.g. PEG), in which the lateral viscoelasticity decreases dramatically with increasing number of monomers. This information clearly demonstrates that the synthetic glycolipids studied represent a more suitable model of the glycocalyx to mimic and investigate the complex interplay of various physical forces in cell-cell recognition processes. The ability of the glycolipids to form a physical network of hydrogen bonds may for example help to protect the cell against the harsh conditions frequently found on the apical side of epithelial cells. This network formation was shown to be a cooperative process (i.e. at a certain number of possible hydrogen bonding sites the network forms in an *"all of a sudden"* type process) and can therefore be viewed as a molecular mechanism in order to switch the macroscopic mechanical properties from viscous to elastic. In addition, due to the fact that the elastic properties of the membrane are controlled or at least modulated by the structure and length of the glycolipids, they can form a soft cushion and so prevent non specific adhesion between cells or influence the adhesion of vesicles, since adhesion is dependent on the elasticity of the membrane. To further investigate the effects of carbohydrate-carbohydrate and carbohydrate-protein interactions and move towards a more realistic physical model of the glycocalyx the functional head group Lewis X was introduced. Rheology studies of Lewis X displayed a fluid crystalline (anisotropic) behavior with an isotropic to nematic transition, demonstrated by a maximum in surface viscosity. This indicates the need to study the role of anisotropy or chirality in membrane physics more intensively not only with respect to mechanical properties as described here, but also for optical or electrical properties. An example is the finding that smectic C fluid crystals display a piezoelectric-like effect (Brand and

Pleiner 1984).

As a consequence of the thermodynamic analysis of glycolipid membranes it was found that although the surface transition pressure and cooperativity change in relation to the head group size, the monolayer maintains its overall stability guaranteeing that the cell membrane will keep its integrity even under harsh extracellular conditions.

The thermodynamic investigation of mixtures between fluorinated and non fluorinated lipids revealed a strong demixing between the two compounds independent of the hydrophilic head groups. Fluorescence microscopy proved the existence of microdomains or artificial lipid rafts, a prerequisite for a variety of biological processes, e.g. cell adhesion. Transfer of the monolayer, including the designed functionalized domains (sialyl Lewis X), onto a solid support and its subjection to a flow of CHO (Chinese Hamster Ovarial) cells, clearly confirmed the impact of these domains on the cell adhesion process. The precise understanding of the microdomain formation process gained throughout this work, will enable the study of the effect of size and concentration as well as the influence of domain shape on cooperative binding between membranes (ligand – receptor). The additional fact that microdomains could be reconstituted in giant lipid vesicles suggests an exciting potential for the design of new cell membrane models with artificial rafts in 3D shells (“phantom cells”). This opens new possibilities for studying cooperative interactions between membranes and proteins in the future.

Appendix

A. Viscoelasticity of PEG-lipids

Here the viscoelasticity of Polyethylenglycol (PEG)-lipopolymers with different head group length is briefly presented. As can be seen, there is a clear reduction in viscoelasticity with increasing the number of polymers from N = 3 (figure A1) to N = 9 (figure A2). This is in contradiction to the lactose lipids presented in chapter 4.1 (details there), in which the viscoelasticity increases with increase of sugar

monomers from N=4 to N= 6 .The reason for this is the strong hydrogen bond network sugars can form as discussed in detail in the chapter mentioned.

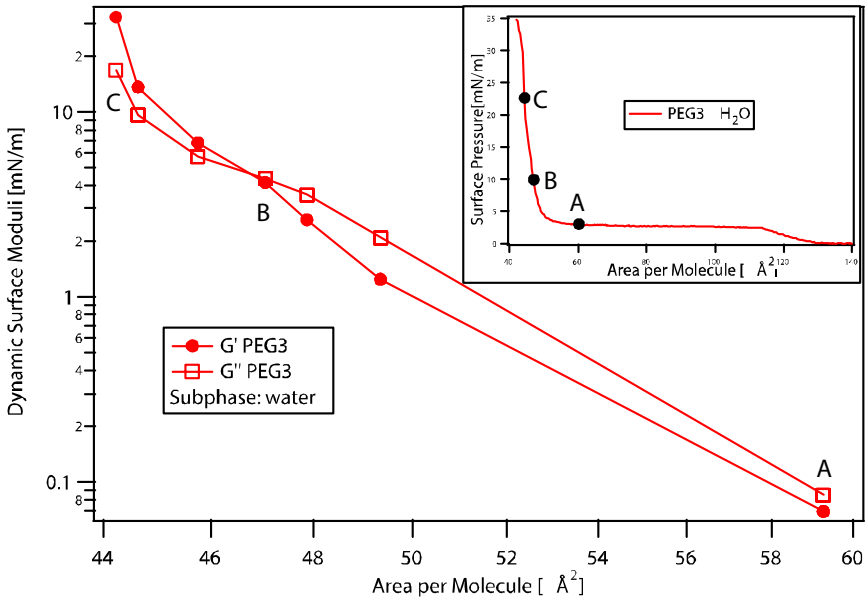

Figure A1 G' and G'' of the PEG 3 lipid.

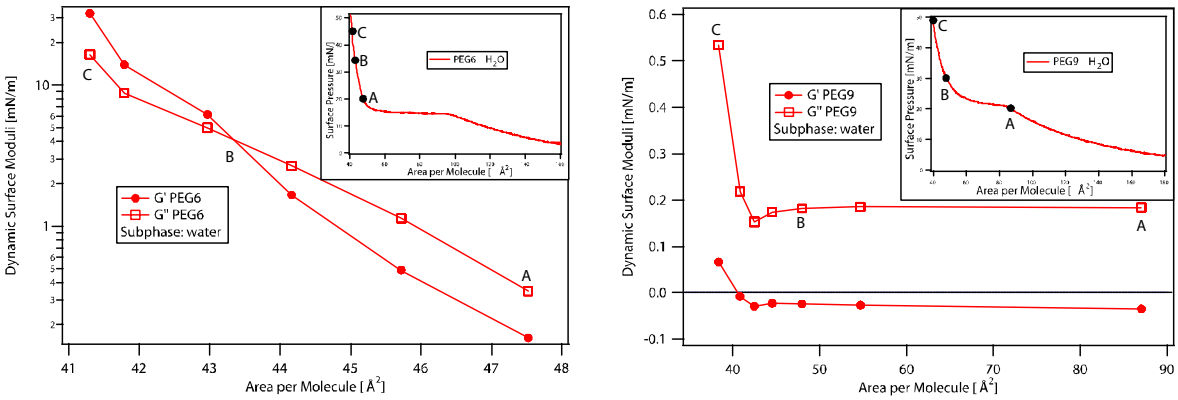

Figure A2 G' and G'' of the PEG 6 (left) and PEG 9 (right) lipid.

B. Preparation of Giant Unilamellar Vesicles (GUVs)

GUVs were prepared using the electroswelling technique. The sample, dissolved in chloroform, was spread on the electrodes and dried over night in a vacuum. A

small amout (1/1000) of the fluorescence probe (Texas Red) was then added. After complete evaporation of the solvent, an electric field of approximately 1V/mm and 10 Hz was applied. To increase the weight of the vesicles the whole setup (electrodes and chamber) was put into a sucrose solution (150 mM) during the formation process. The operating temperature was set above the chain melting temperature of the vesicles. After two hours the vesicles were put into a glucose solution with slightly higher osmolarity (> 150mM) in order to avoid that the vesicles burst. Lastly, small amounts of the sample were put on a cover slide and observed under the microscope. The diameter of these vesicles ranged between 5 and 50 μm.

Literature

Ahrens, H., T. R. Bækmark, et al. (2000). “Hydrophilic/Hydrophobic Nanostripes in Lipopolymer Monolayer.” ChemPhysChem **1**: 101.

Alberts, B., D. Bray, et al. (1994). Molecular Biology of The Cell. New York & London, Garland Publishing, Inc.

Albrecht, O., H. Gruler, et al. (1978). “Polymorphism of phospholipid monolayers.” Journal de Physique I **39**(3): 301-13.

Alexander, S. (1977). J. Phys. II France **38**: 983-987.

Andelman, D., F. Brochard, et al. (1987). “Phase transitions in Langmuir monolayers of polar molecules.” Journal of Chemical Physics **86**(6): 3673-81.

Benvegnu, D. J. and H. M. McConnell (1992). “Line tension between liquid domains in lipid monolayers.” Journal of Physical Chemistry **96**(16): 6820-4.

Brand, H. R. and H. Pleiner (1984). “Macroscopic dynamics of chiral smectic C.” Journal de Physique I **45**(3): 563-73.

Brandrup, J. and E. H. Immergut (1975). Polymer Handbook, Wiley Interscience.

Brockman, H. (1994). “Dipole potential of lipid membranes.” Chem Phys Lipids **73**(1-2): 57-79.

Brooks, C. F., G. G. Fuller, et al. (1999). “An Interfacial Stress Rheometer To Study Rheological Transitions in Monolayers at the Air-Water Interface.” Langmuir **15**: 2450 - 2459.

Bunn, C. W. and E. R. Howells (1954). “Structures of Molecules and Crystals of Fluorocarbons.” Nature **174**: 549 - 551.

Burack, W. R., Q. Yuan, et al. (1993). “Role of lateral phase separation in the modulation of phospholipase A2 activity.” Biochemistry **32**(2): 583-9.

Caffrey, M. (1987). “Kinetics and mechanism of transitions involving the lamellar, cubic, inverted hexagonal, and fluid isotropic phases of hydrated monoacylglycerides monitored by time-resolved X-ray diffraction.” Biochemistry **26**: 6349 - 6363.

Cevc, G. (1993). Phospholipids Handbook. New York, Marcel Dekker.

Curatolo, W. (1987). “The physical properties of glycolipids.” Biochim Biophys Acta **906**(2): 111-36.

Dietrich, C., L. A. Bagatolli, et al. (2001). “Lipid rafts reconstituted in model membranes.” Biophys J **80**(3): 1417-28.

Dietrich, C., Z. N. Volovyk, et al. (2001). “Partitioning of Thy-1, GM1, and cross-

linked phospholipid analogs into lipid rafts reconstituted in supported model membrane monolayers." Proc Natl Acad Sci U S A **98**(19): 10642-7.

Gabius, H. J. and S. Gabius (1997). Glycoscience, Chapmann & Hall.

Gaines, G. L. (1966). Insoluble Monolayers at Lipid-Gas Interfaces, Interscience, New York.

Gege C, Schneider MF,et al. (2003) Artificial Rafts of Glycolipids with Partially Fluorinated Membrane Anchors – Impact on Cell Adhesion. Submitted

Geyer, A., C. Gege, et al. (1999). "Carbohydrate-Carbohydrate Recognition between LewisX Glycoconjugates." Angew Chem Int Ed Engl **38**(10): 1466 - 1468.

Geyer, A., C. Gege, et al. (2000). "Calcium-Dependent Carbohydrate-Carbohydrate Recognition between Lewis(X) Blood Group Antigens. Angew Chem Int Ed Engl **39**(18): 3245-3249.

Giorgione, J. R., Z. Huang, et al. (1998). "Increased activation of protein kinase C with cubic phase lipid compared with liposomes." Biochemistry **37**(8): 2384-92.

Goldenfeld, N. (1992). Lectures on Phase Transitions and the Renormalization Group. Massachusetts, Addiso-Wesley Pubishing:.

Hakomori, S. I. (1991). "Carbohydrate-Carbohydrate Interaction as an Initial Step in Cell Recognition." Pure & Appl. Chem. **63**(4): 473 - 482.

Harper, P. E., D. A. Mannock, et al. (2001). " X-ray diffraction structures of some phosphatidylethanolamine lamellar and inverted hexagonal phases." Biophys J **81**: 2693 - 2706.

Harris, J. M. (1992). Poly(ethyleneglycol) Chemistry. New York.

Hato, M. and H. Minamikawa (1996). Langmuir **12**: 1658.

Hinz, H. J., H. Kuttenreich, et al. (1991). "Stereochemistry and size of sugar head groups determine structure and phase behavior of glycolipid membranes: densitometric, calorimetric, and X-ray studies." Biochemistry **30**(21): 5125-38.

Jacobson, K. and C. Dietrich (1999). “Looking at lipid rafts?” Trends Cell Biol **9**(3): 87-91.

Keller, D. J., H. M. McConnell, et al. (1986). “Theory of Superstructures in Lipid Monolayer Phase Transition.” J. Phys. Chem. **90**: 2311 - 2315.

Köberl, M., H. J. Hinz, et al. (1998). “Temperature scanning simultaneous small- and wide-angle X-ray scattering studies of glycolipid vesicles: areas, expansion coefficients and hydration.” Chem Phys Lipids **91**: 13 - 37.

Kraegel, J., G. Kretzschmar, et al. (1996). “Surface rheology of monolayers.” Elsevier. Thin Solid Films **284**(285): 361-4.

Landau, L. D. and E. M. Lifschitz (1987). Lehrbuch der Theoretischen Physik. Berlin.

Landersjö, C., C. Höög, et al. (2000). J Phys Chem B **104**: 5618.

Larrson, K. (1988). Physical properties - structural and physical characteristics. The Lipid Handbook. J. L. H. F. D. Gunstone, and F. B. Padley. London, Chapman and Hall**:** 321 - 337.

Lipowsky, R. (1991). “The conformation of membranes.” Nature **349**: 475 - 481.

Maffettone, P. L., M. Grosso, et al. (1996). “Extensional Flow of a Two-Dimensional Polymer Liquid Crystal.” Macromolecules **29**: 8473-8478.

Mathe, G., A. Albersdorfer, et al. (1999). “Disjoining Pressure and Swelling Dynamics of Thin Adsorbed Polymer Films under Controlled Hydration Conditions.” Langmuir **15**: 8726 - 8735.

Mathe, G., C. Gege, et al. (2000). “Equilibrium Swelling Behavior of Solid Supported Poly(ethylene glycol) Lipid Monolayers. Effects of Short Chain Lengths.” Langmuir **16**: 3835 - 3845.

McConnell, H. M. (1991). “Structures and Transitions in Lipid Monolayer at the Air-Water Interface.” Annu Rev Phys Chem **42**: 171 - 95.

Miller, A. and H. Mohwald (1987). “Diffusion limited growth of crystalline domains in phospholipid monolayers.” Journal of Chemical Physics **86**(7): 4258-65.

Möhwald, H. (1995). *Structure and Dynamics of Membranes.*, Elsevier: Amsterdam.

Morath, S., A. Stadelmaier, et al. (2002). "Synthetic lipoteichoic acid from Staphylococcus aureus is a potent stimulus of cytokine release." J Exp Med **195**(12): 1635-40.

Mouritsen, O. G. (1983). "Studies on the lack of cooperativity in the melting of lipid bilayers." Biochim Biophys Acta **731**(2): 217-21.

Naumann, C. A., C. F. Brooks, et al. (1999). "Viscoelastic Properties of Lipopolymers at the Air-Water Interface: A Combined Interfacial Stress Rheometer and Film Balance Study." 15: 7752-7761.

Oliveira Jr, O. N., D. M. Taylor, et al. (1992). "Modelling the surface potential-area dependence of a stearic acid monolayer." Thin Solid Films **210/211**: 76-78.

Pabst, G., M. Rappolt, et al. (2000). "Structural information from multilamellar liposomes at full hydration: Full q-range fitting with high quality x-ray data." Phys Rev E **52**: 4000 - 4009.

Pallas, N. R. and B. A. Pethica (1985). Langmuir **1**: 509.

Perez, S., N. Mouhous-Riou, et al. (1996). "Crystal and molecular structure of a histo-blood group antigen involved in cell adhesion: the Lewis x trisaccharide." Glycobiology **6**(5): 537-42.

Pozzoli, G., G. Vita, et al. (1997). Melt-Proccessable Perfluoropolymers. In Modern Fluoropolymers., Wiley.

Riess, J. G. (2002). "Fluorous micro- and nanophases with a biomedical perspective [Review]." Tetrahedron **58**(20): 4113-4131.

Riess, J. G. and J. Greiner (2000). "Carbohydrate- and related polyol-derived fluorosurfactants: an update." Carbohydr Res **327**(1-2): 147-68.

Rundlöf, T., C. Landersjö, et al. (1998). Magn. Reson. Chem. **36**: 773.

Sackmann, E. (1996). *Structure and Dynamics of Membranes. From Vesicles to Cells.* E. Sackmann and R. Lipowsky. Elsevier: Amsterdam.

Sano, Y., T. Sasaki, et al. (1991). Photon Factory Activity Rep. **9**: 196.

Schneider M.F., Andelman D. and Tanaka M. (2003) Electrostatically Driven Stripe Phase Formation of Fluorinated Lipid Monolayers at the Air/Water Interface. In Preparation.

Schneider MF, Marsh D et al. (1999) Network formation of lipid membranes: triggering structural transitions by chain melting. Proc Natl Acad Sci U S A 96(25):14312-7.

Schneider, M.F., Lim, K., et al. (2002). "Rheology of Glycocalix Model at Air/Water Interface." PCCP 4(10):1945-52

Schneider, M. F., G. Mathe, et al. (2001). "Thermodynamic Properties and Swelling Behavior of Glycolipid Monolayers at Interfaces." J. Phys. Chem. B **105**: 5178.

Schneider, M. F., R. Zantl, et al. (2002). "Hydrophilic/Hydrophobic Balance Determines Morphology of Glycolipids with Oligolactose Head Groups." Biophysical Journal.

Scott, H. L., Jr. (1975). "Some models for lipid bilayer and biomembrane phase transitions." Journal of Chemical Physics **62**(4): 1347-53.

Seddon, J. M., G. Cevc, et al. (1984). "X-ray diffraction study of the polymorphism of hydrated diacyl- and dialkylphosphatidylethanolamines." Biochemistry **23**: 2634 - 2644.

Shin, S., N. Collazo, et al. (1993). "Comment on molecular dynamics simulations of monolayers of fluorinated amphiphiles." Journal of Chemical Physics **98**(4): 3469-74.

Simons, K. and E. Ikonen (1997). "Functional rafts in cell membranes." Nature **387**(6633): 569-72.

Smondyrev, A. M. and M. L. Berkowitz (1999). "Molecular dynamics simulation of fluorination effects on a phospholipid bilayer." Journal of Chemical Physics **111**(21): 9864-70.

Tamada, K., H. Minamikawa, et al. (1996). Langmuir **12**: 1666.

Vogel, J., G. Bendas, et al. (1998). "The role of glycolipids in mediating cell adhesion: a flow chamber study." Biochim Biophys Acta **1372**(2): 205-15.

Vogel, V. and D. Mobius (1988). "Hydrated polar groups in lipid monolayers: effective local dipole moments and dielectric properties." Thin Solid Films **159**: 73-81.

Warren, B. E. (1969). X-ray diffraction. Reading, MA, Addison-Wesley.

Weis, R. M. and H. M. McConnell (1985). "Cholesterol stabilizes the crystal-liquid interface in phospholipid monolayers." Journal of Physical Chemistry **89**(21): 4453-9.

Wiener, M. C., R. M. Suter, et al. (1989). "Structure of the fully hydrated gel phase of dipalmitoylphosphatidylcholine." Biophys J **55**: 315 - 325.

Publications

1) Winter DC, Schneider MF, O'Sullivan GC, Harvey and Geibel JP Rapid effects of aldosteron on sodium-hydrogen exchange in isolated colonic crypts. J. Membrane Biol. (1999) 170, 17-26.

2) Schneider MF, Marsh D, Jahn W, Kloesgen B, Heimburg T. Network formation of lipid membranes: triggering structural transitions by chain melting. Proc Natl Acad Sci U S A (1999) Dec 7;96(25):14312-7.

---

3) Schneider MF, Mathe G, Tanaka M, Gege C, Schmidt RR (2001) Thermodynamic properties and swelling behavior of glycolipid monolayers at interfaces. J. Phys. Chem. B 105:5178-5185.

4) Schneider MF, Lim K, Fuller GG and Tanaka M (2001) Rheology of Glycocalix Model at Air/Water Interface.PCCP 4(10):1945-52

5) Schneider MF, Zantl R, Gege C, Schmidt RR and Tanaka M (2002) Hydrophilic/Hydrophobic Balance Determines Morphology of Glycolipids with Oligolactose Head Groups. Biophys. J., In Press

6) Gege C, Schneider MF, Schumacher G.,Limozin L, Rothe U,Bendas G, Tanaka M, and Schmidt, RR (2003) Artificial Rafts of Glycolipids with Partially Fluorinated Membrane Anchors – Impact on Cell Adhesion. Submitted

7) Schneider MF, Andelman D and Tanaka M (2003) Electrostatically Driven Stripe Phase Formation of Fluorinated Lipid Monolayers at the Air/Water Interface. In Preparation.

8) Vautrin V, Zemb T, Schneider MF, Tanaka M (2003) Balance of pH and Ionic Strength Influences on chain melting transition in catanionic vesicles. Submitted

9)Tanaka M, Schneider MF, Brezesinski G (2003) In-planeMorphology of Synthetic Oligolactose Lipid Monolayers – Impact of Saccharide Chain Length. ChemPhysChem, In Press.

CURICULUM VITAE

MATTHIAS F. SCHNEIDER

PERSONAL INFORMATION

- Date of Birth : 02. Feb 1971
- Place of Birth : Schweinfurt, Bayern, Germany

UNIVERSITY EDUCATION

2000 - Lehrstuhl für Biophysik TU München

Promotion (PhD- Thesis)

- Physik der Gylkokalix (Physics of the Glycocalix)

1995 - 1999 Physik Fakultät Universität Göttingen

Student

- Physik Hauptdiplom
- Diplomarbeit at the Max Planck Institut for biophysikalische Chemie, Title : "Thermodynamik von Membranen und Membrannetzwerken".
- Diplomprüfung : Oktober 1999 (Score : 1,6)

1994 - 1995 Physik Fakultät Universität - GH Siegen

Student

- Physik Grundstudium
- Vordiplom : August 1995 (Score: 2,0)

1993 - 1994 Physikalische Technik FH - Rüsselsheim

Student

- Grundstudium

ADDITIONAL RESEARCH EXPERIENCE

1997 Yale Medical School New Haven, CT, USA

Guest Scientist

- Department of Physiology, Prof. Dr. John Geibl
- Subject : "Rapid Effects of Aldosteron on Sodium-Hydrogen Exchange using Laser Confocal Microscopy"
- From : March – November (9 Month)

2001 Stanford University Stanford, CA, USA

Visiting Scientist

- Department of Chemical Engineering (Prof. Dr. Gerry. G. Fuller)
- Subject : "Rheology of Glycolipid Monolayer"
- May 2001 (5 Weeks)

CIVIL SERVICE (ERSATZDIENST)

1991 – 1992
Leopoldina Krankenhaus Schweinfurt, Bayern, Germany.

PRIMARY EDUCATION

1989 – 1992
Abitur, FOS Schweinfurt, Bayern (Technischer Zweig)

1982 – 1989
Gymnasium Bad Königshofen (Rhön Grabfeld)

1978 – 1982
Grundschule Stadtlauringen (Ldkr Schweinfurt)